# NUMERICAL MODELING OF CHEMICALLY REACTING CARBON PARTICLES IN DENSE PARTICULATE MEDIA

by

Pankaj Kumar Sahu

A thesis submitted in partial fulfillment of the requirements for the degree of

Master of Science

in

Chemical Engineering

Department of Chemical and Materials Engineering
University of Alberta

## Abstract

This work presents the numerical study of chemically reacting char particles in dense particulate media applied to fixed and fluidized beds. Our main goal was to approximate 3D fixed bed particles into 2D axisymmetric geometry using a representative element, which is found in Chapter 1. Dry air was made to pass at different Reynolds number of 10, 50 and 100 into a row of 10 spherical char particles($d_p$ = 0.02 m). The inflow temperature was kept at 1000K. We incorporated six gaseous chemical species, $O_2, CO, CO_2, H_2, H_2O$ and $N_2$ in addition to solid carbon, taking into account 3 heterogeneous and 4 homogeneous semi-global reactions. The particles were assumed to be non-porous. A Pseudo Steady State approach using commercial CFD solver, ANSYS® Fluent™14.0[1] was applied to solve the Navier Stokes equation for the flow field, coupled with energy and species conservation equations. Combustion and gasification were represented by varying composition of the inlet gas as, i) $Y_{O_2}$=0.233 and $Y_{H_2O}$=0.001 and ii) $Y_{O_2}$=0.11 and $Y_{H_2O}$=0.074, respectively. Comparisons of the temperature and mass fraction of $CO_2$ on the particle surface as well as along the axis were made. The maximum difference in axial temperatures between the two cases was observed to be ∼8% for $Re = 10$. A 2.8% maximum difference in surface averaged temperature was observed for $Re = 50$. Effect of the P-1 radiation model has also been investigated. The 2D and 3D simulations are illustrated and analyzed to emphasize the validity of the 2D model.

Chapter 2 provides the study of influence of heat transfer in solids, as well as combustion and gasification in 2D-channel bed. Investigations were made at different Reynolds number to analyze the temperature and mass fraction of $CO_2$ along the axis. A maximum temperature difference of 3.6% was observed along the axis for $Re = 100$. Study was also performed to evaluate the carbon consumption rates, temperature and mass fraction of $CO_2$ on the particle surface. The peak axial temperature of 2750 K was seen at $Re = 100$ during combustion, while gasification managed to increase the peak temperature to ∼1900 K. Additional parameters such as the $\text{Damkohler}_{\text{II}}$ number and Lewis number were also investigated.

Chapter 3 includes comparisons between fixed bed and fluidized bed conditions using new 2D approximation. Fluidized beds-like geometry have been depicted by introducing spacing between the particles. Two different arrangements were tried, with spacing:-$d_p$ and $0.5d_p$. This model was compared to the previous chapter and it was found that the temperature in fluidized beds tends to be higher by ∼15% compared to fixed beds.

## Acknowledgements

I wish to thank a lot of people who have contributed in one way or another towards this work. But first, I would like to express deepest gratitude and regards to my supervisor, **Dr. Petr Nikrityuk**. He has been a tremendous mentor for believing in me and encouraging me throughout the entire course of this thesis program. His exciting spirit towards research and enthusiastic approach towards any scientific problem is highly contagious. He was patient enough to teach me the basics of the involved science, simulation software and answer even the silliest of doubts. Apart from scientific concepts, he was also an advisor in terms of extreme work load management, time management and career goals. I would again like to thank him for all his support.

I would also like to thank my research group mate, Md. Omar Reza who has been a very supportive colleague and helpful friend in times of distress and doubt. Learning the various softwares during the thesis would not have been possible without his help and advice. I would also like to thank all my friends at 11615, Edinboro Road, Edmonton for providing me a temporary place to eat and sleep during times when I had to spend 2-3 days continuously at the university. Also, I would like to thank my friends at University of Alberta: Rohan Gaikwad, Abdul Wasay, Amrit Bhinder, Rohit Sivakumar, Yathirajan BM, Lokesh Baskararajan, Aharnish Hande, Talat Iqbal, Prakash Jayachandran and Prateek Kumar. I would also like to thank my best friends in India: Aakash Golia, Prateek Kumar and Hitesh Parwani for their support.

A special mention should be made for my dearest friend, **Nitya Iyer** for her kindness and support during the time of this project. She always provided me with a helping hand and constantly supported me through words of motivation to reach my goal. Finally, I am greatly thankful to my mother, father and sister for all the sacrifices that they made for me. Their prayers and advice have been strong pillars of support throughout the entire project.

# Table of Contents

# List of Tables

# List of Figures

# Chapter 1

# Introduction

Fixed bed reactors have been used extensively in the chemical industry for a number of applications ranging from distillation, filtration, catalytic chemical reaction, gasification and heat storage. The primary reason for this versatile usage is due to the fact that they enhance the contact between two different phases in a chemical process. Some[4] refer to fixed beds as the workhorses of the process industries. Reliability, conversion, capital and energy consumption are some of the limiting factors associated with the design of modern-day reactors. Testing a pilot scale reactor by designing, setting-up and testing is both expensive in terms of time, capital and manual labor. Hence, CFD based computational methods have been adopted to design, scale up and troubleshoot gas-solid reactors. Before the advancement of modern computers, scientists relied upon laboratory experiments and set-up to perform their desired study of fixed bed reactors. We present a short literature review describing the study performed beforehand regarding bed reactors and our motivations to carry out the work mentioned in this report.

## 1.1 Literature Review

**Study of porous media:** We start by sheding some light on the study of porous media with focus upon flow dynamics. Ergun [5] derived an equation for the pressure drop required for a fluid to flow through a column is given in terms of the friction factor, $f_p$ and Reynolds number, $Re$. Many experimental [6, 7] studies were performed to prove the validity of the Ergun equation. These studies tried to incorporate different materials, flow rates and diameter in the fixed bed to validate a large range of Reynolds number. Furthermore, Chhabra et al. [8] performed a comprehensive literature review for the flow of non-Newtonian fluids in fixed and

fluidized beds.

Darcy [9] gave a constitutive equation based on experiments to desribe the flow through a porous medium, which was derived theoretically by Whitaker [10]. Liu et al. [11] modified the Kozeny-Carman theory by combining the one-dimensional flow model with a two-dimensional tortuosity model, curvature ratio and a pore cross-sectional area variation. Thus, a modified equation for the pressure drop through the porous media was obtained where the dependence of porosity was described as $\epsilon^{-11/3}(1-\epsilon)^2$ for the Darcy's flow region different from the Kozeny - Carman's theory ($\epsilon^{-3}(1-\epsilon)^2$). Barak and Bear [12] studied the parameters affecting flow through a porous medium at high Reynolds number. The flow was assumed to be homogeneous and Newtonian whilst the porous medium was homogeneous and anisotropic in nature. They compared the phenomenon through different porous medium and observed that there is no particular equation to define thie flow behaviour.

**Packed beds:** To better understand the void fraction distribution, Benenati and Brosilow [13] studied a packed bed of spheres comparing the distribution to a damped oscillatory wave. Experiments were performed for five different cases of the ball diameter($d$)and voidage was studied using a epoxy resin to fill into the interstices. The voidage was taken unity at the wall as there was a single point of contact which gradually decreased from the wall to the center of the bed. Eisfeld and Schnitzlein [14] tried to correlate the effect of the walls of the packed bed container on the pressure drop across the bed using experiments. They also tried to develop a pseudo-continuous model based on the Navier-Stokes equation taking into consideration the fluid-solid interaction due to the boundary of the particles in the packing[15]. This was validated theoretically with previous studies of pressure drop and axial velocity.

Dixon et al. [16] attempted to better understand the drag-coefficients($C_d$) and heat flow in the steam reforming industry, where Reynolds number range from 500 to 10,000 at the particle-particle and wall-particle contact points. They studied the four most common modifications at the contact points mentioned in literature, namely *gaps*(shrinkage of the particle spheres)[17, 18, 19, 20], *overlaps*(expanding the particle spheres)[21, 22, 23], *bridges*(introduction of a cylinder at the contact points between the spheres)[24, 25, 26] and *flattening*[27] the spherical particles near the particle-particle and wall-particle contact points. They observed that the first two approximations(gaps & overlaps) cause an increment of 3% error in the pressure drop for an increment of 1% error in voidage. Also, these lead to an error of ap-

proximately 4% for the 99% gap and 101% overlap sizes. They recommended that the bridges method is most reliable if used with an effective thermal conductivity. Approximations using gap and overlap methods lead to a high error in both drag coefficient and particle-particle heat transfer rate unless the modification is extremely minimal. However, this again requires extremely fine mesh at the contact regions.

**Experiments on fixed beds:** Glaser and Thodos [28] studied the heat and momentum transfer charcteristics for a randomly packed fixed bed of solid metallic particles. Different geometry and size of particles and gas compositions such as hydrogen and carbon dioxide in addition to air were tried out during the experiments. Gai and Dong [29] studied the gasification of non-woody biomass in a downdraft fixed bed gasifier using air. In this study, the temperature profiles, composition of the producer gas and realease of sulphur and chlorine compounds during gasification were used to investigate the effect of operating conditions on the performance of the gasifer. The yield, efficiency and the low heating value(LHV) of the fixed bed gasifier were calculated.

Gordillo and Annamalai [30] investigated the effect of equivalence ratio(ER) and steam to fuel(SF) ratio on the temperature profile, gas composition, efficiency and the heating value in a dairy biomass fixed bed gasifier. The influence of SF ratio was found to be more than the ER ratio and temperature influences the compostion of the outlet gas by increasing the mass fraction of CO and $H_2O$ with a decrease in $CO_2$ and $H_2$. Grieco and Baldi [31] studied a counter current moving bed coal gasifier by dividing the gasifier into two major zones: drying/pyrolysis at the top and oxidation/gasification as the bottom analytically. The two zones were coupled during the calculations. In the pyrolysis zone, efforts were made to study the model inside the particles and this was again coupled with the model of the entire zone.

**Numerical modelling of non-reacting fixed beds:** Inorder to explain the results obtained from fixed beds, numerical modelling of fixed beds has also received considerable attention by researchers Yoon et al. [32], Amundson and Arri [33], Bhattacharya et al. [34] and Hobbs et al. [35]. These models assume a uniform gas/solid plug flow in the reactor and the gas temperature is kept equal to the temperature of the solid phase. The gas phase kinetics have also been neglected in these studies. Jakobsen et al. [36] suggested a split between the flow and the chemistry model parts to provide a more optimal method of solution for each operator. The behaviour of this scheme was then evaluated using the simulations from two industrial processes, namely the synthesis gas and methanol production processes

which is performed in multitube fixed bed reactors at the Statoil methanol plant at Tjeldbergodden in mid Norway. Skaare [37] gives a comprehensive literature review of wall-cooled fixed bed reactors.

Jang and Chiu [38] attempted to study the effect of turbulence, porosity and particle size on the fluid flow and the heat transfer over a sintered bed both numerically and experimentally. The 3-D numerical model assumed the bed as a packed 4-row bed of spheres where the uniform-sized spheres are present in face-centered cubic arrangement. No chemistry was taken into consideration in this study. Bunt and Waanders [39] studied the volatization rate of trace elements such as Pb, Hg, Se and Cd which are left behind after the gasification of low rank grade C bituminous Highveld coal in South Africa. The study was also carried out for North Dakota lignite coal and comparisons were made between the two cases. Hg was found to be the most volatile in both the cases and is present in elemental Hg form in the gas phase during fixed bed gasification. However, the order of volatilities among the different trace elements varied for the two cases.

**Numerical modelling of reacting beds:** Gerun et al. [40] numerically investigated the oxidation zone in a downdraft gasifier with a focus on the tar cracking chemical mechanism. Air is used as the oxidizer for the pyrolysis gas and RNG $\kappa$ - $\epsilon$ turbulent model is used in order to both compromise accuracy and efficiency. The results were compared with the experimental data and found to agree satisfactorily. Cerutti et al. [41] studied the extraction of vegetable oils using fixed bed columns experimentally and numerically. When solving numerically, the total oil mass extracted showed a maximum error of 20% compared to the experimental data. The numerical model used a non-dimensional transient model for the mass transfer and the governing equations were solved using the finite volume method. Hallett et al. [42] studied the effect of using non-uniform particle size of the fuel in fixed bed combustion/gasification.

Yoon et al. [32] studied moving bed(countercurrent) gasifiers using a steady state homogeneous model. The model was compared with a commercial Lurgi pressurized gasifier and slagging reactor and the agreement between the results was good. One of the major assumptions introduced in the model was that the reactor was divided into two distinct zones, namely an adiabatic core representing majority of the reactor and then a colder boundary layer surrounding the adiabatic core. There is no heat loss from the adiabatic core to the boundary layer. Only the boundary layer is affected by the heat loss to the walls. However, this has little effect on the performance of the Lurgi gasifier. Similarly, Amundson and Arri [33] performed a numerical study

on char paticle gasification in Lurgi reactor. The paper attempts to explain the working phenomenon of a counter-current gasifier in the combustion zone using a shrinking core model. The developed model was used to predict the gas composition, temperature distribution and the maximum temperature in the reactor, with distinct zones for combustion and gasification. Cho and Joseph [43] have improvised these works and included heterogeneous gas-solid temperatures. Further, a pseduo steady state assumption was made to compute the solution of the material and energy balance equation. The results were compared with plant data from Morgantown Energy Technology Center gasifier with good agreement.

**CFD modelling of fixed beds:** Numerical methods to solve basic conservation equations describing fluid flow coupled with the heat and mass transfer using computational fluid dynamics (CFD) has received significant attention in the recent years.*e.g.* see review by Dixon et al. [44] CFD has also attracted considerable attention in the recent years CFD modelling enables study of the system without any external changes to the system. In case of experimental studies, the observer or the researcher changes the system to an extent to study the system and hence, the results are not completely inherent of the system.Also, CFD methods save considerable amount of time, labor and capital costs which are inherently present during the study of pilot scale plants.

**1D:** DeLemos [45] presented one-dimensional numerical model to simulate the combustion of air and methane in a porous media. Four different thermo-mechanical models were tried out in this study. The results differed considerably based on the model used for the numerical simulations. The laminar combusting flow with radiation model was further studied by Coutinho and de Lemos [46]. This group has also worked upon the numerical model of turbulent combusting flow in inert porous media[47] and in moving beds[48]. Pivem and de Lemos [49] from the same group extensively studied the effect of physical properties such as Reynolds number, porosity, thermal conductivity and various other factors using numerical simulations in a crossflow moving thermal bed.

**2D:** Behnam et al. [50] attempted to study the radial heat transfer in fixed beds using a 3D velocity fields from CFD simulations. The information from the simulations was used to extract a 2-D temperature field which was then compared to a 2D pseudo-continuum model. Chen et al. [51] developed a comprehensive 2D heterogeneous CFD reactor model for the catalytic dehydrogenation reaction of syngas

over a supported metal catalyst. Similarly, Xi Gao and hong Luo [52] studied the catalytic coupling reaction of carbon monoxide(CO) – diethyloxalate(DEO) in a fixed-bed reactor. Here, an exponent-function reaction kinetic model was used to study the flow characteritics and the coupling reaction in the fixed bed reactor.

The convetional Ergun equation fails to take into account the effect of particle size and this was proved by Keyser et al. [53]. They used CFD to study the effect of particle size on the pressure drop within a fixed bed. Using an experimental setup, pressure drop measurements were made across beds with the same average particle size, particle sphericity and bed voidage but different particle size distribution(PSD). It was found that the pressure drop across the beds were different though the Ergun equation suggested the same pressure drop. This group suggested a novel method to simulate the coal particles in a fixed bed using the mathematical procedure called the Voronoi tessellation. By this method, a 3-dimensional computational space is sub-divided into randomised convex polyhedra. Each of these polyhedra represented a single coal particle. The polyhedra were further modified to accomodate the average sphericity and the overall bed voidage by translating and squashing each of the polyhedra in a single direction. Meshing of the geometry involved fitting of a cubical mesh into the void spaces between the polyhedra. It was observed that a lower PSD results in a lower pressure drop across the bed, with all other properties remaining the same. Also, the glas flow rates was found to be higher than the inlet superficial velocity for some channels, while it was quite low or almost zero(stagnant) for some channels.

**3D:** Freund et al. [54] studied the three-dimensional (3D) flow field and local concentration in a randomly packed isothermal bed applying Lattice-Boltzmann method, where a first-order reaction on the solid surface was implemented. Dixon et al. [55] investigated the flow in a $120^o$ segment of a packed tube taking into account intraparticle reactions and gradients for the steam reforming process. Nijemeisland and Dixon [56] used CFD simulations to study the flow and heat transfer properties through a packed bed of solid spheres. The RNG $\kappa$ - $\epsilon$ model was used to employ turbulent conditions in this study. Augier et al. [57] studied the transport and transfer properties in packed beds consisting of spherical particles using CFD simulations. They also developed a dense packed model using Discrete Element Method to study the real granular media.

Logtenberg et al. [58] studied the fluid flow and heat transfer characteristics in packed bed reactor where the reactor was represented with a finite element model consisting of 10 spheres with a tube-to-particle diamater ratio of 2.43. The Reynolds

number was varied from $Re$ = 42 - 3344 and the veclocity vector profiles near the wall-particle contact points were observed. The studies were made for both a wall-heated and wall-cooled bed. However, this study doesn't take into account the chemistry in the reactors. Cooper and Hallett [59] developed a heterogenous numerical model for studying fixed bed combustion. They tried to incorporate the oxidation of CO in the gas-phase, axial heat conduction in the solid and gas phase as well as the effects of ash and grate. Nijemeisland and Dixon [17] successfully compared the flow and heat transfer characteristics in a fixed bed consisting of 44 spheres with a tube-to-particle diameter ratio of 2 using both CFD simulations and experiments.

Taskin et al. [4] compared the wall segment model with the complete wall full-bed model of a fixed bed reactor with cylindrical packing to enable reduced computational load for future studies. The wall segment(WS) model is represented as a 120° segment of the complete wall(WS) model. However, they only considered only the momentum and energy conservation equations in both the cases. The $\kappa - \epsilon$ turbulent scheme with RNG model was considered in this model. The overall bed voidage in both the cases was kept at 0.5. The agreement between the radial profiles of temperature and axial velocity was found to be good at overall 120° section and central 60° sections(better agreement).

**Motivation:** The majority of CFD modeling is dedicated to the fluid flow in the void space and the interphase heat transfer. There has been very little work to study the flow and heat transfer characteristics of chemically reacting carbon particles in a packed bed. Recently, Schulze et al. [60, 61] carried out comprehensive three dimensional numerical studies of chemically reacting char particles in a fixed bed coal gasifier using 3D representative column consisting of random packed particles.

There has been very little to negligible work on the numerical study of chemically reacting particles in dense particulate media, including flow dynamics, energy and species characteristics to study processes inside of combustion and gasification zones. However, 3D CFD simulations involving these three governing equations require lot of processing time and computational power. Keeping this in mind, we aim to develop a 2D axisymmetric geometry derived from a 3D row of particles to study conditions similar to a fixed bed/fluidized bed reactor.

# Chapter 2

# Development of a 2D model to approximate 3D structured packed beds

Coal in fixed beds have been used for combustion and gasification to produce syn-gas for more efficient power generation using gasifiers. Hence, information about the temperature and species concentration(solid and gas species) inside chemically reacting fixed bed is of utmost interest. These studies can be used to further improve the efficiency and output of a fixed bed gasifier. In this view, modelling of dense particulate media to study fixed beds could help in understanding and optimization of the combustion and gasification process. As a part of this process, selection of an effective numerical model is quintessential for this task. Hobbs et al. [62] provided an extensive review of study on the numerical modelling of fixed bed combustion and gasification processes. This paper identified 37 models out of which 5 are 0-D models, 27 are 1-D models, and only 4 are 2-D models. The 1D models are able to predict only axial profiles of basic parametrers. However, 1D models fail to predict flame location and temperature differences between the solid and gas phase in the entrance region of the fixed bed. Moreover, 1D models need more assumptions referring to heat and mass transfer submodels characterising particle-gas interactions [63, 64, 59]. 1-D numerical modelling of fixed bed gasifiers by researchers, Yoon et al. [32], Amundson and Arri [33], Hobbs et al. [35] assume an uniform gas/solid plug flow in the reactor and the gas temperature is kept equal to the temperature of the solid phase. However, the transport equations for both phases(gas and solid) and the gas phase chemical kinetics have been neglected in these studies.

Numerical methods to solve basic conservation equations describing fluid flow coupled with the heat and mass transfer using computational fluid dynamics (CFD) has received significant attention in the recent years.e.g. see review by Dixon et al. [44] Augier et al. [57] studied the transport and transfer properties in packed beds consisting of spherical particles using CFD simulations. They also developed a dense packed model using Discrete Element Method to study the real granular media. However, the majority of CFD modeling is dedicated to the fluid flow in the void space and the interphase heat transfer. There has been very little work to study the flow and heat transfer characteristics of chemically reacting carbon particles in a packed bed. Freund et al. [54] studied the three-dimensional (3D) flow field and local concentration in a randomly packed isothermal bed applying Lattice-Boltzmann method, where a first-order reaction on the solid surface was implemented. Dixon et al. [55] investigated the flow in a 120 segment of a packed tube taking into account intraparticle reactions and gradients for the steam reforming process. Recently, Schulze et al.[60, 61] carried out comprehensive three dimensional numerical studies of chemically reacting char particles in a fixed bed coal gasifier using 3D representative column consisting of random packed particles.

However, these studies are computationally very expensive and time consuming. Wehinger et al.[65] carried out 3D detailed simulations of fixed beds for the catalytic dry reforming of methane consisting of 113 spherical solid particles taking into account heat conduction inside the particles. Detailed surface mechanism for the dry reforming of methane including 42 chemical reactions was utilized. The computational grid used in simulations comprises of 3.2 millions cells leading to more than 100 days which were necessary to complete simulations.

Analysis of the literature shows that 2D models describing mesoscale (several particles) processes in a fixed bed are rare[34, 66, 67]. These models are unable to predict velocity distribution between particles within the bed. Motivated by this fact, we approximate a 3-D model of a fixed bed of particles into a 2-D asymmetric model to understand flow dynamics and heat transfer characteristics of gas phase as well as heterogenous and homogeneous kinetics, with the advantage of less processing time and resources.

## 2.1 Model Formulation

We preferred a structured cubic(SC) packing for the 3D arrangement of particles in the packed bed with a porosity of $\sim$0.48, due to their low pressure drops and high overall heat transfer efficiency[68]. It should be noted that the porosity of SC packing

is closer to randomly packed fixed beds consisting of monodisperse particles[69] in comparison to FCC($\epsilon = 0.26$). In the present study, a row of spherical coal char particles with a radius of $\mathbf{r_p = 10mm}$ are placed in a stationery position in a hot environment. The velocity of the inlet gas is measured in terms of the Reynolds number given by:

$$Re = \frac{\rho_{in}\, u_{in}\, d_p}{\mu_{in}} \tag{2.1}$$

where $\rho_\infty$ and $\mu_\infty$ are the density and molecular viscosity, respectively, corresponding to the inflow temperature $T_{in}$ and the gas composition. The inlet gas composition was considered to be '*dry air*', where $Y_{O_2} = 0.233$ and $Y_{H_2O} = 0.001$. All calculations are accomplished at a total pressure of 1 bar.

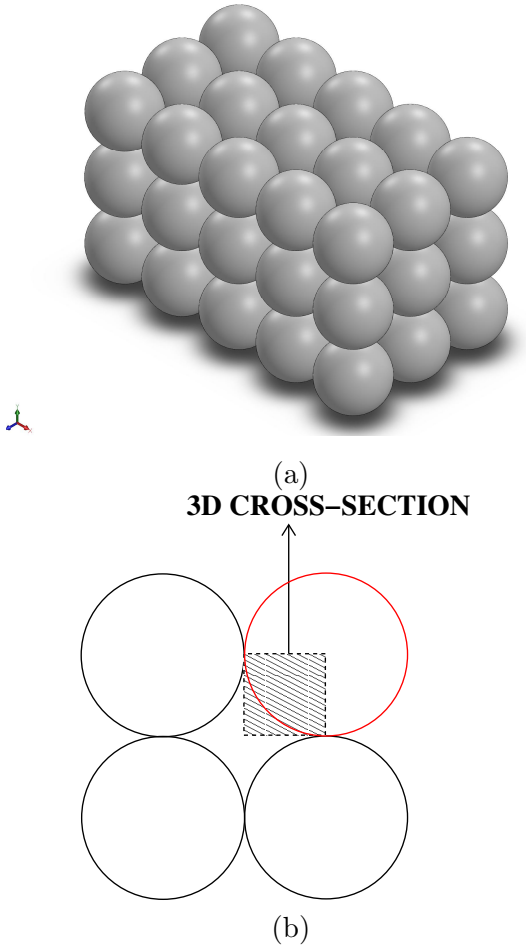


Figure 2.1: (a) 3-D representation of the fixed bed with SC packing, (b) 3-D cross section of the fixed bed highlighting the computational domain;

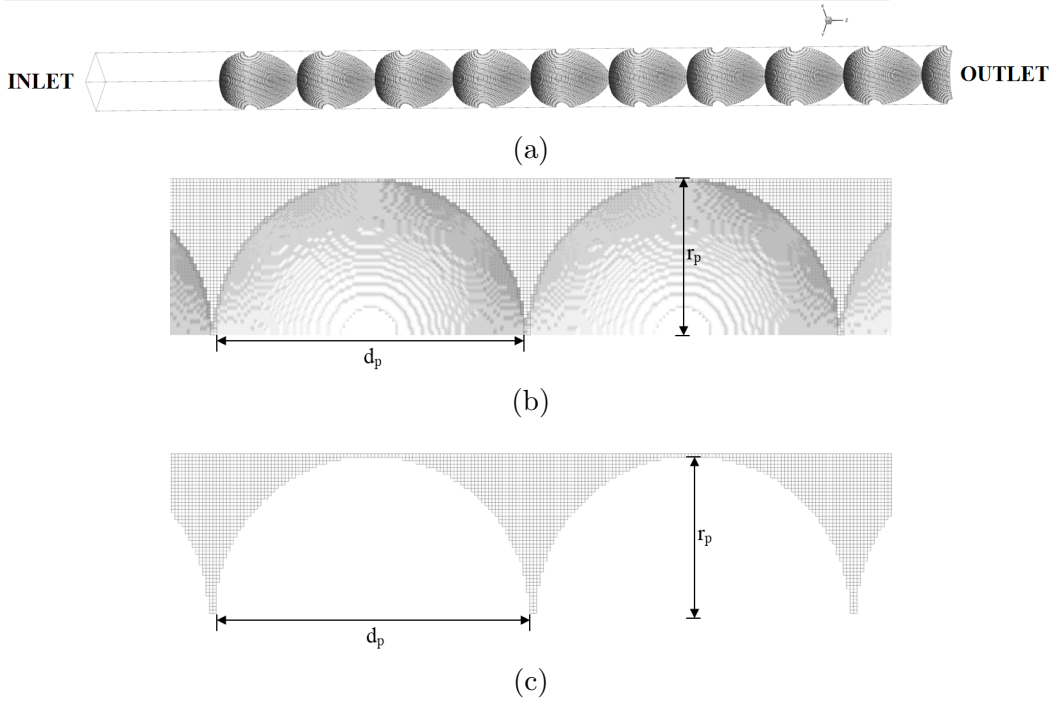


Figure 2.2: (a) Schematic representing the 3D domain, (b) Zoomed view of the meshed 3-D domain showcasing the stair-case mesh structure, (c) Cut section view of the 3-D mesh;

A fixed bed row of particles is illustrated in Fig.2.1(a). A cross-sectional view of this 3-D figure is represented in Fig. 2.1(b). The highlighted part in this section is considered for the 3D geometry, which covers $\frac{1}{4}^{th}$ of the entire sphere. The flow rate for this highlighted part is:

$$\dot{m} = \rho_\infty \cdot \left( r_p^2 - \frac{\pi r_p^2}{4} \right) \cdot u_\infty \tag{2.2}$$

The highlighted section arranged, in a row, one behind the other gives us the 3-D computational domain, as shown in Fig. 2.2(a). The meshed 3-D domain is shown in Fig.2.2(b) with the cut-section view of the mesh illustrated in Fig.2.2(c). The first step of the 2-D approximation is the assumption of a cylidrical representative element, as shown in Fig.2.3(b). A cross-sectional view has been shown in Fig.2.3(a). The second step in the approximation involves the conversion of the cylindrical element into an axysymmetric 2-D geometry, as shown in Fig.2.3(c).

The principle behind the approximated 2D geometry from the 3D domain is that the flow rate remains the same between the 3-D and 2-D models, though the cross-

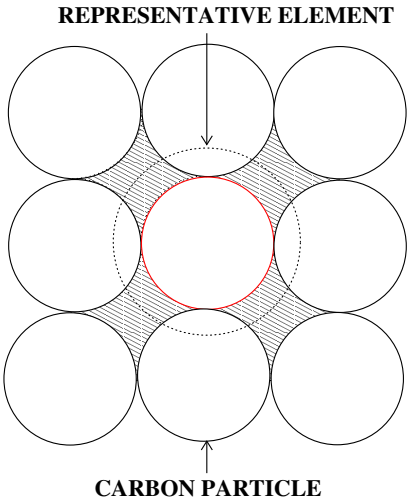


(a)

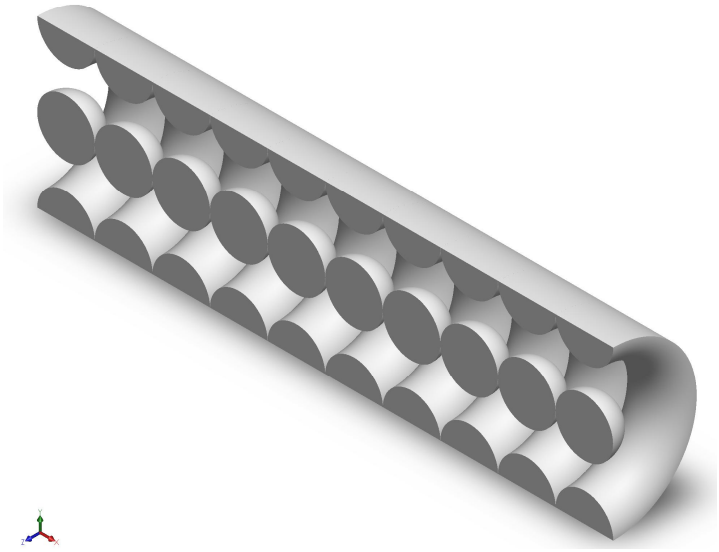

(b)

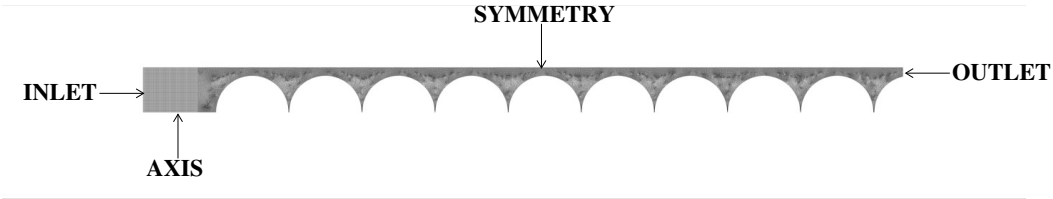


(c)

Figure 2.3: (a) Cross-sectional view of the 3-D domain illustrating the representative element, (b) 3-D isometric view of the representative element, (c) Schematic of the 2-D axisymmetric geomtery of the representative element

sections may be different. The radius of the 2D cylindrical representative element is then calculated to be $1.4467r_p$.

$$\begin{aligned} 4(4r_p^2 - \pi(r_p)^2) &= \pi(r_x^2 - r_p^2) \\ \implies r_x^2 &= \frac{16}{\pi} r_p^2 - 3r_p^2 \\ \implies r_x^2 &= \left(\frac{16}{\pi} - 3\right) r_p^2 \\ \implies r_x &= 1.4467 r_p \end{aligned} \tag{2.3}$$

Using the above radius, we find the radius of the width of the inlet of the 2-D configuration as,

$$\begin{aligned} r_{in} &= \frac{r_x - r_p}{2} + r_p \\ \implies r_{in} &= \frac{1.4467r_p - r_p}{2} + r_p \\ \implies r_{in} &= 1.2234 r_p \end{aligned} \tag{2.4}$$

The surface area of the 3-D geometry by the stair-step meshing method is found to be higher than that of a sphere($4\pi r^2$) by a factor of 1.5 [2]. The ratio of the 2D domain was calculated to be 0.55 which was found to be $\sim$ 15 % higher than the 3D structured packing.

The flow rate of the 3-D cross section taken into consideration for the simulations is given by,

$$\dot{m}_{in} = \rho \cdot U_{in} \cdot S_{in} \tag{2.5}$$

where $S_{in} = r_p^2$ is the inflow cross-sectional area. The total 3-D cross-sectional area is

$$\dot{m}_{\in} = 16 \cdot \dot{m}_{in} \tag{2.6}$$

The 2-D cross-sectional velocity,$u_0$ can then be calculated as,

$$u_0 = \frac{\dot{m}_{\in}}{\rho \cdot S_0} \tag{2.7}$$

where $S_0 = \pi \cdot r_x^2$ is the cross-sectional area of the 2-D geometry.

The representative element highlighted by the dotted lines is shown in Fig. 2.3(a). The 3D and 2D models are then compared in terms of velocity, temperature and mass fraction of $CO_2$ along the symmetrical edge. The inflow temperature is kept at 1000 K. Three different values of Reynolds number are considered for the simulations : $Re = 10, 50$ and 100.

### 2.1.1 Chemistry

The model takes into consideration six gaseous chemical species namely, $O_2$, CO, $CO_2$, $H_2$, $H_2O$, and $N_2$. The chemistry is modeled using semi-global homogeneous and heterogeneous reactions as mentioned below [70]:

*heterogeneous* (surface) reactions:

$$C + \frac{1}{2}O_2 \rightarrow CO \tag{R1}$$

$$C + O_2 \rightarrow CO_2 \tag{R2}$$

$$C + CO_2 \rightarrow 2CO \tag{R3}$$

$$C + H_2O \rightarrow CO + H_2 \tag{R4}$$

*homogeneous* (gas phase) reactions:

$$CO + \frac{1}{2}O_2 + H_2O \rightarrow CO_2 + H_2O \tag{R5}$$

$$CO + H_2O \rightarrow CO_2 + H_2 \tag{R6}$$

$$CO_2 + H_2 \rightarrow CO + H_2O \tag{R7}$$

The rate and kinetics of these reactions are provided in Table 2.1.1. The kinetics of reaction.R7 was calculated simultaneously with reaction.R6 using thermodynamic equilibrium. It should be noted that these semi-global heterogeneous and homogeneous chemical reactions are widely used to model industrial combustors or gasifiers using computational fluid dynamics software, e.g. see [71]. However at the same time, it is a well-known fact that global reaction rates are often only valid in a narrow range of conditions and should be used very cautiously.

| Reaction No. | $A_r$ | $n_T$ | $E_A(J/kmol)$ | Refs |
|---|---|---|---|---|
| R1 | $3.007 \times 10^5\,\mathrm{m\ s^{-1}}$ | 0 | $1.4937 \times 10^8$ | [72] |
| R2 | $593.83\,\mathrm{m\ s^{-1}\ K^{-1}}$ | 0 | $1.4965 \times 10^8$ | [72] |
| R3 | $4.605\,\mathrm{m\ s^{-1}K^{-1}}$ | 1 | $1.751 \times 10^8$ | [73] |
| R4 | $11.25\,\mathrm{m\ s^{-1}\ K^{-1}}$ | 1 | $1.751 \times 10^8$ | [73] |
| R5 | $2.24 \times 10^{12}\,\mathrm{m^{2.25}\ kmol^{-0.75}s^{-1}}$ | 0 | $1.6736 \times 10^8$ | [70] |
| R6 | $2.75 \times 10^9\,\mathrm{m^3kmol^{-1}s^{-1}}$ | 0 | $8.368 \times 10^7$ | [74] |
| R7 | $9.98 \times 10^{10}\,\mathrm{m^3kmol^{-1}s^{-1}}$ | 0 | $1.205 \times 10^8$ | – |

Table 2.1: Kinetic coefficients for the chemical reactions; (*Gasification Processes: Modeling and Simulation*)[2]

### 2.1.2 Assumptions and Governing Equations

Several assumptions are introduced in order to solve the mathematical CFD-based model.

1. The consumption time of the particle is always large compared to the convective and diffusion time scales for the gas phase. Hence, Pseudo-Steady-State(PSS) approach has been assumed,(refer [75, 76]).
    - Further discussions on PSS can be found in works of Higuera [77], Safronov et al. [76] and Kestel et al. [78].
2. The gas flow was treated as an incompressible ideal gas.
3. The representative element is considered to be axysymmetrical with a symmetrical gasflow.
4. The porosity of the particles is not taken into account which results in neglecting the intraparticle diffusion. The surface reaction model is used to simulate the interaction between reacting solid surface and gas phase.
5. The particles consists of carbon only. In particular, the volatilization of the particles is not included due to the steady-state character of the model.
6. The radiation of the gas phase is modeled using the P-1 model.
7. The buoyancy effect is neglected.

These assumptions facilitate the formulation of governing equations for the model. The mass and momentum conservation equations take the following form, refer [2]:

$$\nabla \cdot (\rho \, \vec{u}) = 0 \tag{2.8}$$

$$\nabla \cdot (\rho \, \vec{u} \otimes \vec{u}) = -\nabla p + \nabla \cdot (\bar{\bar{\tau}}) \tag{2.9}$$

where $\rho$ is the density, p is the pressure, and $\vec{u} = (u_x, u_r)^T$ is the velocity vector. In eq. 2.9 $\otimes$ denotes the dyadic product of two vectors. The density of an incompressible ideal gas is given by

$$\rho = \frac{P}{R_g T \sum_i \frac{Y_i}{M_i}} \tag{2.10}$$

The stress tensor, $\bar{\bar{\tau}}$ is comprised of

$$\bar{\bar{\tau}} = \eta \left\{ [\nabla \vec{u} + (\nabla \vec{u})^T] - \frac{2}{3} \nabla \cdot \vec{u} \right\} \tag{2.11}$$

where $\eta$ represents the molecular viscosity.

The species and energy conservation equations are represented by the following equations respectively,

$$\nabla \cdot (\rho \, \vec{u} \, Y_i) = \nabla \cdot (\rho \, D_i \, \nabla Y_i) + R_i \tag{2.12}$$

$$\nabla \cdot (\rho \, \vec{u} \, h) = \nabla \cdot (\lambda \nabla T - \vec{q_r}) - \sum_i \frac{h_i^0}{M_i} R_i \tag{2.13}$$

where $i$ represents each of the participating reactants $O_2$, $CO_2$, $CO$, $H_2$ and $H_2O$. $Y$ is the mass fraction and $D$ is the mass diffusion coefficient of the species. The mass fraction for $N_2$ is calculated as $Y_{N2} = 1 - \sum_i Y_i$. $h$ is the enthalpy, $h^0$ is the enthalpy of formation and $M$ is the molecular weight of the species while $\vec{q_r}$ stands for the gas-phase radiation source. The P-1 radiation model requires the solution of an additional transport equation for the incident radiation term $G$ as shown below, [1],

$$\nabla \cdot \left( \frac{\nabla G}{3\alpha} \right) - \alpha G + 4\alpha n^2 \sigma T^4 = 0 \tag{2.14}$$

The species net production rate $R_i$ is computed as the sum of the Arrhenius reaction sources over $r = N_R$ reactions in which the species are involved,

$$R_i = M_i \sum_r^{N_R} \widehat{R}_{i,r} \tag{2.15}$$

Here the Arrhenius molar rate of creation/destruction $\widehat{R}_{i,r}$ is calculated as

$$\widehat{R}_{i,r} = \left( \nu''_{i,r} - \nu'_{i,r} \right) \left( k_r \prod_{j=1}^{N} [C_{j,r}]^{\left( \eta'_{j,r} - \eta''_{j,r} \right)} \right) \tag{2.16}$$

for a homogeneous reaction, where $\nu'_{i,r}$ is the stoichiometric coefficientfor reactant $i$ in reaction $r$ and $\nu''_{i,r}$ is the stoichiometric coefficient for product $i$ in reaction $r$. $\eta'_{j,r}$ and $\eta''_{j,r}$ are the forward and backward rate exponents for each reactant and product species $j$ in reaction $r$.

## 2.2 Boundary Conditions

The governing equations can be solved provided that boundary conditions are specified at the inlet and outlet boundary as well as at the symmetry axis and the upper side of the computational domain. We use the Neumann boundary conditions for the symmetry axis as well as the upper side, which can be expressed in the form as follows:

$$\frac{\partial p}{\partial r} = 0,\ \frac{\partial \vec{u}}{\partial r} = 0,\ \frac{\partial Y_i}{\partial r} = 0,\ \frac{\partial T}{\partial r} = 0 \tag{2.17}$$

The values for the gas velocity, masss fractions and temperature at the inlet boundary are given by:

$$\vec{u} = \vec{u_{in}},\ Y_i = Y_{i,\text{in}}, T = T_{\text{in}} \tag{2.18}$$

This is also a convenient way to input our study pre-requisites such as the Reynolds number or the inlet temperature. We use the outflow boundary condition with an overall mass balance correction at the outlet boundary(see [79]). We know that there is a "no-slip" boundary condition on a chemically non-reacting solid surface implying that the fluid velocity at the solid wall is zero. But, if there is a heteregenous chemical reaction occuring at the solid surface, the velocity in the normal direction from the surface can be non-zero. This flow which is induced by heteregenous reactions at the surface is called Stefan flow and is represented by the following form(see [2]):

$$\mathbf{n} \cdot \vec{u} = \frac{\dot{m}_C''}{\rho} \tag{2.19}$$

Our system consists of heterogeneous reactions which affects mass and energy balance at the interface between the particle surface and the gas phase. Hence, there is a significant influence by the heterogeneous raeactions on the boundary conditions for the gas species and the temperature. At the surface, the convective and diffusive mass fluxes of the gas-phase species are balanced by the production/destruction rates of the gas-phase by surface reaction as described by the Reactions(R1 - R4)(refer to [80]).

$$\rho_{\mathrm{s}} D_{i,\mathrm{m}} \frac{\partial Y_{i,\mathrm{s}}}{\partial n} - \dot{m}_C^{''} Y_{i,\mathrm{s}} = \underbrace{M_i \hat{R}_{i,\mathrm{s}}}_{heterog.reac.} \quad ; \tag{2.20}$$

$$\dot{m}_c'' = \sum_i M_i \hat{R}_{i,\mathrm{s}} \tag{2.21}$$

$$\mathbf{n} \cdot \lambda \nabla T|_{solid} - \mathbf{n} \cdot \lambda \nabla T|_{gas} = \underbrace{\sum_r \Delta_R H_{r,j} R_{r,j,s}}_{heterog.reac.} + \underbrace{\epsilon_{\mathrm{s}} \sigma (T_{\mathrm{s}}^4 - T_{\mathrm{in}}^4)}_{radiation} \tag{2.22}$$

$$\tag{2.23}$$

where $R_{j,\mathrm{s}}$ is the production rate of species $j$ due to the surface reaction $r$, $\dot{m}_C^{''}$ is the net mass flux between the surface and the gas in kilogram per square meter per second, the index "gas" refers to the gas side at the wall and $\mathbf{n}$ is the vector normal to the wall. $\epsilon_{\mathrm{s}}$ stands for the emissivity of the particle surface($\epsilon_{\mathrm{s}} \approx 1.0$ for solid carbon).

NOTE: These boundary conditions are valid for all steady and transient cases of the numerical model(refer,[80]).

The commercial software, ANSYS® Fluent™14.0[1] was used to solve the governing equations combined with the boundary conditions. A semi-implicit(SIMPLE) scheme was used for pressure-linked equations during the pressure-velocity coupling. Next, the discretization scheme used for convective terms in all the equations is called quadratic upstream interpolation for convectice kinematics or QUICK scheme. The under-relaxation factors for the species and energy were kept at 0.5 at the start and then were gradually increased as the simulations progressed on. Due to the strong couling between the species and energy conservation equations, the under-relaxation factors were $T$ and $Y_i$ were set to 9.0. When the maximum normalized residuals for all equations were $< 10^{-9}$ and a constant surface deposition rate of solid carbon was obtained for the species. the convergence iterations were considered to be converged and stopped.

### 2.2.1 Numerical Software and Validation

Mesh generation of the 3D and 2D geomtery is performed in Gambit and Fluent v14.0 is used for the numerical simulations. The conservation of mass( 2.8), momentum( 2.9), energy( 2.13) and species( 2.12) is applied at the particle surface. The effect of the Stefan flow and the heat loss due to radiation are also included in the problem set-up. Mathematical formulation of all boundary conditions including heterogeneous reactions and P1-radiation model can be found in works [81, 76].

The kinetic coefficients $k_r$ of chemical reactions (R1) through (R7) are calculated using the extended Arrhenius expression[2],

$$k_r = A_r \, T_S^{n_T} \, exp^{\frac{-E_A}{R T_S}} \tag{2.24}$$

where $A_r$ is the pre-exponential factor, $n_T$ is the temperature exponent, and $E_A$ is the activation energy. The values for $A_r$, $n_T$ and and $E_A$ with corresponding units are given in Table 2.1.1. Notice that the CO oxidation-reaction order (reaction R5) is not related to the stoichiometry of the reaction due to the global character of this reaction. It should also be noted that the reaction C + $2H_2$ is not included in considerations because the rate of reaction is much lower than those of the other heterogeneous reactions. The model and software validation applied to modeling of chemically reacting carbon particles have been published in following works:

- [76] - validation against analytical two-film model (the influence of the Stefan flow has been illustrated numerically),
- [81] - validation against Bejarano & Levendis experiment Bejarano and Levendis [82],
- [78, 83] - validation against Makino et al experiment [84].

Applied to 3D simulations carried out in this work the final Cartesian grid consists of $1.2 \cdot 10^6$ control volumes (CV), see Fig. 2.2c. A stair-step meshing method was utilized. It should be noted that the use of stair-step approximation of a sphere leads to the increase in surface area by a factor 1.5, for details see [85].

Final grid for 2D simulations comprises of $46 \cdot 10^3$ control volumes, see Fig.2.3c. This resolution was chosen based on the grid study perfomed for three diferent grids with $13 \cdot 10^3$ CV, $46 \cdot 10^3$ CV and $113 \cdot 10^3$ CV, respectively.

### 2.2.2 Effect of P1- Radiation model

The effect of P-1 radiation model has been performed in our study during combustion and gasification. However, we wanted to independently study the P-1 radiation model with prime focus upon the geometry of the channel. This helps validate the results during the case of combustion and gasification.

The P-1 radiation model is considered to be the most basic form of the P-N model. The radiation flux can be given by the following equation, refer [79]:

$$q_r = -\frac{1}{3(a + \sigma_s) - C\sigma_s} \nabla G \tag{2.25}$$

where $a$ is the absorption coefficient, $\sigma_s$ is the scattering coefficient, $G$ is the incident radiation, $C$ is the linear-anisotropic phase function coefficient. This equation can be simplified by using a parameter, $\Gamma$:

$$\Gamma = \frac{1}{3(a+\sigma_s) - C\sigma_s} \tag{2.26}$$

Thus, Eq. 2.25 can be written as,

$$q_r = -\Gamma \nabla G \tag{2.27}$$

We also write the transport equation for the incident radiation, $G$ as

$$\nabla \cdot (\Gamma \nabla G) - aG + 4a\sigma T^4 = S_G \tag{2.28}$$

where $\sigma$ is the Stefan-Boltzmann constant and $S_G$ is a radiation source defined by the user. Combining Eq. 2.27 and Eq. 2.28, we obtain the following equation

$$-\nabla \cdot q_r = aG - 4a\sigma T^4 \tag{2.29}$$

The above equation is used by FLUENT to account for the heat sources due to radiation. The absorption coefficient for the gas radiation is calculated by the use of the cell-based Weighted-Sum-of-Gray-Gases Model [79, 86].

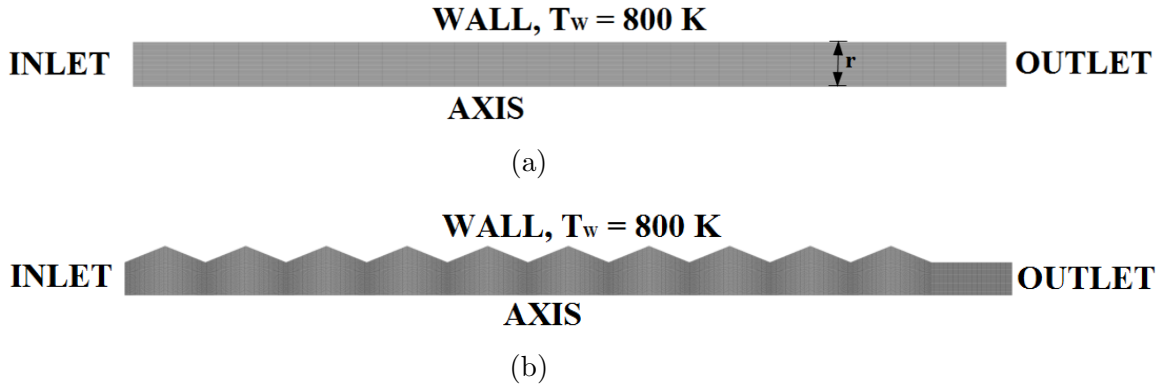


Figure 2.4: Meshed domain used for the (a) simple axisymmetric geometry, (b) complex axisymmetric geometry

We made a geometry-based study of P-1 radiation model and wsggm-cell based model using a tube-shaped geometry for a simple and complex domain represented by 2-D axisymmetric geometry as shown in Fig2.4(a) and (b) respectively. The radius of the tube was taken as 1 cm and the length of the tube was taken as 2 m. The

temperature at the inlet was taken as 1000K and the wall temperature was maintained at 800K. The Reynolds number was kept at 50. The inlet gas composition was taken as, $Y_{CO_2} = 0.99$ and $N_2$ as the remaining constituent. Variations were made at the symmetry wall to change the shape from a simple line to a zig-zag(complex) boundary. The main motive was to gain insight into the effect of radiation in a domain with enhanced surface areas using temperature plots along the axis. Fig.2.5 and Fig.2.6 illustrate the temperature contour profiles for the simple and complex tube. From Fig.2.7, we see that the temperature along the axis for the complex tube is remains lower than the simple tube with and without radiation. This goes to prove that the high surface area of the complex geometry indeed plays a vital role in order to uniformize the temperature with the channel much faster compared to the simple tube. This can also be further proved by the following equation,

$$Q = U \cdot A \cdot \Delta T \tag{2.30}$$

where '$Q$' is the heat transferred through an area '$A$' with a heat transfer coefficient '$U$' with a temperature difference of '$\Delta T$'. As the heat transfer coefficient remains the same, a higher area would lead to a higher heat transferred for the same temperature difference. The conclusions drawn from this study motivated us to report the effect of radiation in the 2D model approximated for our study. The results will be further discussed in Section.2.4.

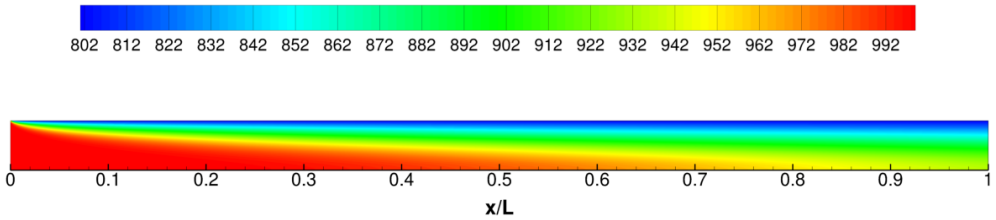


(a) No Radiation

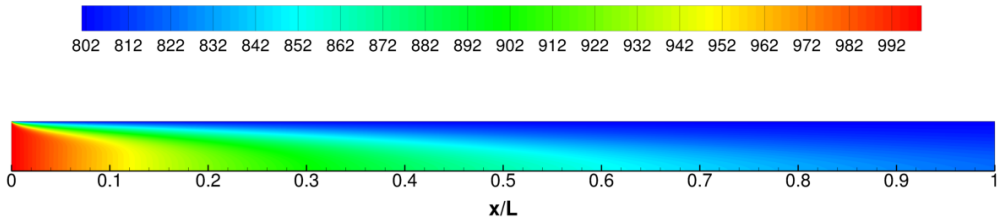


(b) Radiation

Figure 2.5: Temperature contour profile with and without radiation for a **simple** tube represented using 2D axysymmetric geometry. Inflow gas composition: $Y_{CO_2}$ = 0.99 at $T_{in}$ = 1000K

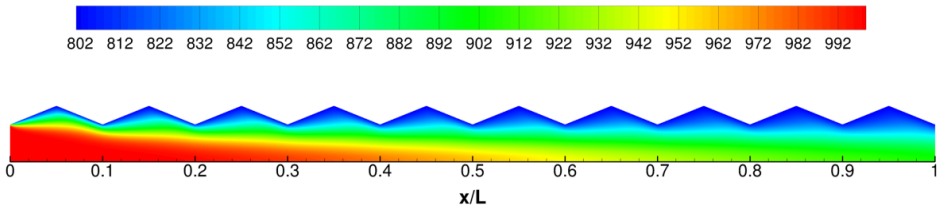


(a) No Radiation

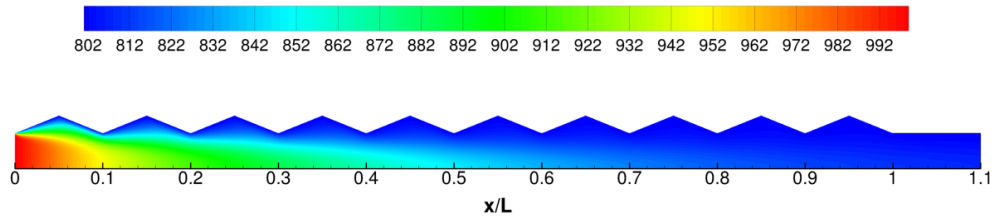


(b) Radiation

Figure 2.6: Temperature contour profile with and without radiation for a **complex** tube represented using 2D axysymmetric geometry. Inflow gas composition: $Y_{CO_2}$ = 0.99 at $T_{in}$ = 1000K

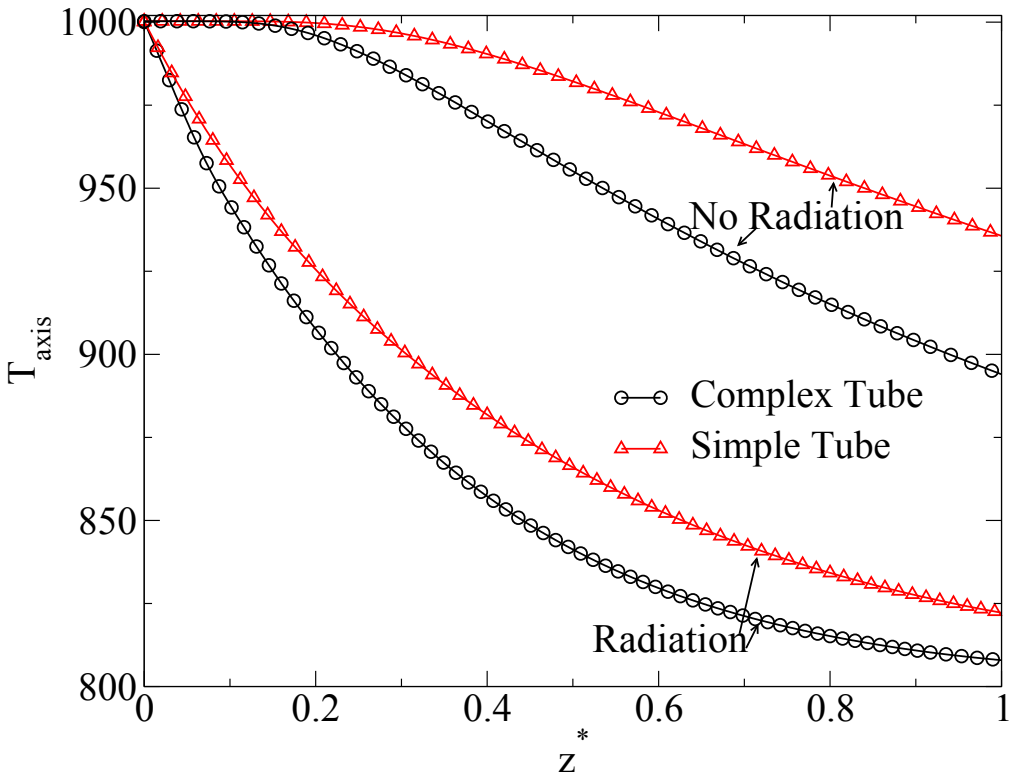


Figure 2.7: Temperature plots comparing the axial temperatures for **simple** and **complex** tubes represented using 2D axysymmetric geometry. Cases with and without radiation have been shown in the figure.

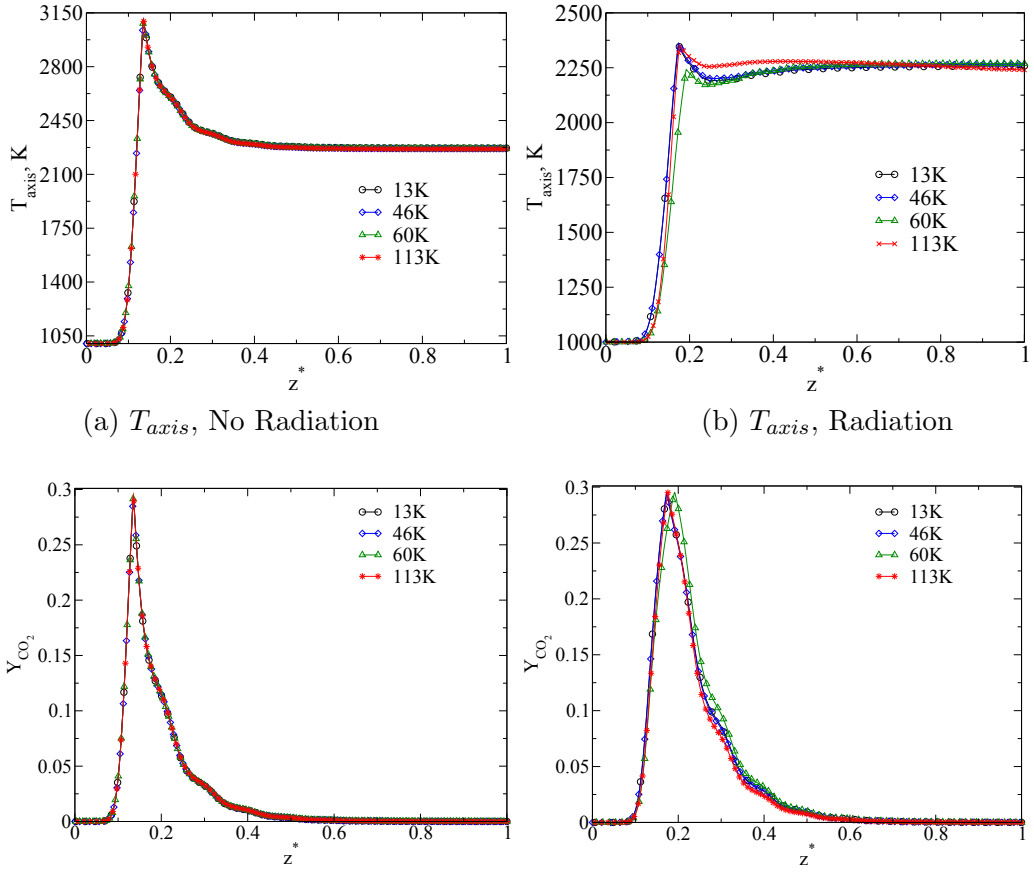


(a) $T_{axis}$, No Radiation

(b) $T_{axis}$, Radiation

(c) $Y_{CO2}$, No Radiation

(d) $Y_{CO_2}$, Radiation

Figure 2.8: Temperature and $Y_{CO_2}$ profiles for performing **grid study** for meshes of sizes: 13K, 46K, 55K, 60K, 71K and 113K. Inflow gas composition was taken as $Y_{O_2} = 0.233$ and $Y_{H_2O} = 0.001$ with $T_{in}$=1000K

### 2.2.3 Grid Study

The accuracy, convergence and numerical stability of a solution are highly dependent on the distribution and number of grid points in the geometry under consideration. The computational geometry is discretized by uniform unstructured triangular type mesh. The full grid view of the domain is shown in Fig. 2.3(c). Simulations were performed for 13k, 46k, 55k,60k, 71k and 113k number of mesh elements with and without P-1 radiation model. Temperature and $Y_{CO_2}$ along the axis were compared for these cases. It was concluded that the simulations with radiation were independent of the size of the elements for all the cases as shown in Fig.2.8(a) and (c). However, when P-1 radiation is included, we observe slightly different profiles for temperature and $Y_{CO_2}$. This was attributed to the cell-based Weighted-Sum-of-Gray-Gases Model [79, 86]. As the name suggests, this model is cell based and

hence, affects the profiles in the presence of radiation. We decided to use the mesh size of 46k, keeping in mind, the computational time required for simulations and profile variations, as seen in Fig.2.8(b) and (d).

## 2.3 RESULTS

### 2.3.1 Flame sheet formation

During combustion, the $CO_2$ diffuses through the stagnant layer and then reacts heterogenously with carbon at the particle surface to release CO. This reaction being endothermic absorbs heat from the inlet air. The CO which is produced at the surface then diffuses outward and reacts with the incoming $O_2$ to form $CO_2$ according to Reaction R5. This leads to a zone of maximum $CO_2$ similar to a flame sheet over the particle. Simultaneously, the $CO_2$ produced at the flame sheet diffuses inward to react heterogenously with the carbon particle surface through Reaction R3. Increase in the Reynolds number of the inlet gas extends the flame sheet further into the channel. This can be attributed to the fact that the increase in the Reynolds number leads to an increase in the flow rate of the inlet gas into the channel leading to an enhancement of $O_2$ in the intraparticle space. Thus, CO diffusing outwards from the particle surface reacts with the overly ample $O_2$ to produce $CO_2$ resulting in a longer flame sheet extending into the channel.

Fig.2.9 presents the $CO_2$ isosurfaces at different Reynolds number with and without radiation for the 3D model. The figures on the left represent the case without radiation while that on the right represent the case with radiation. The flame sheet is represented by the contour with the highest mass fraction of $CO_2$. As discussed before, the effect of Reynolds number, is clearly visible in this figure. The increase in Reynolds number results in an extension of flame sheet within the channel as seen in Fig2.9(a),(b) and (c). Radiation affects the flame sheet over the particle bed by elongating it over an additional particle.

### 2.3.2 Comparison of 2D and 3D model

Simulations were performed for 2D and 3D models at varying Reynolds number of 10, 50 and 100. The inlet gas composition was taken as $Y_{O_2} = 0.233$ and $Y_{H_2O} = 0.001$ with $T_{in} = 1000$K, which represents the case of combustion within fixed bed gasifiers. The P-1 radiation model was considered for this study. The results have been compared in terms of velocity($||U||$), temperature($T$), mass fraction of $CO_2$. Comparisons have also been made on the surface as well as along the axis to gain

deeper insight into the validity and robustness of the model.

Before proceeding to the comparison of parameters with combustion, we performed a cold run comparison between the 2D and 3D model to evaluate the development of velocity within the channel bed, without any heat transfer or chemical reactions. Fig. 2.10 shows the comparison of the velocity magnitude for all the cases studied. Fig. 2.10(a) illustrates the cold run case, where the species and energy equations are turned off to only study the influence of the model on the flow velocity. The inflow temperature of the gas is kept at 300K. The velocity profile within the channel, when the fluid enters the row of particles, is much higher than the inlet superficial velocity. This is contrary to the popular assumption in literature of a plug flow within the reactor bed[87, 88, 89]. The velocity profile follows a sinusoidal profile, where each peak of the curve represents the position of the center of the particle. Though the models have the same inlet flow rate, the peak velocity was observed to be slightly higher(8.33%) for the 2D model. This suggests that the model agree with each other in terms of development of fluid velocity within the fixed bed. However, the velocity increases and decreases at a slightly faster rate as it flows over the particles in the 2D model.

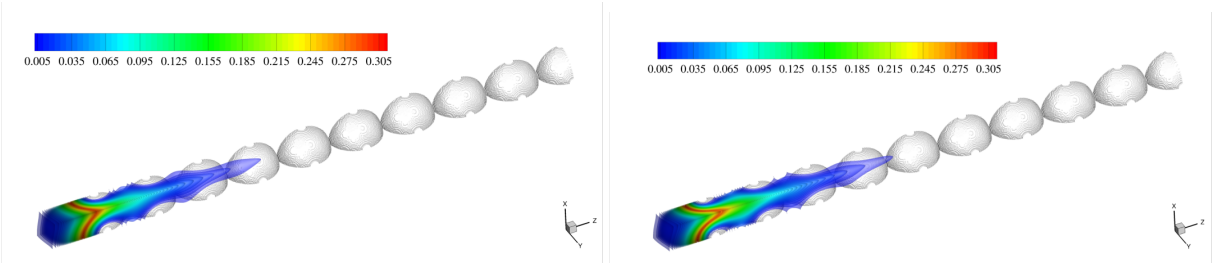


(a) Re 10

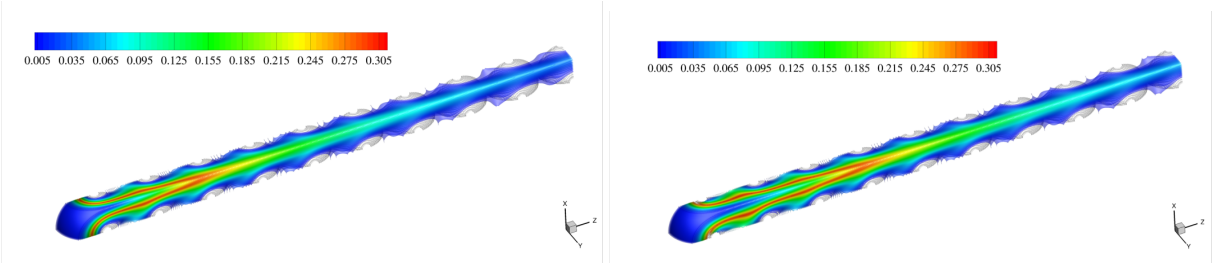


(b) Re 50

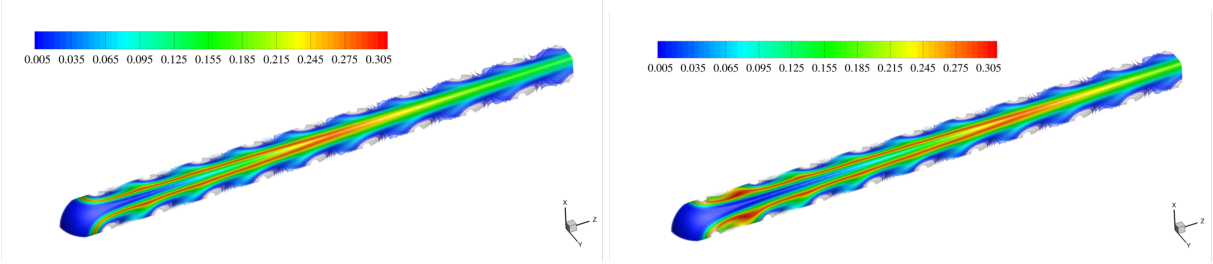


(c) Re 100

Figure 2.9: $CO_2$ isosurfaces at different *Re* depicting the effect of radiation; Figures on the *left* represent the case *without radiation* and figures on the *right* represent the case with *radiation*

The cold flow study is followed by the comparison of the velocity profiles between the two models at three different Reynolds number of 10, 50 and 100 as shown in 2.10(b), (c) and (d) respectively. The inlet gas composition was taken as $Y_{O_2} = 0.233$ and $Y_{H_2O} = 0.001$ with $T_{in}$=1000K. The peaks of the curves represent the maximum width of a particle resulting in an increase of the gas velocity. It can be concluded from Fig.2.10 that the agreement between the two models is very good.

However, the velocity gradient is higher in the 2D model between the particles, compared to the 3D case. Apart from the local fluctuations in the velocity profile of the gas phase, we also notice an increase in the average velocity profile for $Re = 50$ and 100. Combustion leads to a massive increment in the gas phase temperature, resulting in a decrease in the density and thus, an increase in the mean flow velocity.

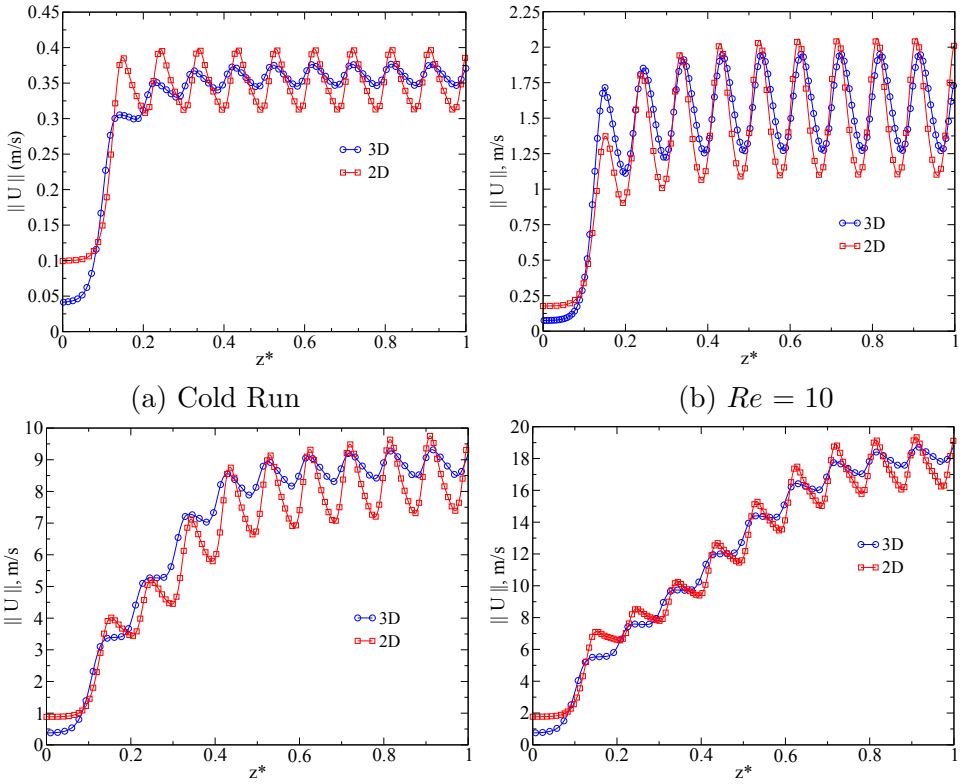


Figure 2.10: Comparison of velocity magnitude for different cases; (a) *Cold gas run* without heat transfer and chemical reactions, with $T_{in}$ = 300 K, (b) Combustion at $Re = 10$ and $T_{in} = 1000K$ (c) Combustion at $Re = 50$ and $T_{in} = 1000K$ (d) Combustion at $Re = 100$ and $T_{in} = 1000K$

Fig.2.11 represents the axial temperature as well the mass fraction of $CO_2$ along the axis for both the models at different $Re$ of 10, 50 and 100. The peak value of $Y_{CO_2} = 0.295$ in the bed remains the same for all the three cases of Reynolds number. However, increase in $Re$ results in a shift of the peak $Y_{CO_2}$ downstream of the bed channel as seen in Fig.2.11(a). This can be attributed to a higher flow rate through the channel for higher $Re$. It should be noted that the mass fraction of $CO_2$ is not zero at the outlet for $Re = 10$ but remains very low ($4 \cdot 10^{-5}$). In this case, the Boudouard reaction goes to completion ($Y_{CO} = 0.35$) and unavailability of

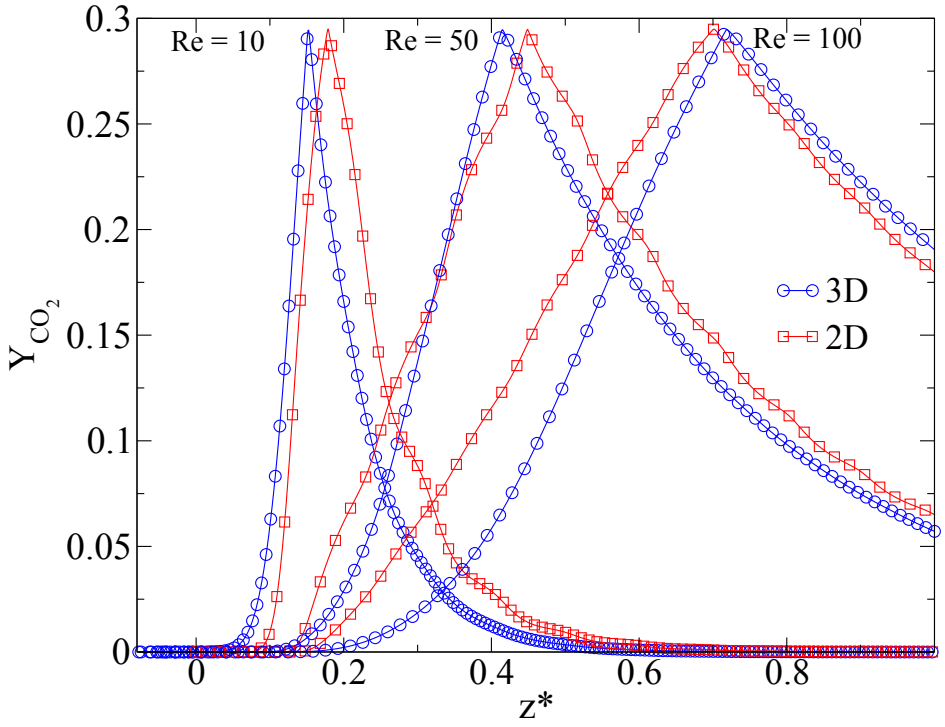


(a)

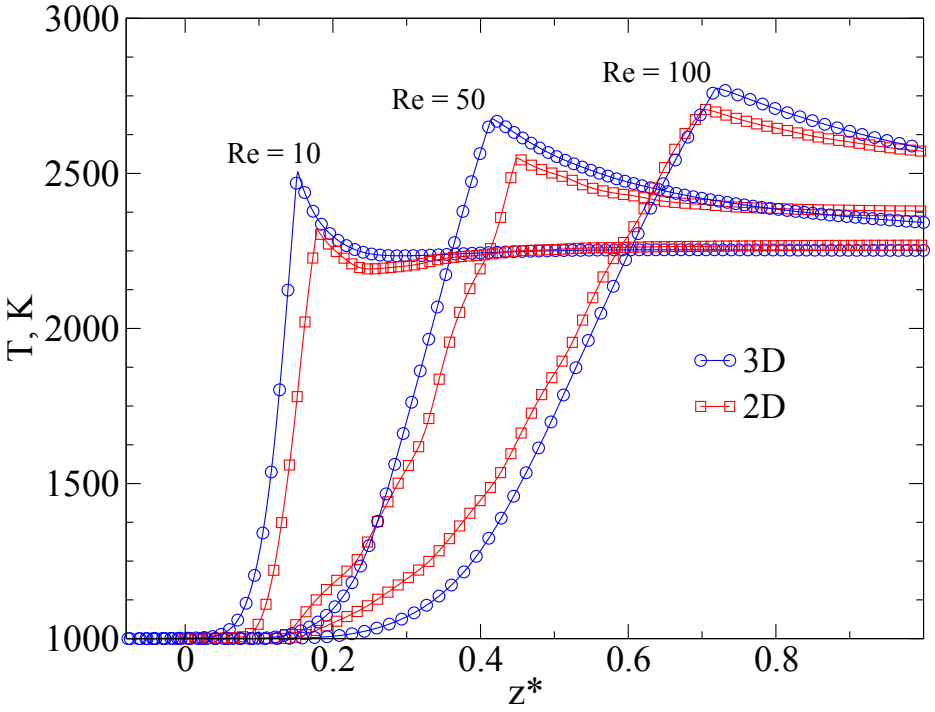


(b)

Figure 2.11: Comparison of mass fraction of $CO_2$ and temperature along the **axis** between the 2D and 3D models for $Re$ = 10, 50 and 100; Inflow gas composition was taken as $Y_{O_2}$ = 0.233 and $Y_{H_2O}$ = 0.001 with $T_{in}$=1000K; P-1 radiation model was included.

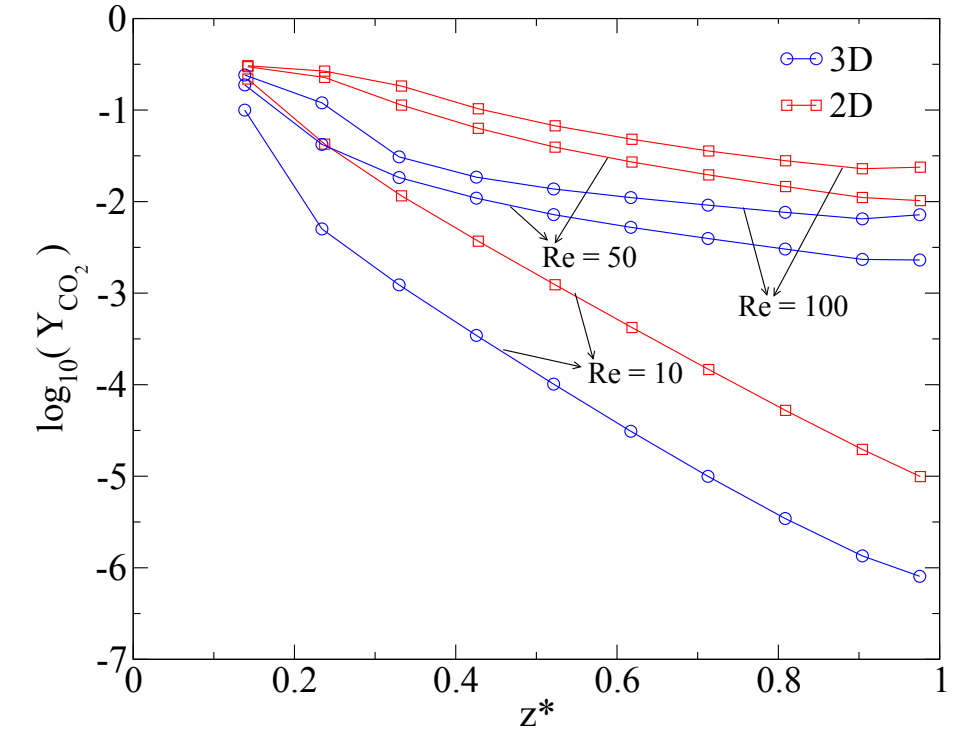


(a)

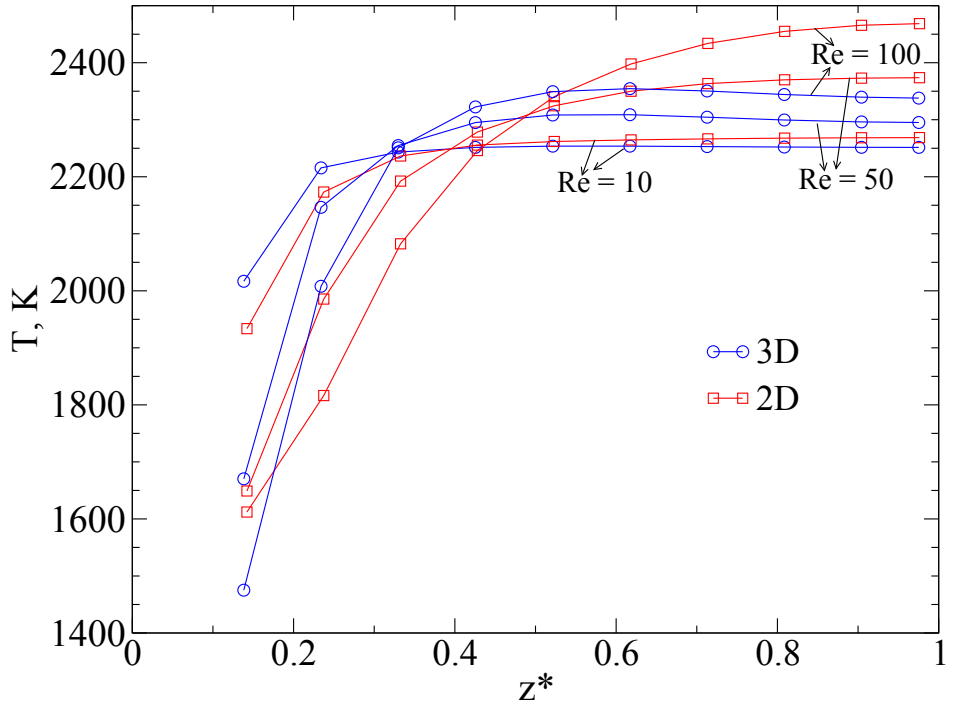


(b)

Figure 2.12: Comparison of **surface averaged** mass fraction of $CO_2$ and temperature between the 2D and 3D models for $Re = 10$, 50 and 100; Inflow gas composition was taken as $Y_{O_2} = 0.233$ and $Y_{H_2O} = 0.001$ with $T_{in}$=1000K; P-1 radiation model was included.

$O_2$ ($Y_{O_2} = 0$) in the gas phase inhibits the further production of $CO_2$. Fig.2.11(b) illustrates the axial temperature profiles for the two models at different Reynolds number. We observe a slight increase in the peak axial temperature for the 2D model at all Reynolds number. The maximum difference in temperature was found to be 7.46% for $Re = 10$. The peak positions were found to be almost the same for both the models. This can be attributed to the surface area difference between the two models.

Comparisons were also made between the surface averaged properties, namely mass fraction of $CO_2$ and particle surface temperature for both the models. It should be pointed out that the logarithmic scale was used for the comparison of $Y_{CO_2}$ for better understanding of the results as shown in Fig.2.12(a). The difference in $Y_{CO_2}$ at the surface of the particles between the 2D and 3D model was found to be minimal with a maximum difference of 5.82% observed at $Re = 50$. Also, the value of $Y_{CO_2}$ on the first particle remains almost the same at every Reynolds number for both the models. The mass fraction of $CO_2$ ($Y_{CO_2}$), then, decreases along the channel and correspondingly, increases for an increase in the Reynolds number. The surface averaged temperature on the particles as shown in Fig.2.12(b). Due to radiation, the cold inlet gas absorbs considerable amount of heat at the inlet of the channel, and then tends to reacts downstream of the channel resulting in an considerable increase in temperature, as can be seen from the figure. The profiles for the 3D and 2D models are similar to each other with a maximum variation of 9.55 % evaluated at $Re = 100$.

The comparison plots are further supported by contour plots for $CO_2$ and temperature for the 3D and 2D models as illustrated in Fig.2.13 and Fig.2.14 respectively. We see that the contour profiles for the 3D and 2D models are in excellent agreement with each other. Hence, it should be noted that the 2D model can be used reliably to study the combustion/gasification processes within a fixed bed gasifier.

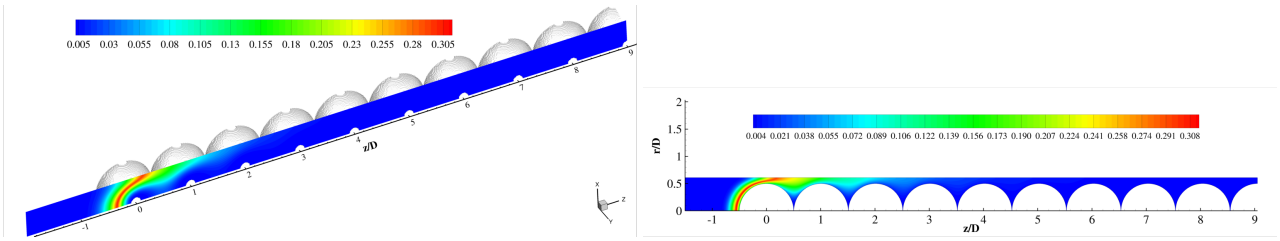


(a) Re 10

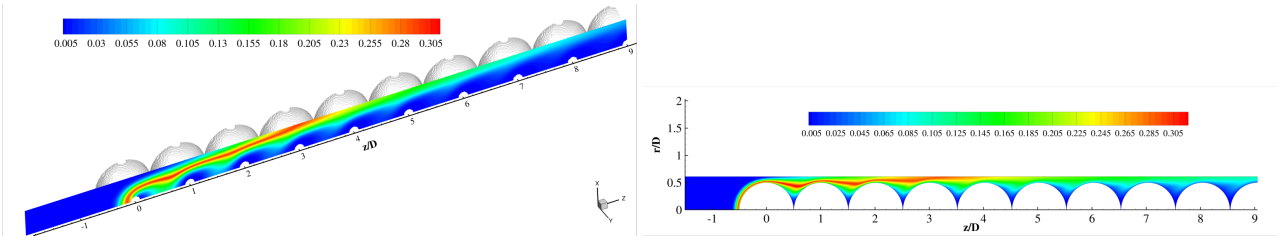


(b) Re 50

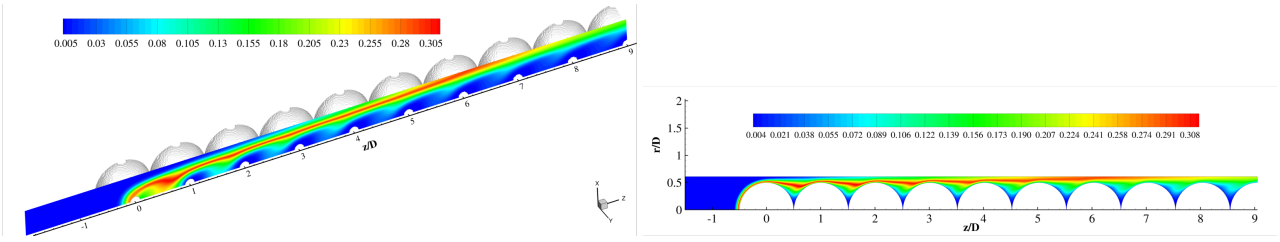


(c) Re 100

Figure 2.13: $CO_2$ contour plots for 3D and 2D models at Reynolds number, $Re$ = 10, 50 and 100; Inflow gas composition was taken as $Y_{O_2} = 0.233$ and $Y_{H_2O} = 0.001$ with $T_{in}$=1000K; P-1 radiation model was included.

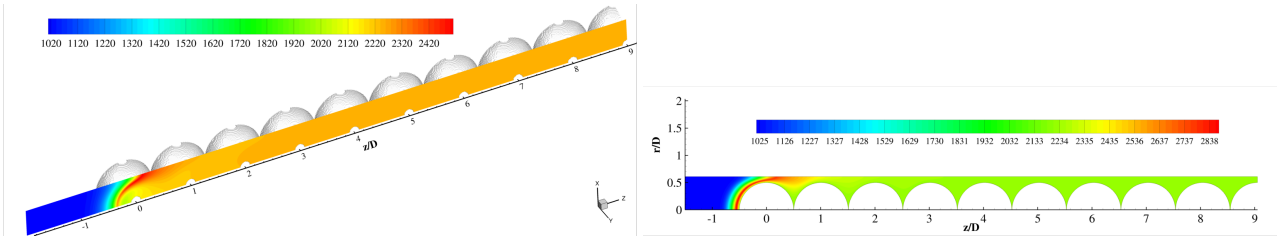


(a) Re 10

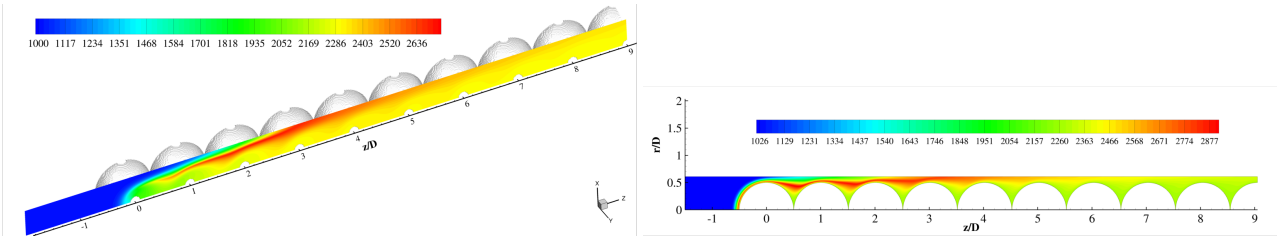


(b) Re 50

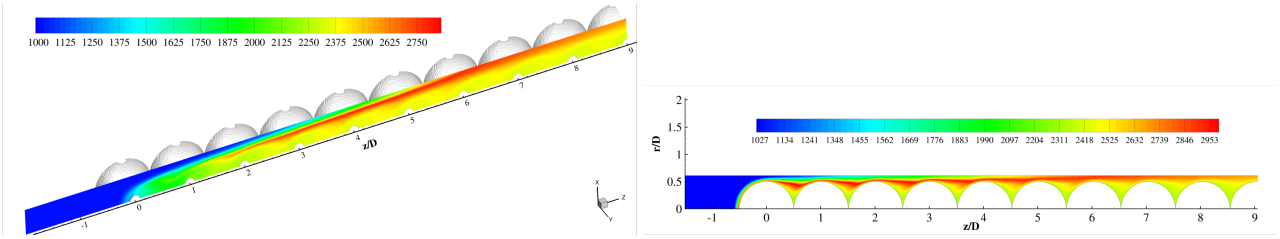


(c) Re 100

Figure 2.14: Temperature contour plots for 3D and 2D models at Reynolds number, $Re$ = 10, 50 and 100; Inflow gas composition was taken as $Y_{O_2}$ = 0.233 and $Y_{H_2O}$ = 0.001 with $T_{in}$=1000K; P-1 radiation model was included.

## 2.4 Effect of gas radiation

The effect of radiation on the combustion characteristics at Reynolds number, $Re$ = 10, 50 and 100 has also been investigated. Fig.2.15 shows the comparison of surfaced averaged temperature($T_S$), *(left)* and carbon mass fluxn($\dot{m}_c''$), *(right)*. Radiation helps the cold inlet air to absorb heat from the particle surface at the inlet of the

fixed bed which is shown by the drop in the particle surface temperature. The hot inlet gas stream reacts downstream leading to an increase in the surface temperature. There is no significant difference in the carbon mass flux for $Re = 10$. However, there is an decrease in the deposition rate by 50% at the inlet of the particle row for $Re = 50$ and 100, owing to the huge drop in surface temperature. The carbon mass flux remains almost the same downstream of the row, with and without radiation, at every Reynolds number. In a fixed bed reactor, particles which come in contact first with the inflow gas stream tend to be consumed faster due a higher consumption rate as seen from these plots.

## 2.5 Summary

This chapter attempts to develop a 2-D model to approximate 3-D structured packed beds in order to save computational time and resources. Simulations were performed at $Re = 10$, 50 and 100 with composition of inlet gas as $Y_{O_2} = 0.233$ and $Y_{H_2O} = 0.001$ and inlet temperature of 1000 K. Comparisons were made between the 2D and 3D model and the results can be summarized as follows:

- The velocity profiles for the two models were in very good agreement with each other with a maximum difference of 8.33% for cold run. The maximum difference in the developed velocity profiles during combustion was calculated to be 18.75 % between the two cases.
- Axial $Y_{CO_2}$ and temperature were also compared for the two models and plots showed excellent agreement. The maximum difference between the peak temperatures was found to be 7.46 % observed for the case of $Re = 10$, with a peak axial temperature of 2500 K for 3D and 2300 K for 2D model.
- Comparison of parameters at the surface were also performed. The difference in $Y_{CO_2}$ between the 2D and 3D model was found to be minimal with a maximum difference of 5.82% observed at $Re = 50$. The surface temperature profiles for the 3D and 2D models showed a maximum deviation of 9.55% evaluated at $Re = 100$.
- As an engineering relevance, further particles can be added to the model and a longer row comparable to the height of a fixed bed in a reactor can be studied using this 2D model.

Finally, it should be noted that the results of Particle Resolved Simulations(PRS) can be used to develop submodels, which can be used for the analysis of dynamics

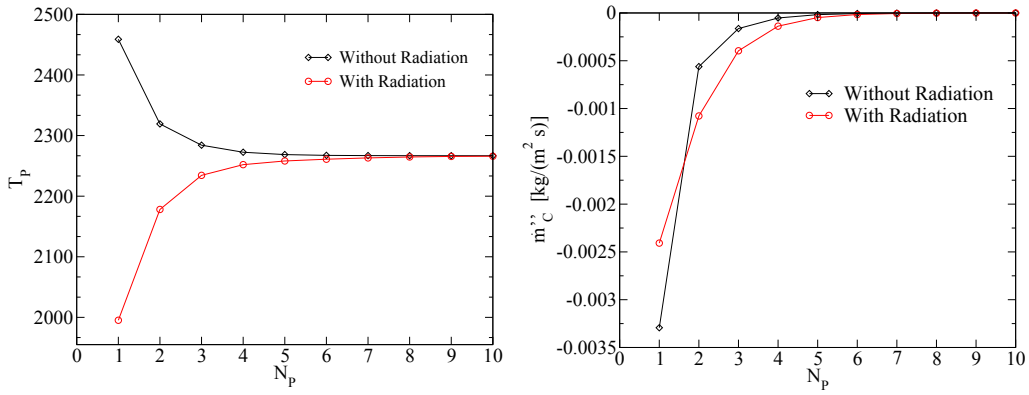


(a) Re 10

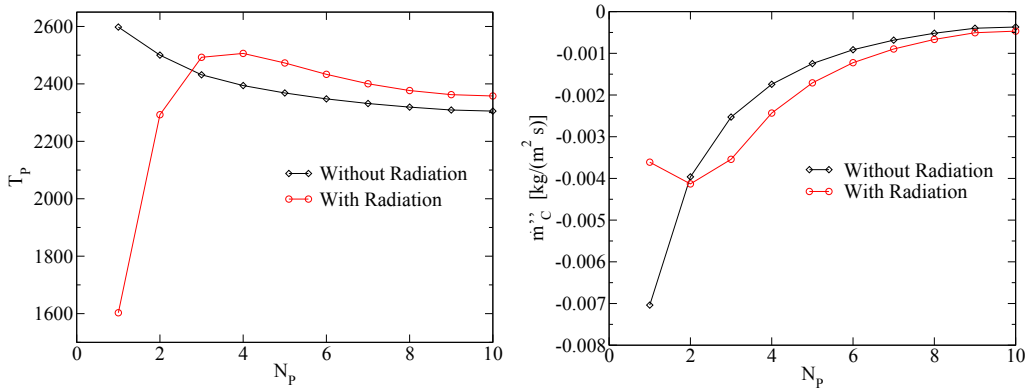


(b) Re 50

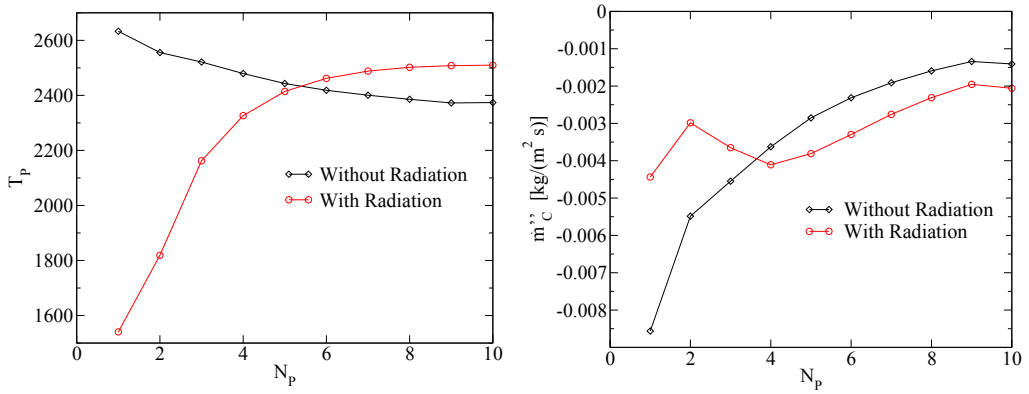


(c) Re 100

Figure 2.15: Comparison of surface averaged temperature and carbon mass flux($\dot{m}_c{}''$)for $Re$ = 10, 50 and 100 with and without radiation; Inflow gas composition was taken as $Y_{O_2}$ = 0.233 and $Y_{H_2O}$ = 0.001 with $T_{in}$=1000K

inside a packed bed reactor. Studying heat characteristics inside char particles during combustion/gasification has been explored further in this thesis which is of particular interest in catalytic fixed bed reactors.

# Chapter 3

# Study of heat transfer and species characteristics within solids

## 3.1 Introduction

Study of particles in the previous chapter involved only the surface of the particle without inclusion of heat transfer characteristics in the solid char particles. Studies using simulations [58, 56] have attempted to the heat transfer characteristics within fixed-bed reactors. These have aimed to resolved wall-particle and particle-particle interactions. Calculations of Nusselt number and effective thermal conductivity were the main subjects of interest in these studies. Szafran and Kmiec [90] customized the governing equations using a UDF code into Fluent 6.1 to expand its abilities. Nusselt and Sherwood numbers were calculated and were in agreement with theory. Guardo et al. [91] also studied effect of free and forced convection using different fluids to study the heat transfer characteristics within fixed bed reactors. However, none of these studies have managed to account for the chemistry of species within the reactor. Studies[4, 54, 92] attempting to study chemistry inside reactors have not focused on heat transfer properties. Very few studies[52, 93] have taken both species and energy along with the fluid dynamics within the reactor. Development of an efficient 2-D model allows to study all these characteristics simultaneously. Hence, this chapter aims at studying the heat transfer characteristics within the solids and species characteristics as combustion and gasification progress within the channel, while taking into account heat transfer in solid particles.

## 3.2 Model Formulation

The geometry in this case is similar to that mentioned in the previous chapter. However, in order to study the solid particles, the domain within the particles needed to be meshed. We quickly highlight the model formulation and assumptions before jumping on to the results.

A series of 10 solid particles with diameter,$d_p$ = 2 cm, are placed one behind another in a single row with the main gas flow flowing around the row of particles. The modeling configuration and the meshed grid are illustrated in Fig.3.1(a) and Fig.3.1(b), respectively. The configuration is considered as axisymmetric. The solid used here was graphite with specific heat of 710 J $kg^{-1}K^{-1}$, thermal conductivity of 0.2 W $m^{-1}K^{-1}$ and density of 1500 kg $m^{-3}$.

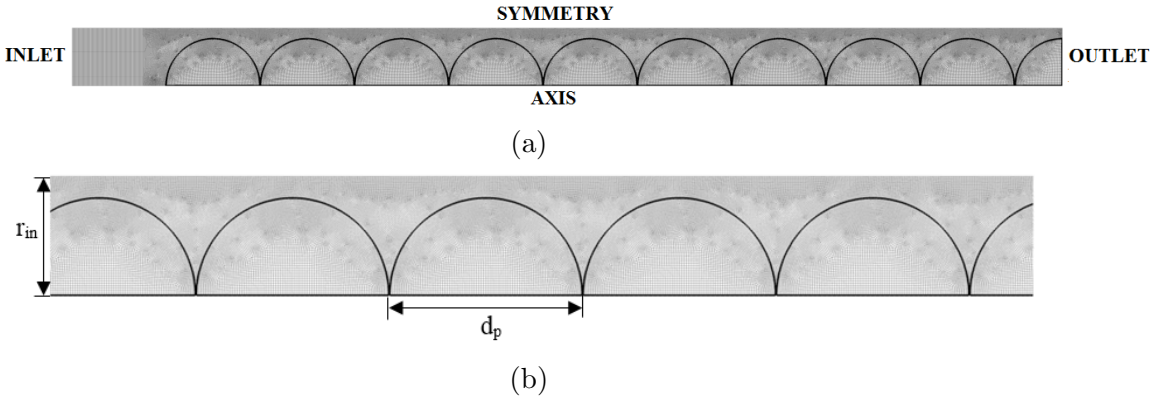


Figure 3.1: Meshed domain of the geometry with solid particles

### 3.2.1 Assumptions

To proceed with the description of the mathematical CFD-based model, several assumptions are introduced in order to solve the problem.

1. The consumption time of the particle is always large compared to the convective and diffusion time scales for the gas phase. Hence, pseudo-steady-state apprach has been assumed.

2. The gas flow was treated as an incompressible ideal gas.

3. The representative element is considered to be axysymmetrical with a symmetrical gasflow.

4. The porosity of the particles is not taken into account which results in neglecting the intraparticle diffusion. The surface reaction model is used to simulate the interaction between reacting solid surface and gas phase.

5. The particles consists of carbon only. In particular, the volatilization of the particles is not included due to the steady-state character of the model.

6. The radiation of the gas phase is modeled using the P-1 model.

7. The buoyancy effect is neglected.

### 3.2.2 Governing Equations and Boundary Conditions

The governing equations and chemistry modeled for this configuration as explained in Section 2.1.2 and Eqns. R1 - R7. It should be noted that, in this case, we balance the heat transferred to the solid particle from the surface with the heat of heterogeneous reactions and loss due to radiation. The surface temperature of the particle is calculated using this particular boundary condition(BC). The temperature inside the particle is calculated using the energy conservation equation solved inside each particle.

## 3.3 Results

The main objective of this study is to analyze the heat transfer due to conduction in solid particles during combustion/gasification. Hence, a number of simulations were performed at Reynolds number of $Re = 10$, 50 and 100 with inlet gas temperature at 1000K. The composition of the inlet gas was taken as $Y_{O_2} = 0.233$ and $Y_{H_2O} = 0.001$ to simulate combustion within the channel and $Y_{O_2} = 0.11$ and $Y_{H_2O} = 0.074$ to simulate gasification within the channel.

### 3.3.1 Comparison of Particles and Solids

The results obtained from the simulations in this chapter were compared with that performed in Chapter.2. *'Particles' denote the case with no heat transfer to the bulk of the particle while 'Solids' involve heat conduction to the bulk of the particle from the surface due to a gradient in temperature.* Comparisons were made along the axis and on the surface to study the temperature, mass fraction of $CO_2$ and surface deposition rate between both the models.

The axial temperature profiles were compared with and without heat transfer in Fig.3.2 and maximum difference of 2.5% was noted for the peak temperatures at

$Re = 100$. The profiles remain roughly the same for $Re = 10$ with a minute 1.9% difference observed for $Re = 50$. Further, Fig.3.3 shows the comparison of $CO_2$ on the surface and along the axis. The peak $CO_2 = 0.295$ remains the same along the axis for both the solids and particles. However, there is a slight displacement in the position downstream of the channel, as observed for solids in Fig.3.3(b). The surface averaged $Y_{CO_2}$, also follows similar trend for both solids and particles at every Reynolds number shown in Fig.3.3(a).

Fig.3.4 presents the surface averaged temperature and carbon mass flux at varying Reynolds number. We see that the temperature for solids seems to be lower than particles as expected. This is due to additional heat transfer due to conduction in solids leading to a decrease in the surface temperature. However, the decrease in temperature varies with Reynolds number. We see that there is negligible change in the temperature profile at $Re = 10$ and a moderate change at $Re = 100$. However, temperature difference of 400K, amounting to $\sim$16% decrease is observed at $Re = 50$ for $N_P = 3$, as seen in Fig.3.4(a). This also results in a sudden decrease in the carbon mass flux for the same, which can be seen in Fig.3.4(b). Apart from this reduction of 16.67%, the carbon mass flux essentially remains the same for at other Reynolds number and particles.

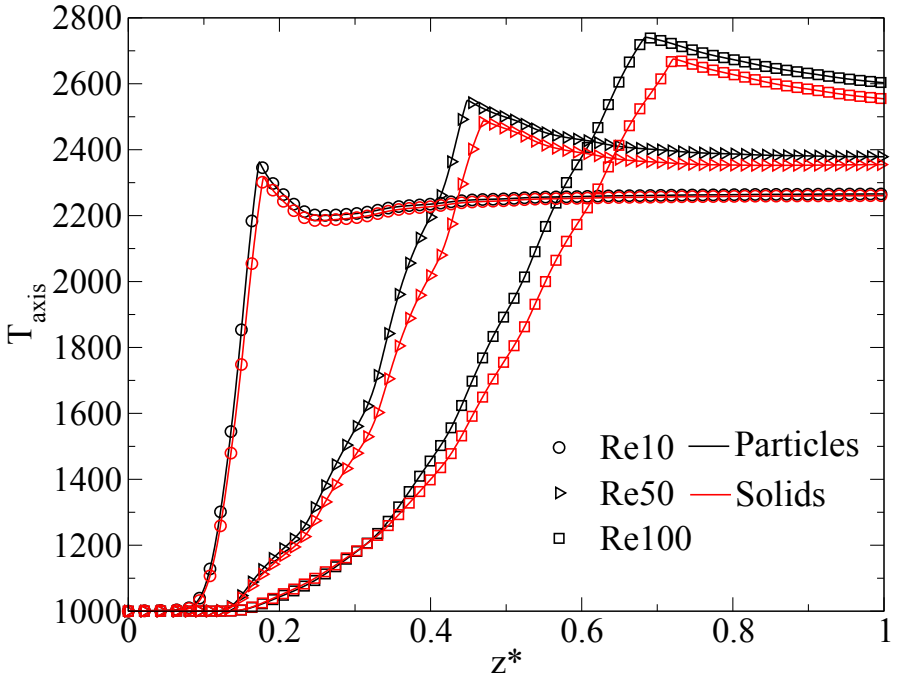


(a) Axial temperature

Figure 3.2: Comparison plots for axial temperature, with and without heat transfer in solids, for Reynolds number, $Re$ = 10, 50 and 100; *"Particles" relates to the case* **without** *heat transfer in solids, "Solids" relates to the case* **with** *heat transfer in solids* $T_{in}$=1000K with $Y_{O_2}$=0.233 and $Y_{H_2O}$=0.001 has been taken for this model

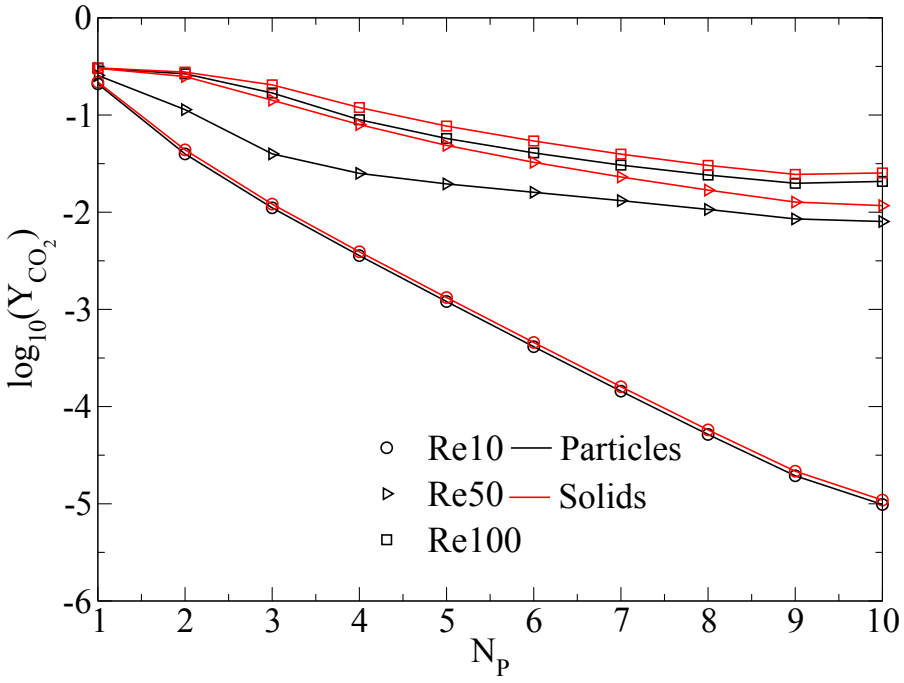


(a) Surface averaged $Y_{CO_2}$. Logarithmic values have been used

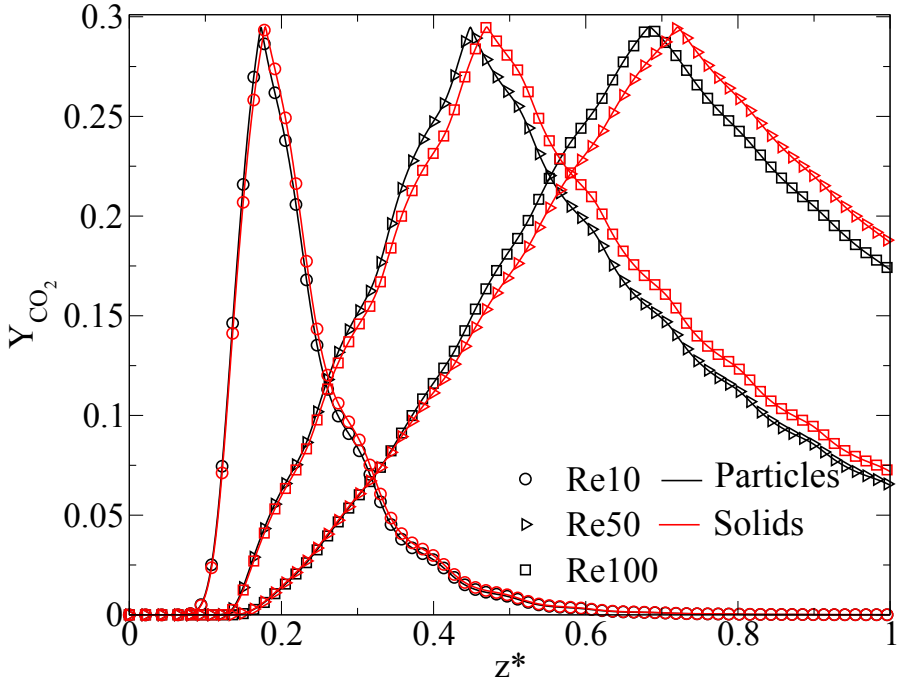


(b) $CO_2$ mass fraction along the axis($Y_{CO_2}$)

Figure 3.3: Comparison plots for mass fraction of $CO_2$ along the axis and on the surfaces with and without heat transfer in solids, for Reynolds number, $Re$ = 10, 50 and 100; *"Particles" relates to the case* **without** *heat transfer in solids, "Solids" relates to the case* **with** *heat transfer in solids* $T_{in}$=1000K with $Y_{O_2}$=0.233 and $Y_{H_2O}$=0.001 has been taken for this model

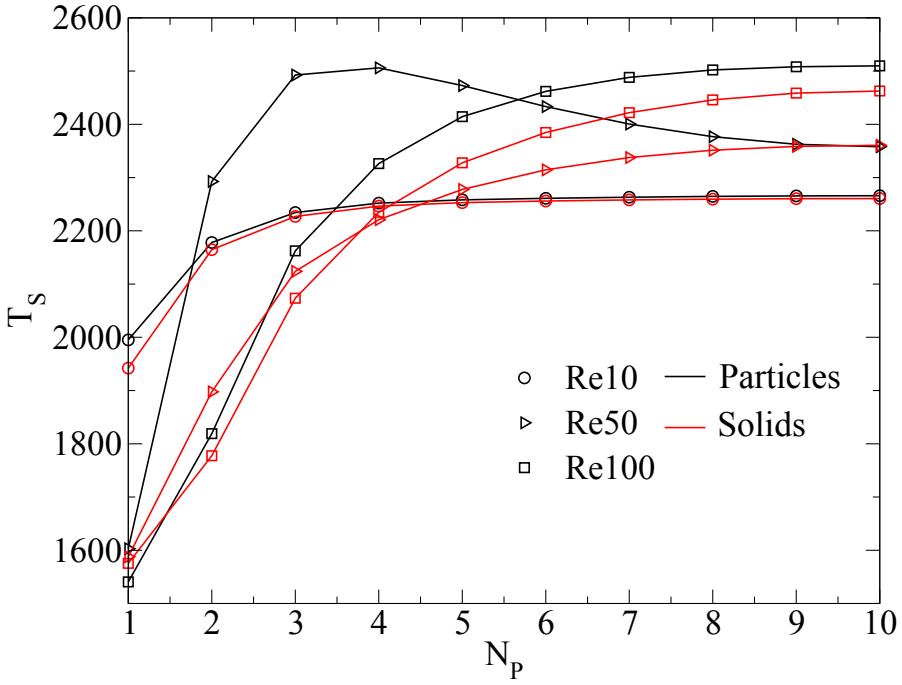


(a) Surface averaged temperature($T_S$)

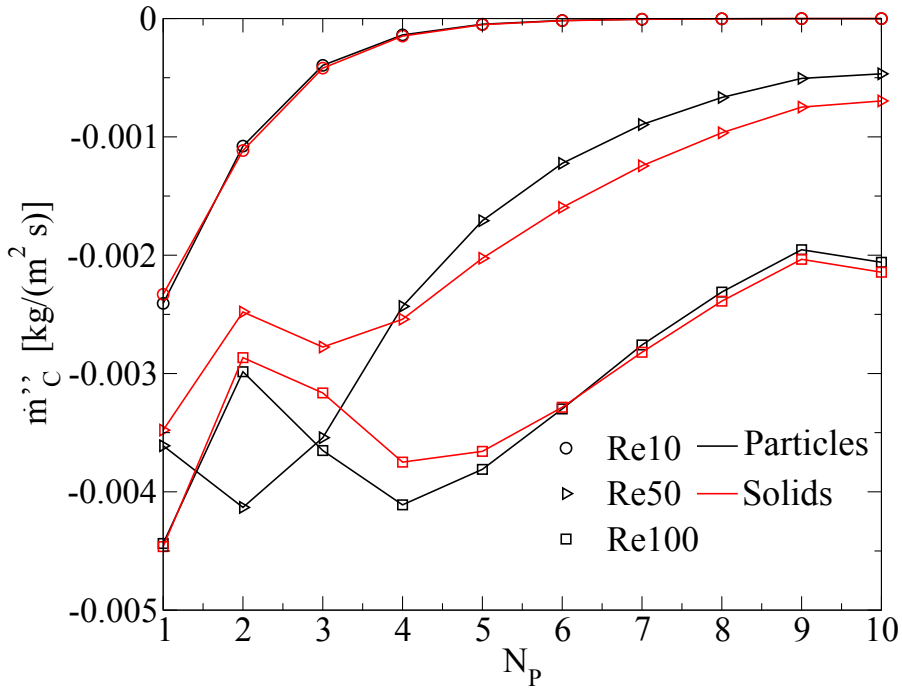


(b) Surface averaged carbon mass flux($\dot{m}''_c$)

Figure 3.4: Comparison plots for surface averaged temperature($T_S$) and surface averaged carbon mass flux($\dot{m}''_c$), with and without heat transfer in solids, for Reynolds number, $Re$ = 10, 50 and 100; *"Particles" relates to the case* **without** *heat transfer in solids, "Solids" relates to the case* **with** *heat transfer in solids*; $T_{in}$=1000K with $Y_{O_2}$=0.233 and $Y_{H_2O}$=0.001 has been taken for this model

### 3.3.2 Combustion

This subsection presents the results obtained for the inlet gas composition of $Y_{O_2}$ = 0.233 and $Y_{H_2O}$ = 0.001 entering the particle column at 1000K. The Reynolds number was varied from 1 to 100 through 50. Radiation brings about similar changes mentioned in the previous chapter. The first visible change is the extension of the flame sheet further down the channel. The extension is more prominent in the case of $Re = 50$ and $Re = 100$ as seen from Fig.3.5(a) and Fig.3.5(b) respectively. The flame sheet extends from 3 to 5 particles for $Re = 50$ and 5 to 7 particles for $Re = 100$.

Fig.3.6 shows the CO contour profiles for all three Reynolds number with and without radiation. From this figure, it can be observed that the flame sheet formed during combustion in the channel prevents any further leakage into the channel due to diffusion of CO and $O_2$. The mass fraction of CO, $Y_{CO}$, beyond the flame sheet is zero and is represented by the blue zone in the channel. This holds true for all the cases of Reynolds number with and without radiation. Fig.3.6(a) shows that for $Re = 10$, the $Y_{CO} = 0.345$ downstream of the channel which should have ideally reacted with the incoming $O_2$. However, due to the low flow rate of the inlet gas, the $O_2$ is not sufficient enough to reach the interior of the channel and ends up getting consumed at the inlet itself. However, for $Re = 50$ and $Re = 100$, we have a much faster incoming gas flow into the channel resulting in a higher trasnport within the channel. This makes use of the high mass fraction of CO and results in a flame sheet which mayb even extend upto to the $7^{th}$ particle in the channel as can be seen in Fig.3.6(c).

Fig.3.7 shows the temperature contour profiles within the channel including the temperature of the particles for the three variations of Reynolds number with and without radiation. The development of flame sheet increases the local temperature within the channel which leads to rise in the temperature of particles in the local vicinity of the flame sheet. Heat transfer due to radiation results in the decrease of the particle temperature near the inlet of the particle column as shown in the bottom subfigures of Fig.3.7(a), (b) and (c). This is due to the high difference in temperature of gas phase and the solid phase evident in the cases without radiation. The heat is transfered to the cold inlet gas enabling it to react with the CO further down the channel, which leads to the local extension of the flame sheet as seen in Fig.3.8.

The effect of radiation has further been highlighted in Fig.3.8 where the inlet gas composition is $Y_{O_2} = 0.233$ & $Y_{H_2O} = 0.001$ and $T_{in} = 1000$K. Fig.3.8(a) represents the $CO_2$ mass fraction along the axis for the case. The peak $Y_{CO_2} = 0.295$ for all

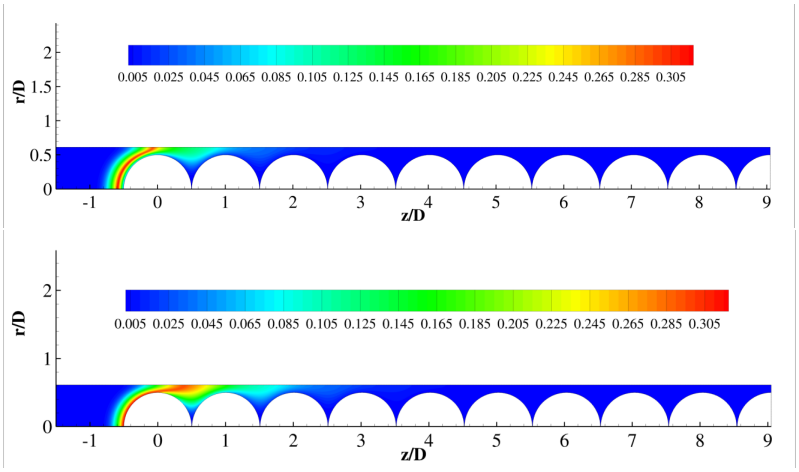


(a) Re 10

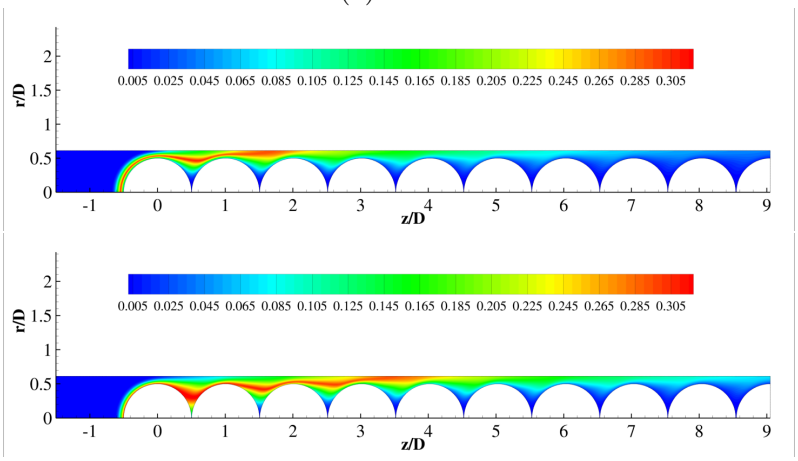


(b) Re 50

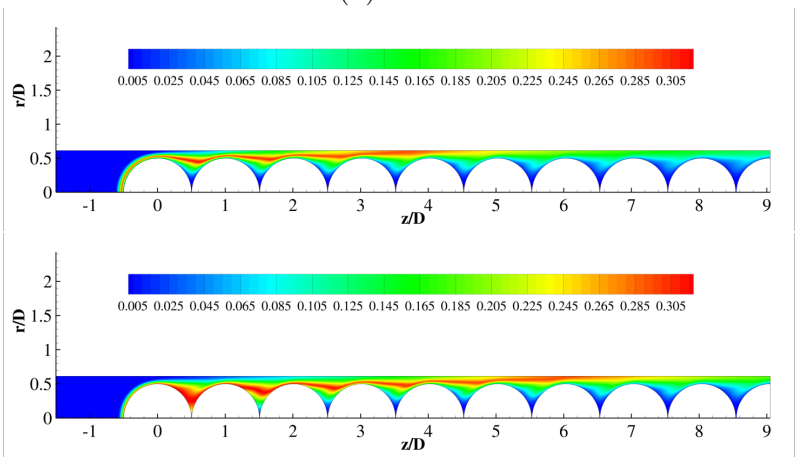


(c) Re 100

Figure 3.5: $CO_2$ contour profiles for $T_{in}$=1000K with $Y_{O_2}$=0.233 and $Y_{H_2O}$=0.001; The top subfigure in each case represents combustion *without radiation* and effect of the P-1 *radiation* model is represented by the bottom subfigure

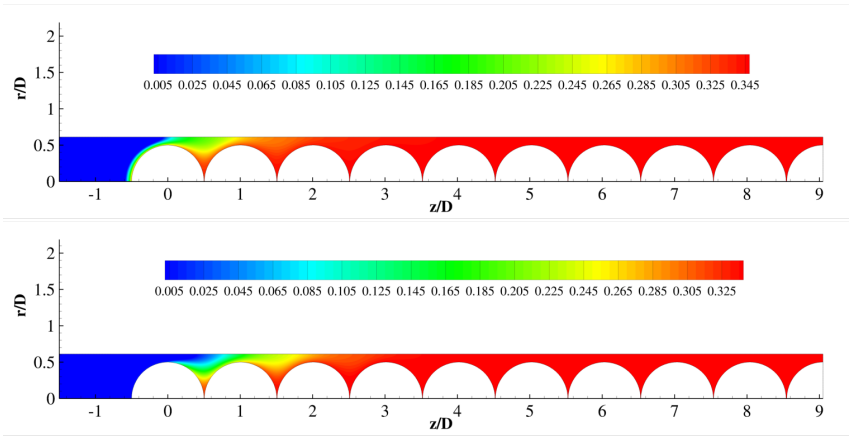


(a) Re 10

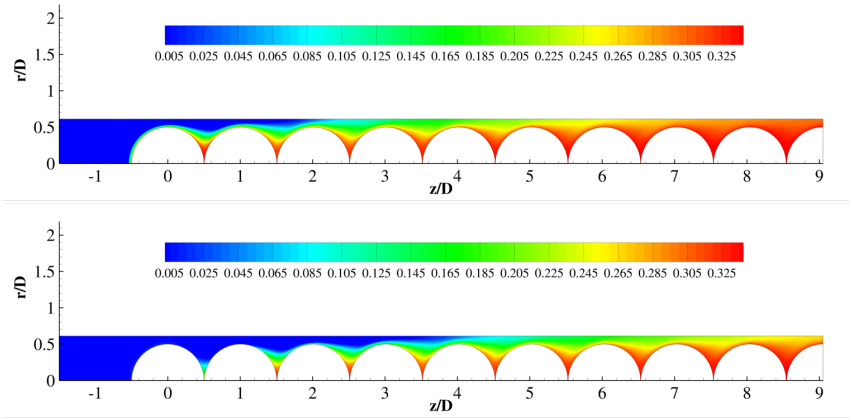


(b) Re 50

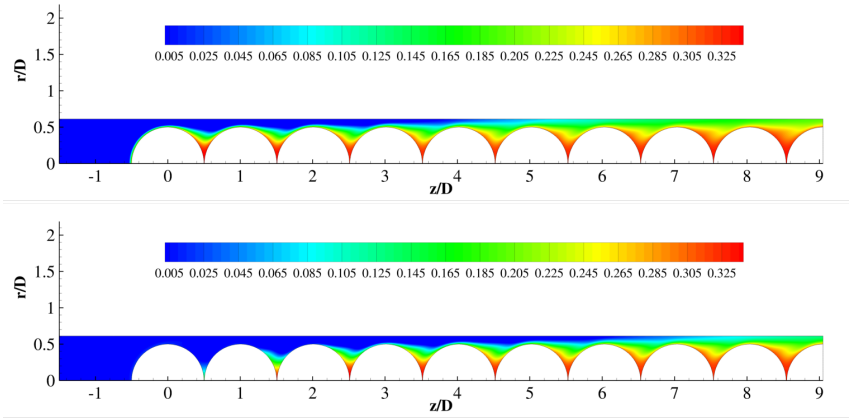


(c) Re 100

Figure 3.6: CO contour profiles for $T_{in}$=1000K with $Y_{O_2}$=0.233 and $Y_{H_2O}$=0.001; The top subfigure in each case represents combustion *without radiation* and effect of the P-1 *radiation* model is represented by the bottom subfigure

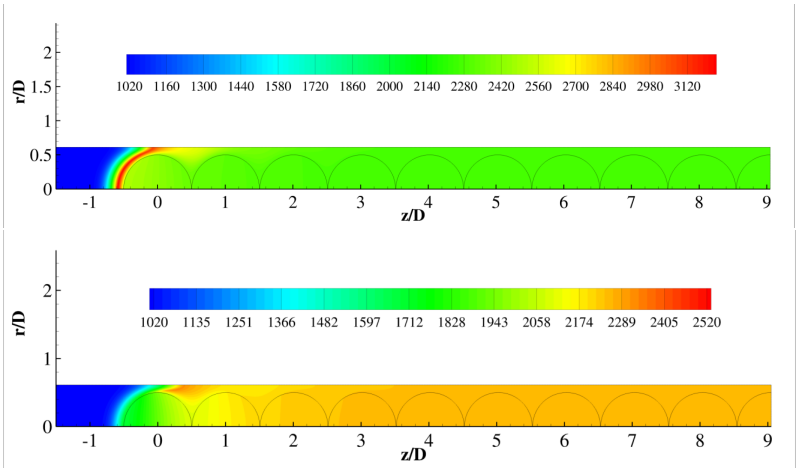


(a) Re 10

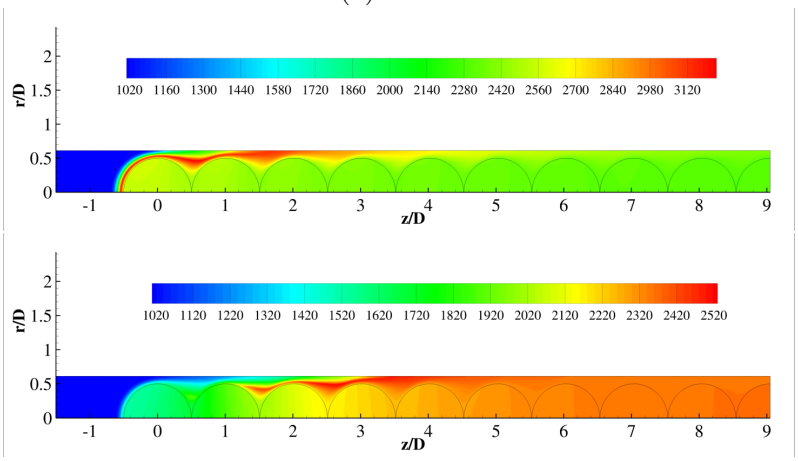


(b) Re 50

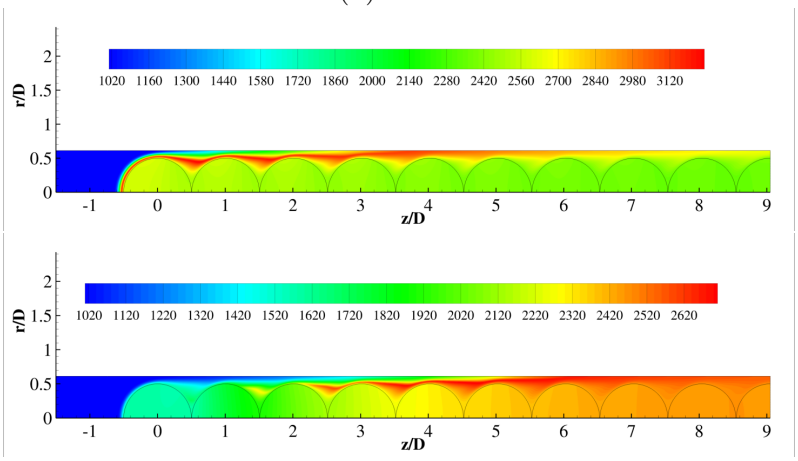


(c) Re 100

Figure 3.7: T contour profiles for $T_{in}$=1000K with $Y_{O_2}$=0.233 and $Y_{H_2O}$=0.001; The top subfigure in each case represents combustion *without radiation* and effect of the P-1 *radiation* model is represented by the bottom subfigure

cases of Reynolds number with and without radiation. However, there is a shift in the peak $Y_{CO_2}$ position downstream of the channel with increasing Reynolds number. The introduction of P-1 radiation model furthers shifts the peak towards the outlet of the channel. Fig.3.8(b) shows the development of the temperature along the axis for varying Reynolds number with and without radiation. Similar to $Y_{CO_2}$, the peak temperature along the axis remains the same for varying Reynolds number with a identical shift in the position. The P-1 radiation model brings interesting changes in the axial temperature profile also. The peak temperature without radiation reaches upto ∼3100 K at all Reynolds number, which decreases significantly with the inclusion of the P-1 radiation model. We also observe an additional shift in the position towards the outlet of the particle channel. The maximum decrease is observed for $Re = 10$ of 25.04% and peak axial temperature of 2675 K at $Re = 100$. This can be attributed to the fact that the cold inlet gas heats up due to radiation at the entrance of the channel and hence, reacts downstream resulting in the rise of ambient temperature. A high Reynolds number tends to be more affected by this phenomena due to the higher gas transport as seen in Fig.3.8(b).

Furthermore, we also plot the particle surface characteristics in terms of carbon mass flux and surface temperature to study the influence of Reynolds number and radiation. Fig.3.9(a) corresponds to the surface averaged temperature of the char particles. Without radiation, the temperature increases with Reynolds number and decreases along the channel. However, introduction of the P-1 radiation model decreases the temperature of the particle nearest to the inflow and increases the temperature of the particles downstream due to an increased carbon mass flux. The effect of radiation is computed to be the highest for $Re = 100$ with a decrease of 40.41% in the surface temperature at the inlet of the particle row. Fig.3.9(b) shows the carbon mass flux at the particle surface for Re = 10, 50 and 100 representing the cases with and without the P-1 radiation model. The mass flux is negative as carbon is consumed from the char particles due to the heterogeneous reactions at the surface. Without radiation, we see that the mass flux increases with increasing Reynolds number due to an increase in the gas transport in the channel. Inclusion of P-1 radiation model, however, leads to decrease in the mass flux from the surface near the inlet(47.85% for $Re = 100$) which explains the drop of temperature as seen earlier. As we move towards the interior of the channel, the mass flux increases due to the enhanced reactivity of the heated inlet gas.

We also attempt to study the transport phenomena coupled with reaction kinetics in terms of the non-dimensional Damkohler number. The Damkohler number for heterogeneous reaction, ReactionR3 is defined as the ratio of the reaction rate

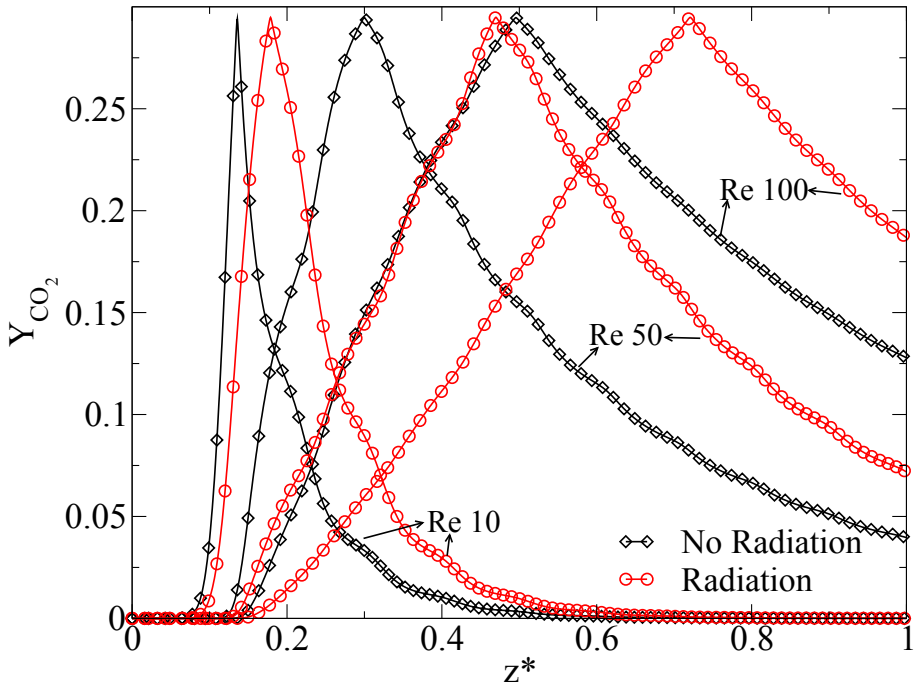


(a) $CO_2$ mass fraction($Y_{CO_2}$)

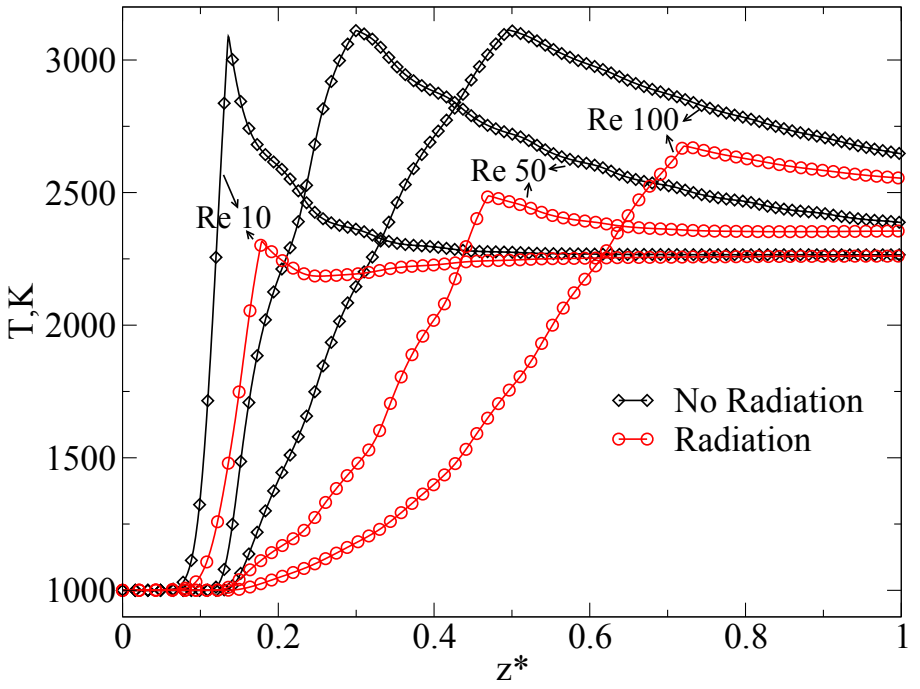


(b) Axial Temperature

Figure 3.8: Comparison of the $Y_{CO_2}$ and temperature profile along the axis for Reynolds number, $Re$ = 10, 50 and 100 at 1000K for cases with and without radiation; $Y_{O_2}$=0.233 and $Y_{H_2O}$=0.001 is taken for the inlet gas

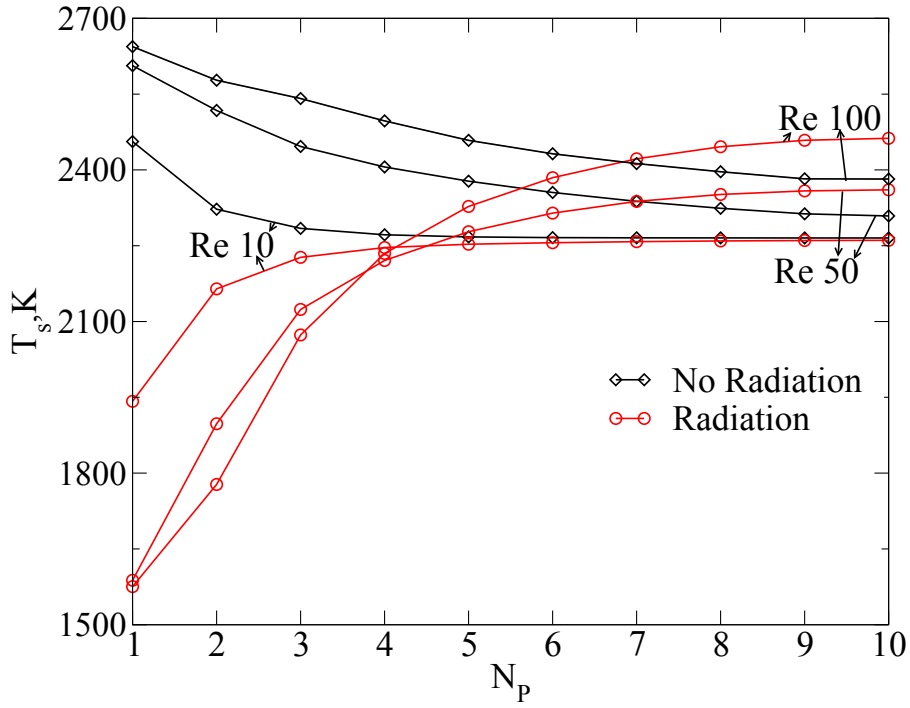


(a) Surface Temperature($T_S$)

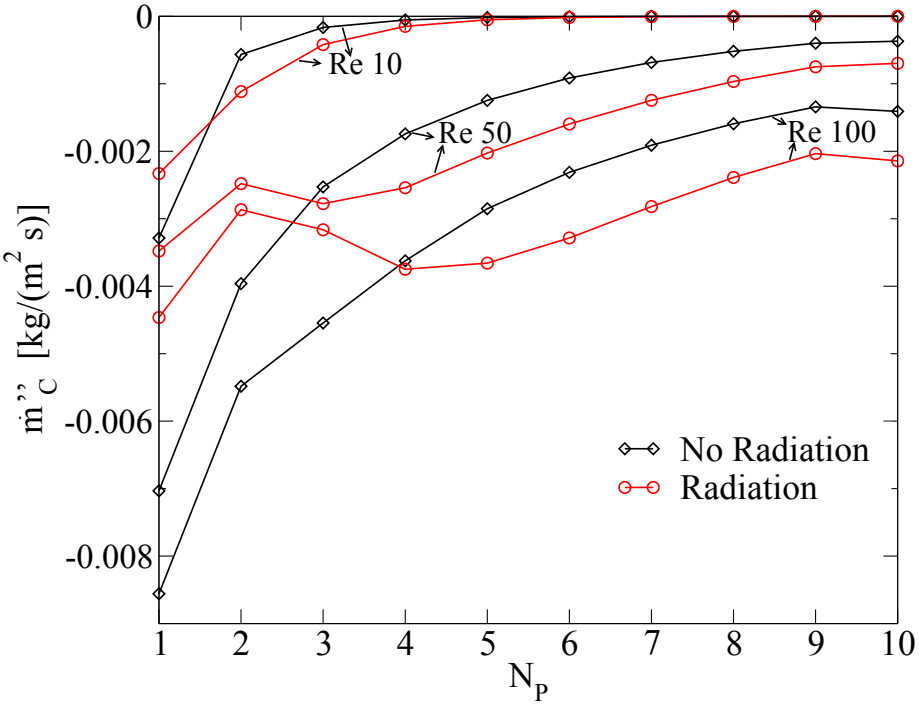


(b) Carbon Mass Flux($\dot{m}_c''$)

Figure 3.9: Comparison of carbon mass flux and temperature on the particle surface for Reynolds number, $Re$ = 10, 50 and 100 at 1000K for cases with and without radiation; $Y_{O_2}$=0.233 and $Y_{H_2O}$=0.001 is taken for the inlet gas

to the mass transfer rate, refer [94, 2], is given by:

$$Da_{\mathrm{II}} = \frac{k_{CO_2}}{\beta} \tag{3.1}$$

where '$\beta$' is the mass transfer coefficient of the gas-solid interface. The transport regimes can be deduced using the following criteria(refer [85]):

- $Da_{\mathrm{II}} < 1$: A kinetically controlled regime with a much slower chemical kinetic rate compared to the mass transfer or diffusion rate.
- $Da_{\mathrm{II}} > 1$: A diffusion controlled regime with mass transfer rate quite slow compared to the chemical kinetic rate.
- $Da_{\mathrm{II}} \approx 1$: Comparable mass transfer and chemical kinetic rates.

We can define the mass transfer coefficient, $\beta$ using the Sherwood number, '$Sh$' given by the equation,

$$\beta = \frac{ShD_m}{d_p} \tag{3.2}$$

where, '$Sh$' is the Sherwood number, '$D_m$' is the mass diffusivity and the $d_p$ is the diameter of the particle. We also define, Lewis number as the ratio of the thermal diffusivity and the mass diffusivity, given by:

$$Le = \frac{\alpha}{D_m} \tag{3.3}$$

where, '$\alpha$' is the thermal diffusivity. In order to characterize the fluid flow withing the channel in terms of mass and thermal diffusivity, we studied the Lewis number throughout the domain. This has been illustrated in Fig.3.10 which represents the Lewis number throughout the domain at $Re = 10$, 50 and 100. We can conclude from the figures that the Lewis number remains $\sim$1 within the channel. It should also be mentioned that for $Le = 1$,

$$Nu = Sh \tag{3.4}$$

where '$Nu$' is the Nusselt number. We use the above findings to plot $Da_{\mathrm{II}}$ for Reaction.R3 which is the dominating mechanism in the present case. The results have been plotted in Fig.3.11 for each Reynolds number. The Damkohler number, $Da_{\mathrm{II}}$ always remains greater than 1 for $Re = 10$ which suggests that diffusion controlled regime is the dominating phenomenon for this case. However, we see that the regime is kinetically controlled for $Re = 50$ and 100 initially at the inlet of the

bed. However, the regime remains within transition regime at the interior of the channel.

In order to compare the surface temperature with the overall particle temperature, illustrations were made in Fig.3.12. The overall temperature of the particle remains lower than the particle temperature for all $Re$ at the first particle, and increases immediately for the second particle. As we proceed along the channel, though the temperature difference decreases, the particle temperature continues to be higher than the surface temperature. The highest difference of ∼185K was observed at $Re = 100$ and $N_P = 4$, as can been seen in the figure.

### 3.3.3 Gasification

This subsection presents the results for an inlet gas composition, where $Y_{O_2} = 0.11$ and $Y_{H_2O} = 0.074$ which corresponds to a gasification atmosphere in an industrial fixed bed gasifier. Simulations were performed at $T_{in} = 1000$K. The P-1 radiation model was toggled to study the effect of radiation on gasification.

Fig.3.13 shows the $CO_2$ contour profiles showcasing the effect of radiation during gasification. There is a formation of a comparatively thicker flame sheet closer to the particle surface. The maximum $Y_{CO_2}$ of 0.162 is less compared to the case of combustion where peak $Y_{CO_2} = 0.312$. This is due to low $Y_{O_2}$ present in the inlet gas which limits the Reaction R5. Radiation affects the flame sheet length similar to that of combustion. Additionally, we find that for $Re = 100$, the flame sheet extends upto the outlet of the channel, and the mass fraction of $CO_2$ decreases as we move from the inlet to the outlet of the particle column.

Fig.3.14 shows temperature profiles within the channel for different cases of Reynolds number. The peak temperatures are much lower than those seen in the case of combustion, as expected. For the case without radiation, the peak temperature is ∼2030°C much lower than ∼3120°C. This is to be expected as $Y_{CO_2}$ produced is also limited in this case. Radiation tends to have the same effect as observed in combustion, leading to a homogeneous temperature in the interior of the channel.

Fig.3.15 shows the comparison of mass fraction of $CO_2$ and temperature along the axis for the case with and without radiation for all the variants of Reynolds number i.e. Re = 10, 50 and 100. We see that the $Y_{CO_2}$ has a peak value of 0.137 for all cases. Shifts similar to that of combustion were observed here as well with increase in Reynolds number, with additional shifts observed with the inclusion of P-1 radiation model.

We also studied the evolution of surface temperature and carbon mass flux for the individual particles with Reynolds number with and without radiation. Fig.3.16(a)

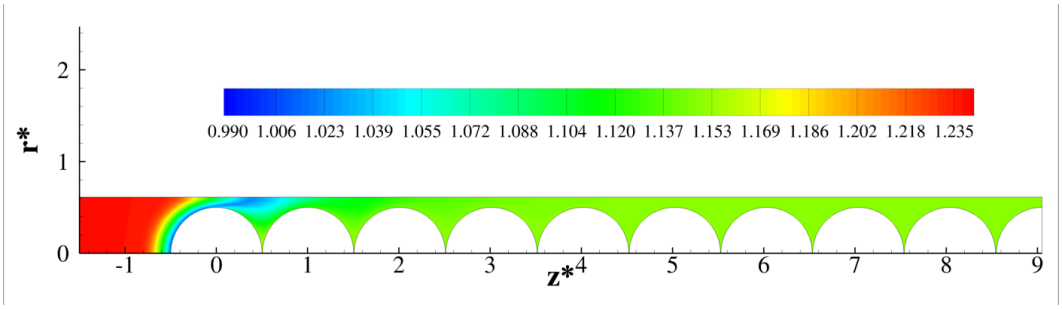


(a) Re 10

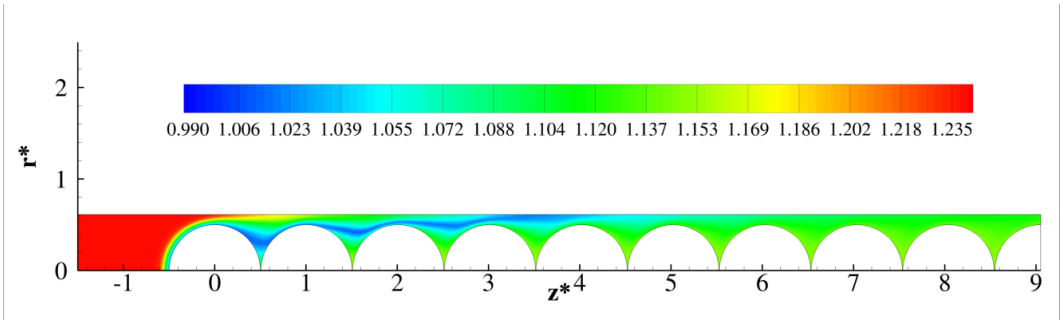


(b) Re 50

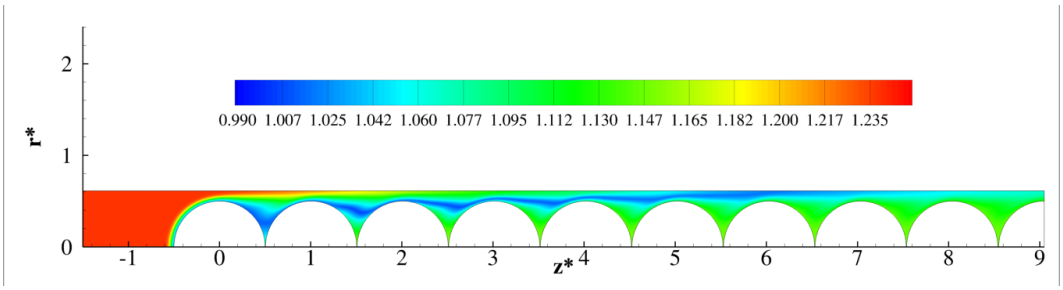


(c) Re 100

Figure 3.10: Contour profiles for Lewis number($Le$) with $Y_{O_2}$=0.233 and $Y_{H_2O}$=0.001; The P-1 *radiation* model has been considered for these cases

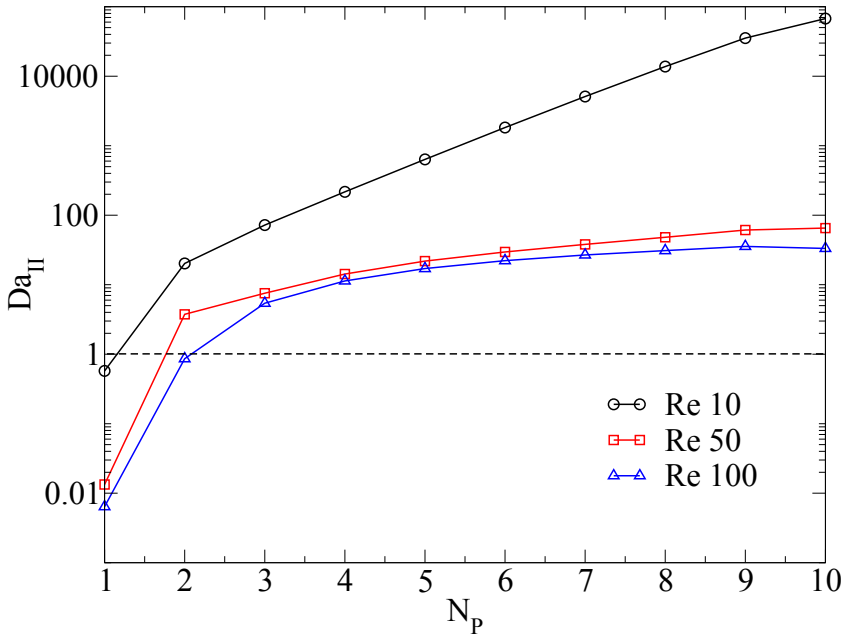


Figure 3.11: Comparison of Damkohler number for each particle at Reynolds number, $Re$ = 10, 50 and 100 at 1000K for cases with radiation; $Y_{O_2}$=0.233 and $Y_{H_2O}$=0.001 is taken for the inlet gas

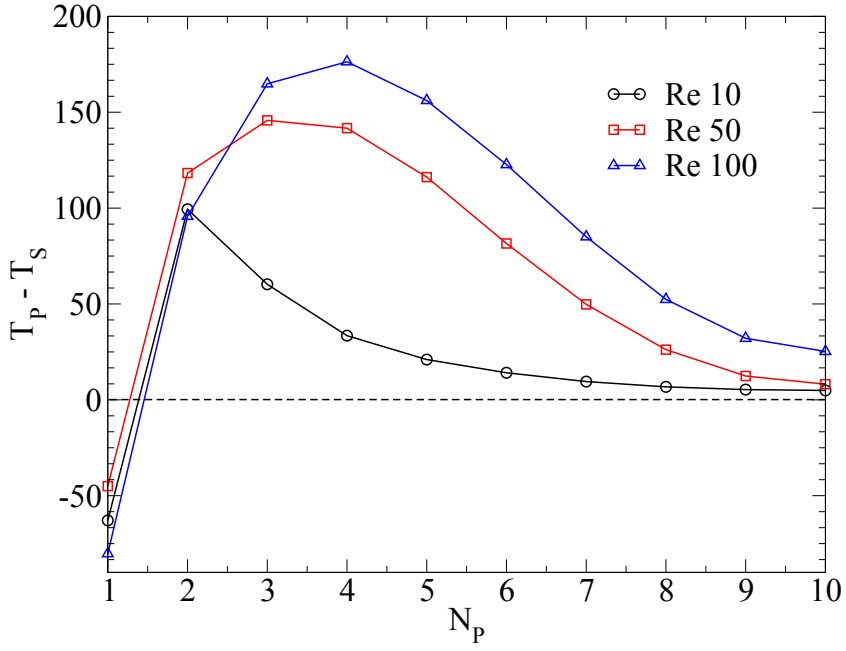


(a) Difference between particle temperature and surface temperature

Figure 3.12: Comparison of volume averaged particle temperature for Reynolds number, $Re$ = 10, 50 and 100 at 1000K for cases with radiation; $Y_{O_2}$=0.233 and $Y_{H_2O}$=0.001 is taken for the inlet gas

gives the plots for the development of the surface temperature($T_s$) of the particles in the column with Reynolds number. For the case without radiation, the surface temperature increases with Reynolds number and decreases as we advance towards the outlet. Radiation decreases the surface temperature near the inlet and increases it towards the outlet, significantly in the case of Re 50 and Re 100. The maximum drop in temperature was observed for $Re = 100$ of $\sim 20\%$. Similar results were obtained for the carbon mass flux plotted in Fig.3.16(b).

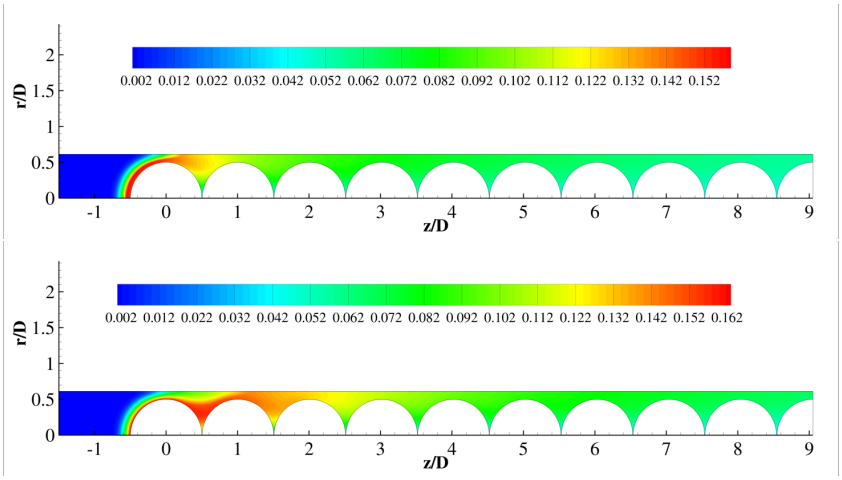


(a) Re 10

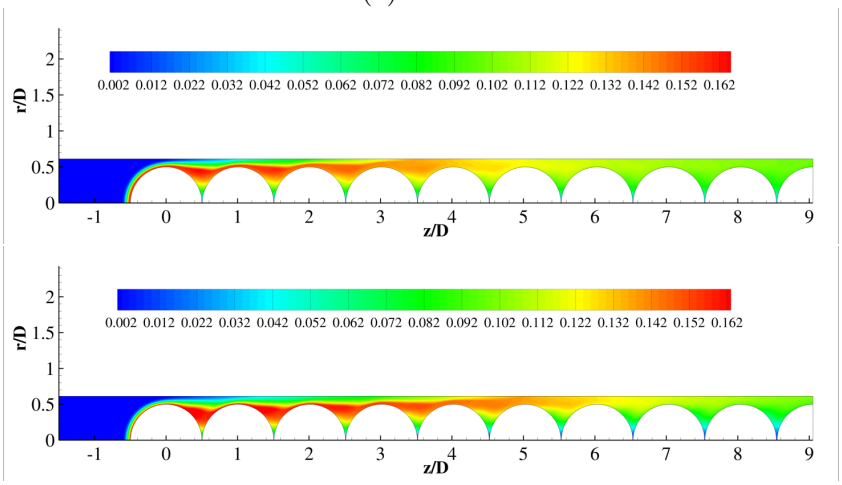


(b) Re 50

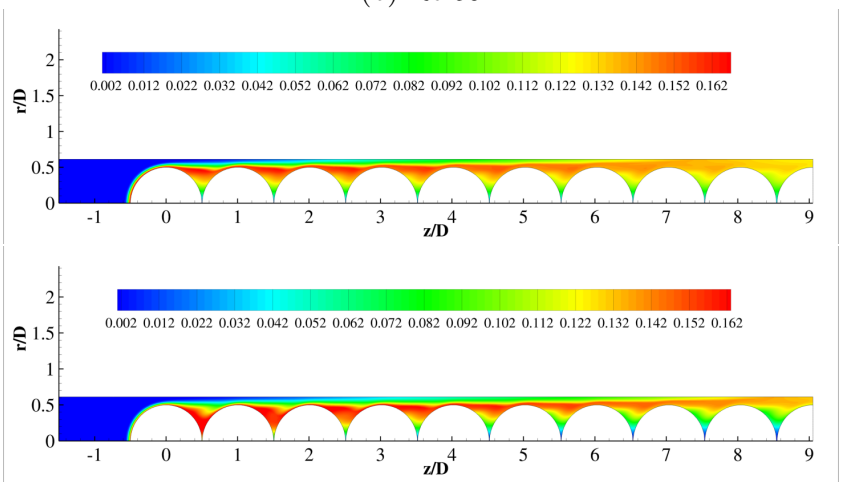


(c) Re 100

Figure 3.13: $CO_2$ contour profiles for $T_{in}$=1000K with $Y_{O_2}$=0.11 and $Y_{H_2O}$=0.074; The top subfigure in each case represents combustion *without radiation* and effect of the P-1 *radiation* model is represented by the bottom subfigure

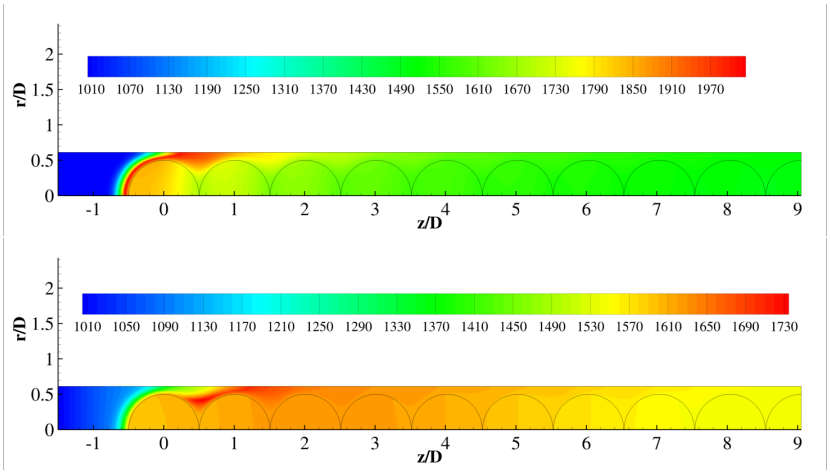


(a) Re 10

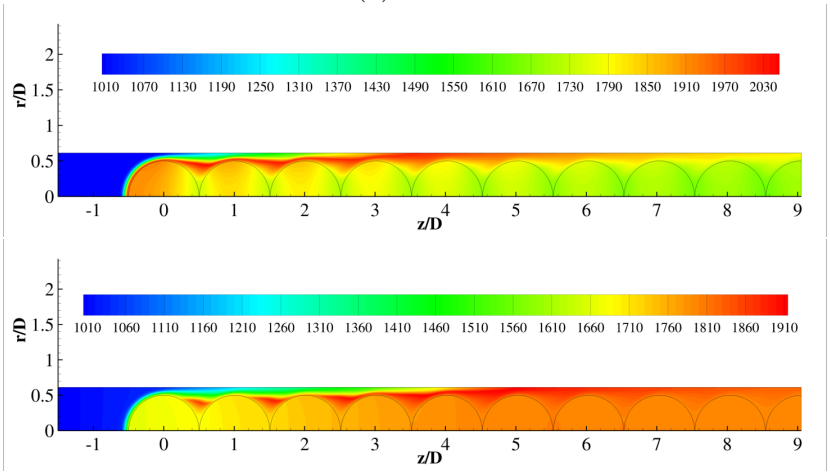


(b) Re 50

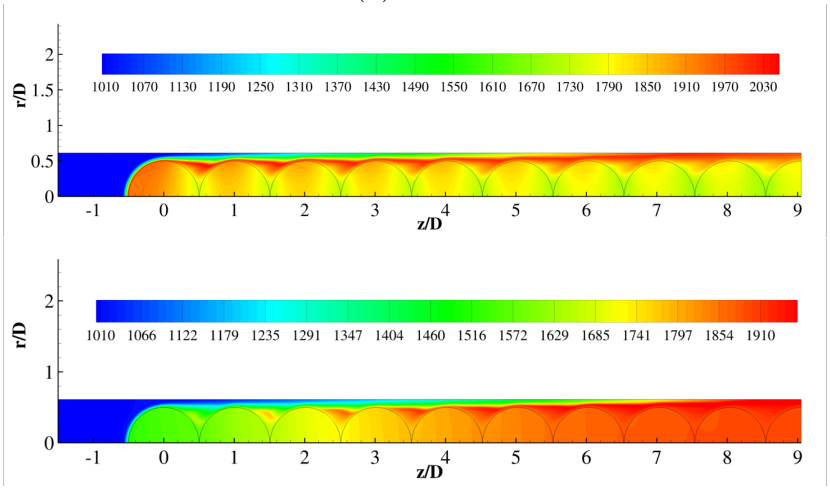


(c) Re 100

Figure 3.14: T contour profiles for $T_{in}$=1000K with $Y_{O_2}$=0.11 and $Y_{H_2O}$=0.074; The top subfigure in each case represents combustion *without radiation* and effect of the P-1 *radiation* model is represented by the bottom subfigure

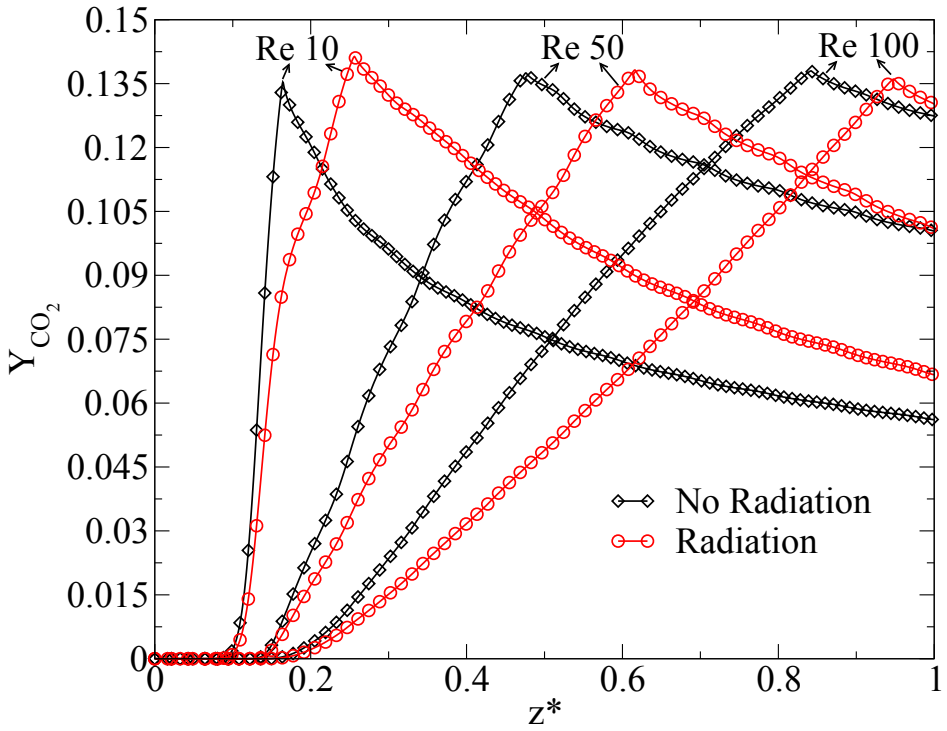


(a) $CO_2$ mass fraction($Y_{CO_2}$)

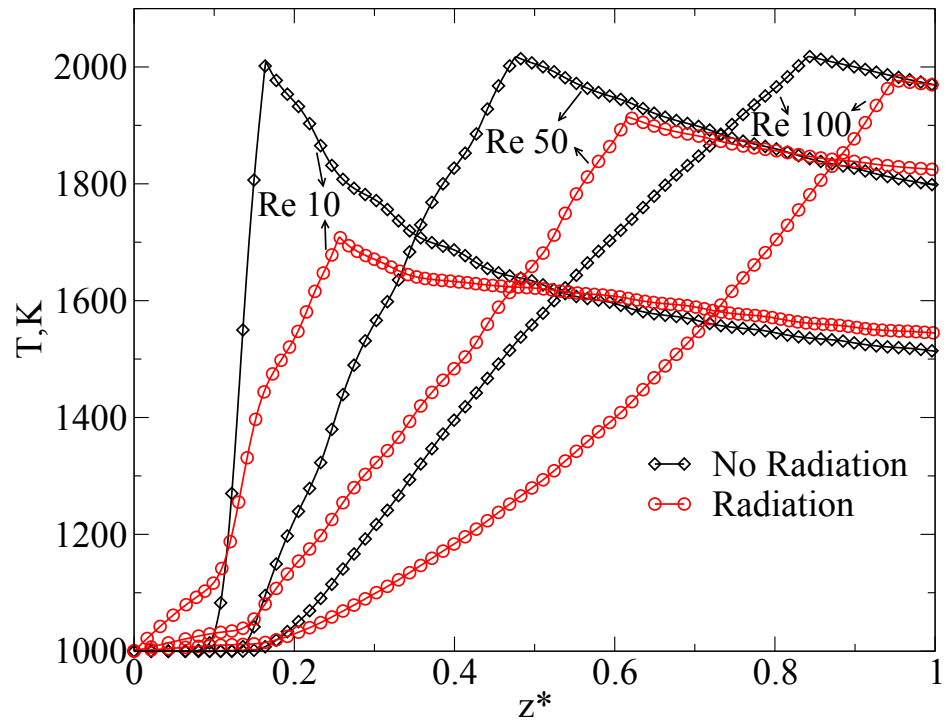


(b) Axial Temperature

Figure 3.15: Comparison of the $Y_{CO_2}$ and temperature profile along the axis for Reynolds number, $Re$ = 10, 50 and 100 at 1000K for cases with and without radiation; $Y_{O_2}$=0.11 and $Y_{H_2O}$=0.074 is taken for the inlet gas

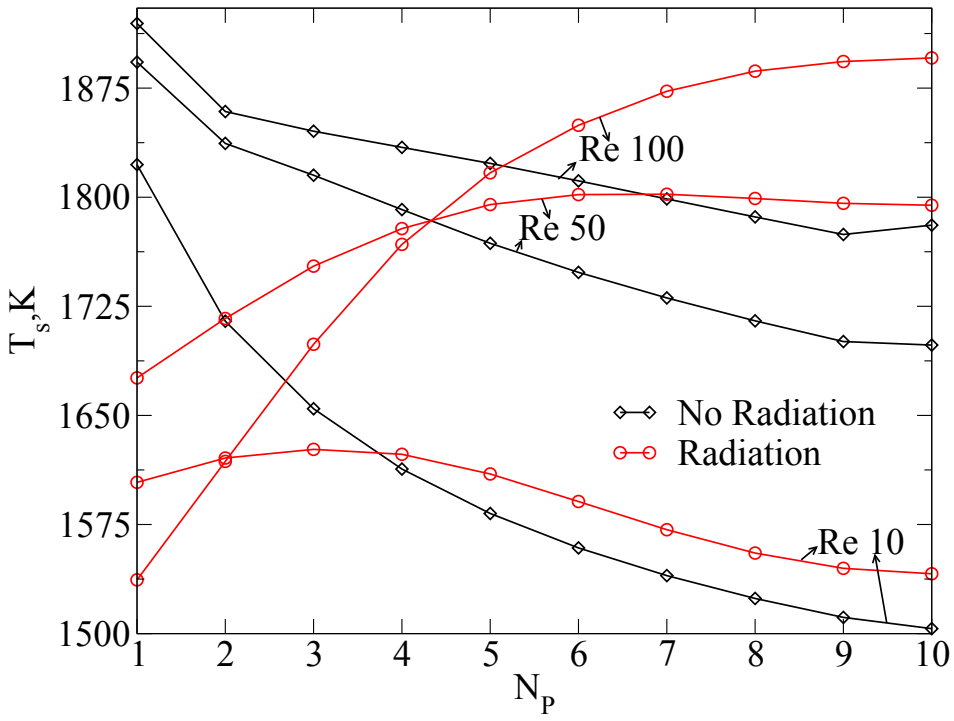


(a) Surface Temperature($T_S$)

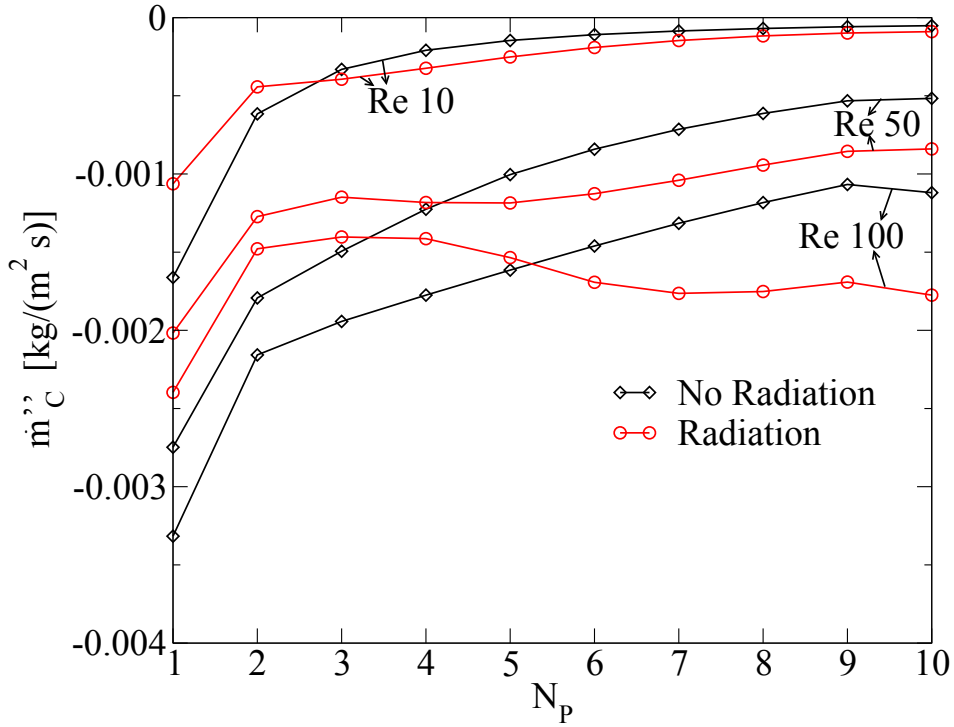


(b) Carbon Mass Flux($\dot{m_c}''$)

Figure 3.16: Comparison of carbon mass flux and temperature on the particle surface for Reynolds number, $Re$ = 10, 50 and 100 at 1000K for cases with and without radiation; $Y_{O_2}$=0.11 and $Y_{H_2O}$=0.074 is taken for the inlet gas

### 3.3.4 Combustion vs Gasification

The previous sections discuss the effect of radiation and Reynolds number during combustion and gasification inside the particle bed applicable to fixed beds. Comparison of the heat transfer and species characteristics between combustion and gasification was also of interest to us to gain deeper insight into these processes.

As expected, the axial temperatures were much higher for combustion than gasification with a 35.31% spike in temperature obtained for $Re = 100$. The surface averaged temperatures are shown in Fig.3.17 with a relatively low surface temperature obtained for gasification. Fig.3.18 shows the carbon mass flux and axial temperature profiles at $Re = 10$, 50 and 100 for combustion and gasification. The carbon mass flux was found to be quite high for combustion at the inlet of the channel with a difference of $\sim 45\%$ observed for $Re = 100$. However, the mass flux was nearly the same towards the outlet of the channel as can be seen from Fig.3.18 (a).

Fig.3.19 shows the comparison of mass fraction of $CO_2$ on the axis of the particle bed and the surface of the particles. The peak $Y_{CO_2}$ for dry air was found to be 0.295 while that for gasification was found to be 0.134. This remains same for all cases of Reynolds number. The $Y_{CO_2}$ doesn't disapper at the outlet for $Re = 10$ but remains extremely low($\sim 10^{-5}$), due to the dominant Boudouard Reaction and $Y_{O_2} = 0$. The surface averaged $Y_{CO_2}$ is higher for gasification due to the increase in the mass fraction of $H_2O$ by an enhanced reaction R4. The Lewis number in this case was also $\approx$1 as shown in Fig.3.20.

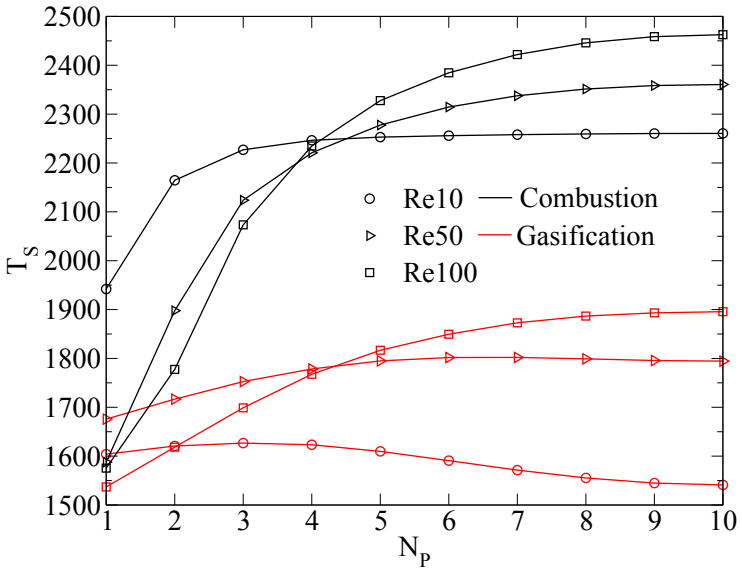


(a) Surface averaged temperature

Figure 3.17: Comparison of surface averaged temperature for combustion and gasification at Reynolds number, $Re = 10$, 50 and 100 at 1000K

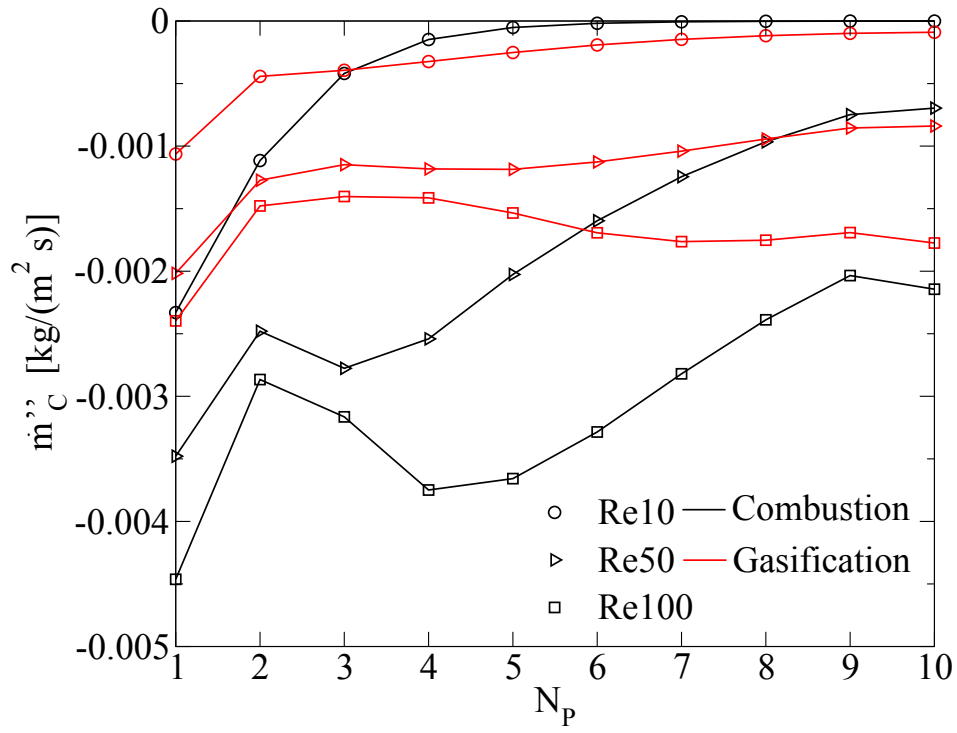


(a) Surface averaged carbon mass flux($\dot{m}_c''$)

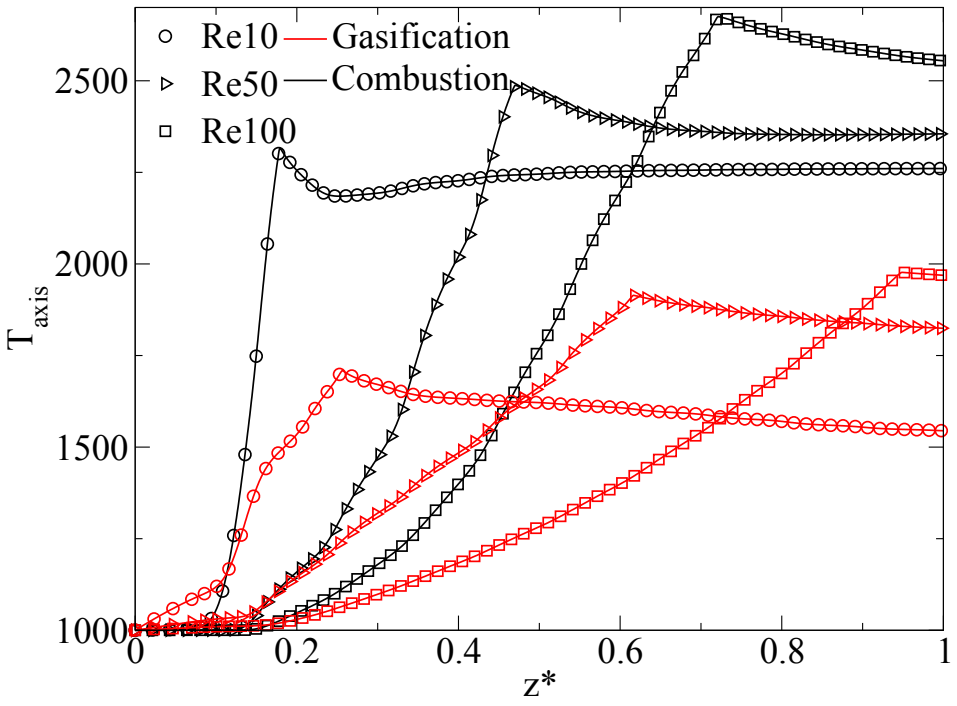


(b) Axial Temperature

Figure 3.18: Comparison of $\dot{m}_c''$ and axial temperature for combustion and gasification at Reynolds number, $Re$ = 10, 50 and 100 at 1000K

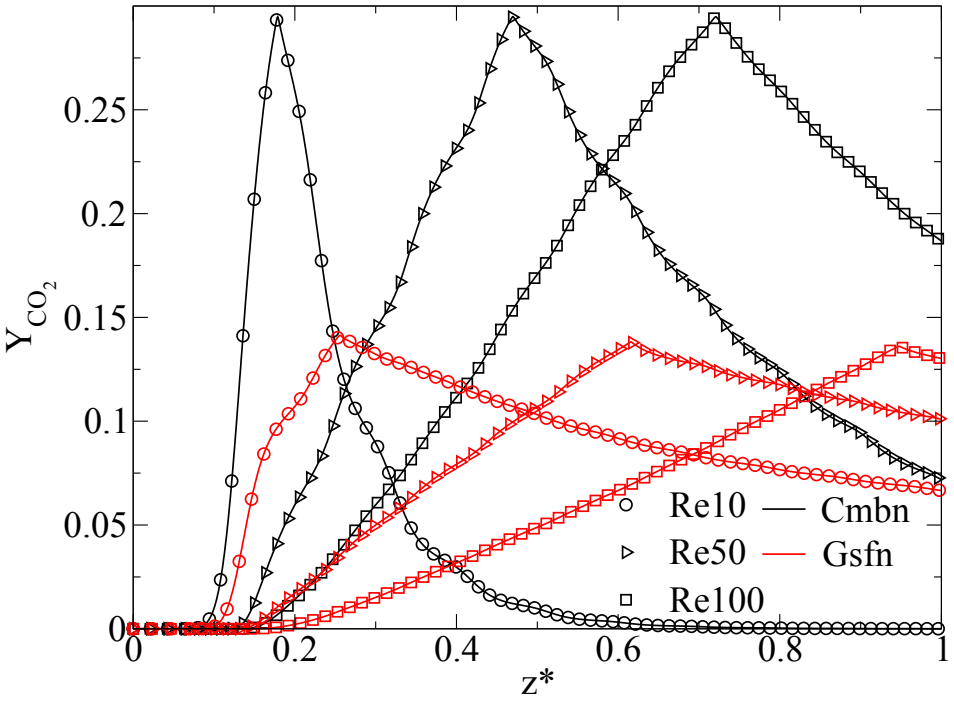


(a) $Y_{CO_2}$ along the axis

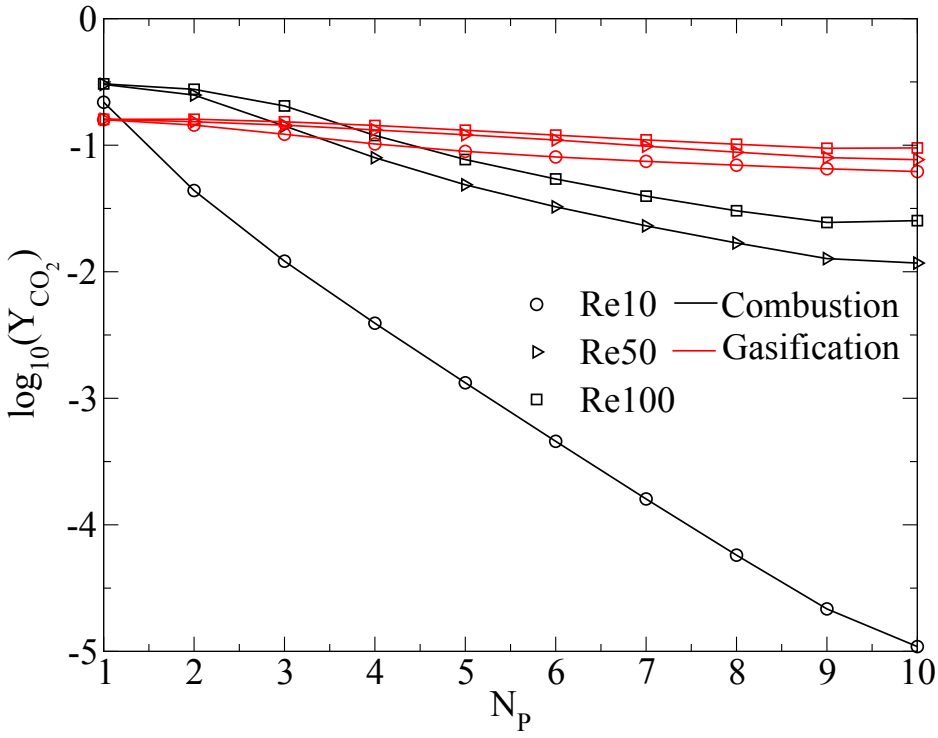


(b) Surface averaged $Y_{CO_2}$

Figure 3.19: Comparison plots for $Y_{CO_2}$ along the axis and surface averaged $Y_{CO_2}$ for combustion and gasification at Reynolds number, $Re = 10$, 50 and 100 at 1000K

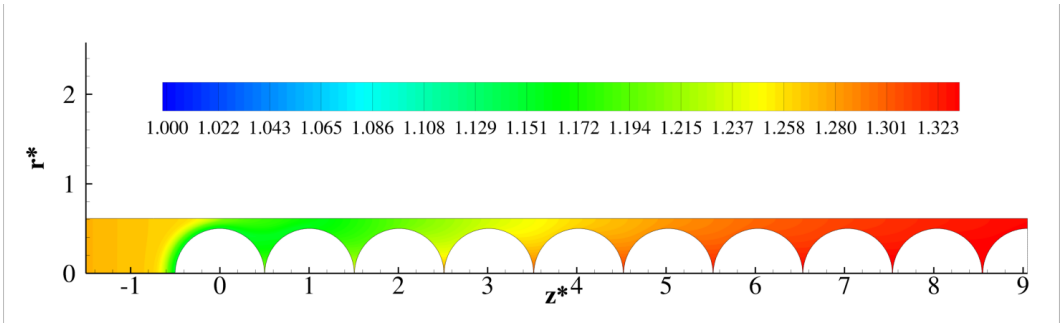


(a) Re 10

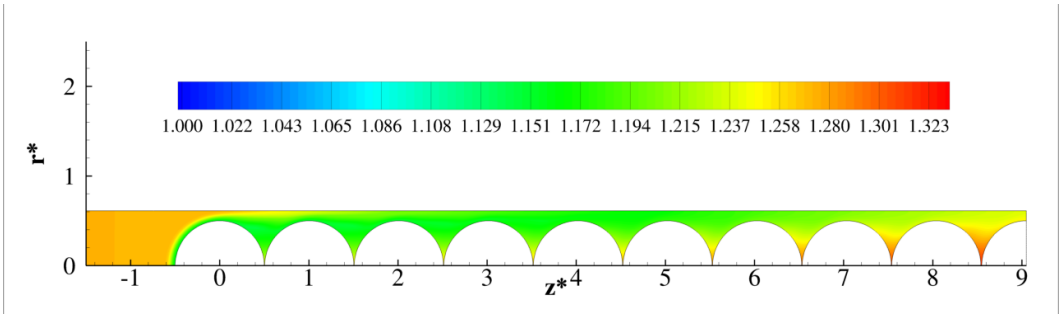


(b) Re 50

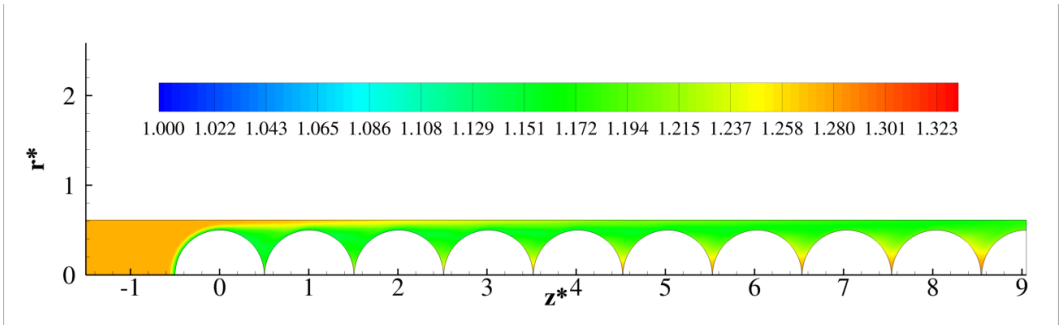


(c) Re 100

Figure 3.20: Contour profiles for Lewis number($Le$) with $Y_{O_2}$=0.11 and $Y_{H_2O}$=0.074; The P-1 *radiation* model has been considered for these cases

## 3.4 Summary

This chapter highlights the differences in the species and temperature characteristics, using heat transfer in solids compared with particles, where heat transfer inside solids is neglected. The chapter, then, also aims to study the characteristics of combustion and gasification processes within particle beds. The results can be

summarized as follows:

- Comparisons of the axial temperature between particles and solids generated similar profiles with a maximum 2.5% difference in the peak temperature at $Re = 100$, with solids to be around 2675 K while for particles, it was 2700K. The peak mass fraction of $CO_2$ was 0.295 and found to be same for the particles and solids at all Reynolds number.

- Surface averaged temperature and carbon mass flux were found to be essentially the same(small scale of decrease) between solids and particles at each Reynolds number, except $Re = 50$ which saw an abrupt decrease in temperature at $N_P = 2$.

- The peak $Y_{CO_2}$ for dry air along the axis was found to be 0.295 while that for gasification was found to be 0.134. The carbon mass flux was found to be quite high for combustion at the inlet of the channel with a difference of $\sim 45\%$ observed for $Re = 100$.

- Lewis number was found to be 1 for the domain and Damkohler number was used to comment on the transport regimes for different Reynolds number.

- From an engineering point of view, the temperature of the particle is lower at the start of the channel by 50 - 70 K during combustion. However, the particle temperature inside the column is much higher as compared to the surface temperature and goes up to a maximum value of 180 K for $Re = 100$.

- As an engineering relevance, it should be mentioned that $Y_{CO_2} = 0.072$ for $Re = 50$ and $Y_{CO_2} = 0.18$ for $Re = 100$ at the end of the particle row during combustion. This is suggestive of that fact that the Boudouard reaction remains incomplete for these cases unlike $Re = 10$. This calls for the need of a longer row of particles for $Re = 50$ and 100.

# Chapter 4

# From non-spaced to spaced

## 4.1 Introduction

Our previous studies were aimed at studying chemically reacting partciles within dense particulate media and understand the flow dynamics, heat trasfer charcteristics and species properties applied to a fixed bed reactor. This led to some interesting findings and conclusions as described in the previous chapters. This present chapter is aimed at understanding the kinetics and heat transfer properties within a fluidized bed reactor. Fluidized beds have been used for catalytic and gas-solid reactions in the industial reactors for more than 50 years. Despite the longevity of its use, the properties affecting the performance have been seldom understood. As a number of uncertanities are associated with scale-up and modeling of moving beds, CFD is a good tool for understanding the physical and chemical phenomena occuring within the reactor. However, using CFD to predict the species and heat transfer characteristics has received very little to negligible attention in literature. It is quite difficult to properly simulate a fluidized bed reactor as suggested by works[95, 96, 97]. Researchers have attempted to understand the fluid flow dynamics within a fluidized bed reactor[98, 95]. These studies aim at studying the bulk fluid dynamics within the fludiized bed with focus upon the particle sizes present in the gasifier and the drag models such as Syamlal–O'Brien, Gidaspow, and Wen–Yu drag models. Zimmermann and Taghipour [99] used CFD to simulate flow dynamics and species characteristics for fluid catalytic cracking within a fluidized gasifier. Drag models suggested by Syamlal and O'Brien and Gidaspow were modified to correctly simulate the bubbling phenomena. Similarly,Behjat et al. [100] attempted to study the flow dynamics and heat transfer within the fluidized bed focussing on the bulk chracteristics of the reactor. However, studying the flow, heat transfer and species

characteristics within a small row of particles could provide valuable information and understanding of such properties can be applied to fluidized beds.

## 4.2 Model Setup

An illustration of the reactor scheme is shown in Fig.4.1 and the principal scheme of the computational domain has been represented in Fig.4.2. To attempt the study of the conversion processes within fluidized beds, spacings were introduced between the particles into our previous arrangement to portray the freely moving solid particles. The spherical coal char particles with a diameter, $d_p = 0.02$ m were placed in a row with equal gaps between each other. The spacing of $d_p$ and $0.5d_p$ has been taken to study two different arrangements as shown in Fig.4.3 and Fig.4.4. The properties of char particles are taken as: specific heat of 710 $J/kg - K$, thermal conductivity of 0.2 $W/m - K$ and density of 1500 $kg/m^3$. The study is performed for two different composition of the inlet gas:- a) $Y_{O_2} = 0.233$ and $Y_{H_2O} = 0.001$ and b) $Y_{O_2} = 0.11$ and $Y_{H_2O} = 0.074$.

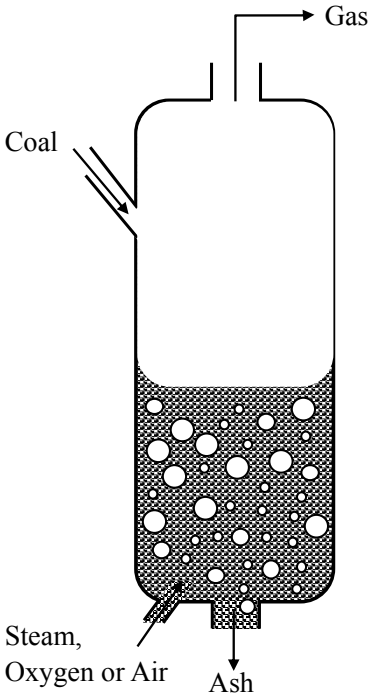


Figure 4.1: Illustration of the reactor scheme[3]

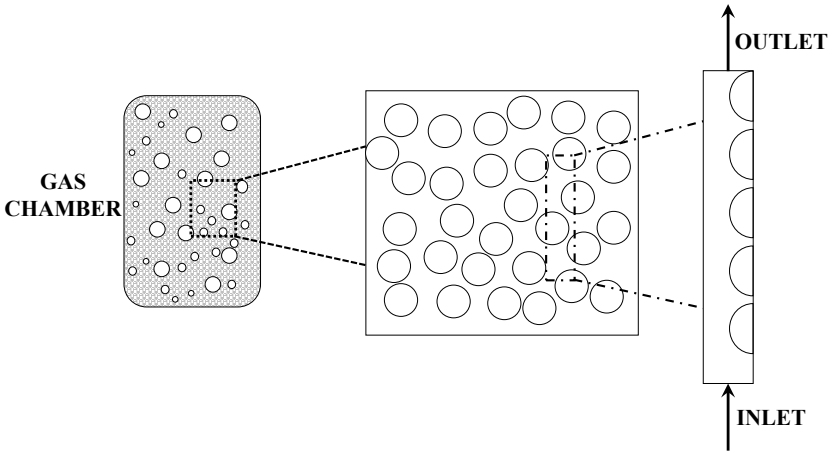


Figure 4.2: Representation of the principle scheme of the computational domain

### 4.2.1 Assumptions

To proceed with the description of the mathematical CFD-based model, several assumptions are introduced in order to solve the problem.

1. The consumption time of the particle is always large compared to the convective and diffusion time scales for the gas phase. Hence, pseudo-steady-state apprach has been assumed.
2. The gas flow was treated as an incompressible ideal gas.
3. The representative element is considered to be axysymmetrical with a symmetrical gasflow.
4. The porosity of the particles is not taken into account which results in neglecting the intraparticle diffusion. The surface reaction model is used to simulate the interaction between reacting solid surface and gas phase.
5. The particles consists of carbon only. In particular, the volatilization of the particles is not included due to the steady-state character of the model.
6. The radiation of the gas phase is modeled using the P-1 model.
7. The buoyancy effect is neglected.

### 4.2.2 Governing Equations and Boundary Conditions

The governing equations and chemistry modeled for this configuration as explained in Section 2.1.2 and Eqns. R1 - R7.

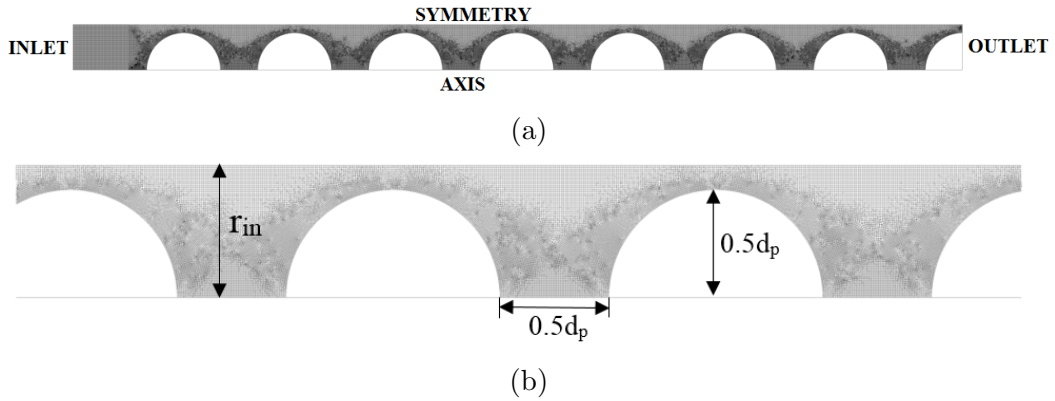


Figure 4.3: (a) Schematic representing the meshed computational domain, where spacing between the particles = $0.5d_p$, (b) Zoomed-in view of the schematic illustrating the geometry of the domain;

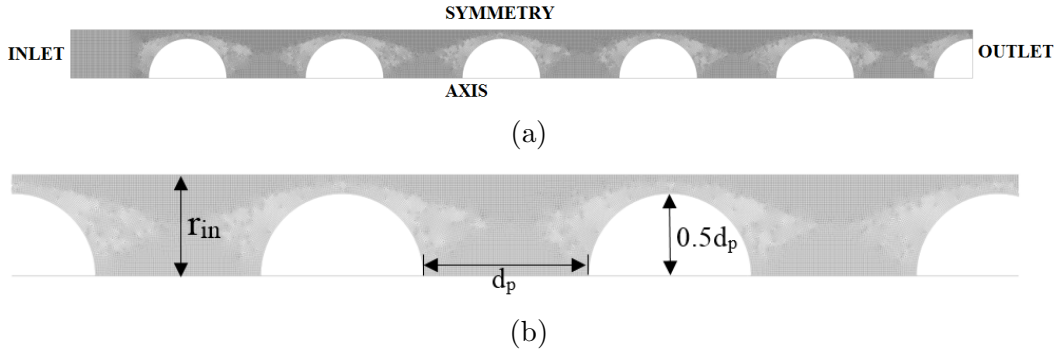


Figure 4.4: (a)Schematic representing the meshed computational domain, where spacing between the particles = $d_p$, (b) Zoomed-in view of the schematic illustrating the geometry of the domain;

## 4.3 Results

We tried to study of combustion and gasification inside a channel of spaced row of particles($0.5d_p$ and $d_p$) and compared the species and heat transfer characteristics for these models. The results have been divided into two sections:- Combustion: $Y_{O_2} = 0.233$ and $Y_{H_2O} = 0.001$ and Gasification: $Y_{O_2} = 0.11$ and $Y_{H_2O} = 0.074$. The fluid flow, energy and species characteristics were also plotted and compared between combustion and gasification for both cases of particle spacings. Further, illustrations have been made made to compare these results within non-spaced particle arrangements.

### 4.3.1 Combustion

Fig.4.5 shows the comparison of the $CO_2$ contours for two arrangements of particles during combustion. Radiation was included in this study. We see that there is not much difference in the contours for $Re = 10$ for the two arrangements. Though the maximum $Y_{CO_2} = 0.345$ remains the same for all Reynolds number, we notice differences in the contours for $Re = 50$ and $Re = 100$.

In the case of $Re = 50$ and $0.5d_p$ spacing, the flame occupies most of the space between the first two particles avoiding their surfaces. Between the second and third particle, the flame is compratively weaker and moves out of the channel eventually. The length of the flame in the channel is the same for both the spacings($0.5d_p$ and $d_p$). For $d_p$, as the space is much wider between the particles, the flame occupies most of the gap due to availability of free space, $O_2$ and CO between the particles. The CO diffusing out from the particle surfaces from either side readily react with the $O_2$ from the inlet gas resulting in the thick flame formation in the gap between the particles. A similar effect can be seen in the case of $Re = 100$ with a longer flame sheet in the channel due to the increased transport of the inlet gas within the channel.

Fig.4.6 represents the temperature contour profiles for the two different geometries. The peak temperature remains the same for $Re = 10$ for both cases with similar temperature contours for the models. Increasing the Reynolds number results in interesting chemical phenomena within the bed. We had observed in Chapter3 that radiation has a significant impact on the temperature profiles with the channel. It results in a decrease in the temperature of the particles located near the inlet, due to transfer of heat due to radiation. This heat transfer heats up the cold inlet gas which ends up reacting with the carbon particles in the interior of the channel resulting in significant increase in the temperature downstream of the channel. However, we do not observe that phenomena for $Re = 50$ for $0.5d_p$, but can be observed for $Re = 100$. For the case of $d_p$ spacing, there is no such effect of P-1 radiation model. Another interesting observation which can be made from contours of $d_p$ spacing is that the peak temperature is limited to a small region within the flame sheet which was observed for Fig.4.5(b) and (c).

We were interested to study the total temperature and mass fraction of $CO_2(Y_{CO_2})$ along the axis for the non-spaced models studied in the previous chapter and the spaced models in this chapter. Comparison plots of the axial temperature and $Y_{CO_2}$ for different Reynolds number have been shown in Fig.4.7. There were quite a few notable observations made as a result of this study. We start our discussion of these results with mass fraction of $CO_2$. We see that the peak $Y_{CO_2}$ is higher for the

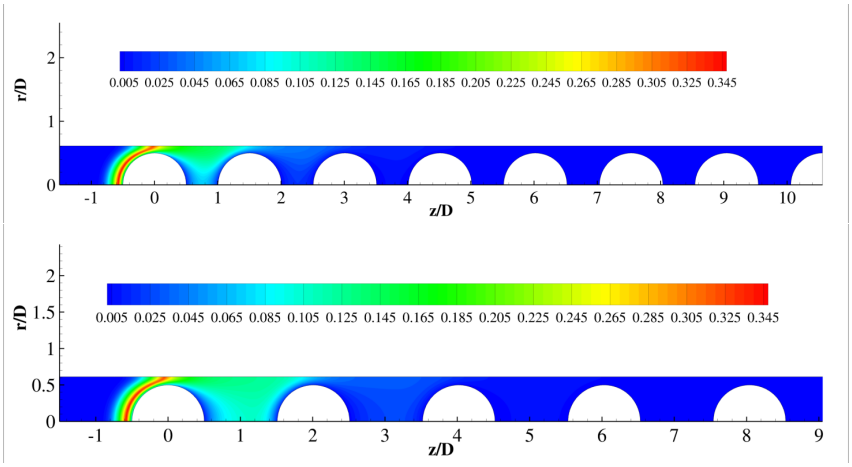


(a) Re 10

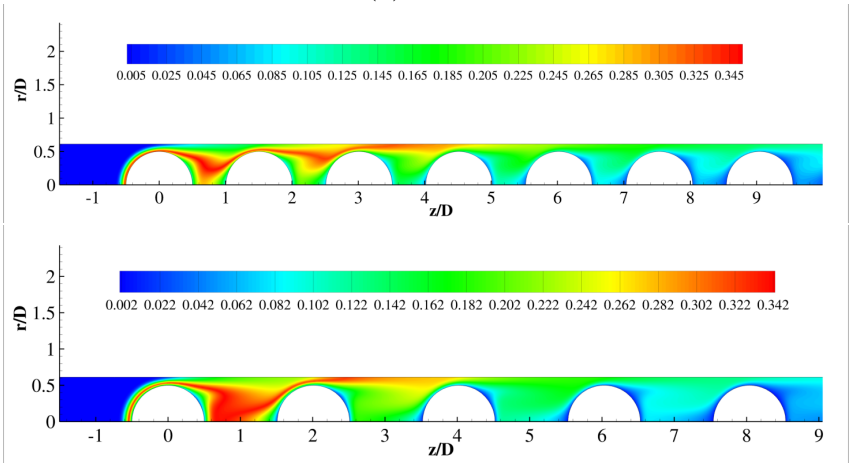


(b) Re 50

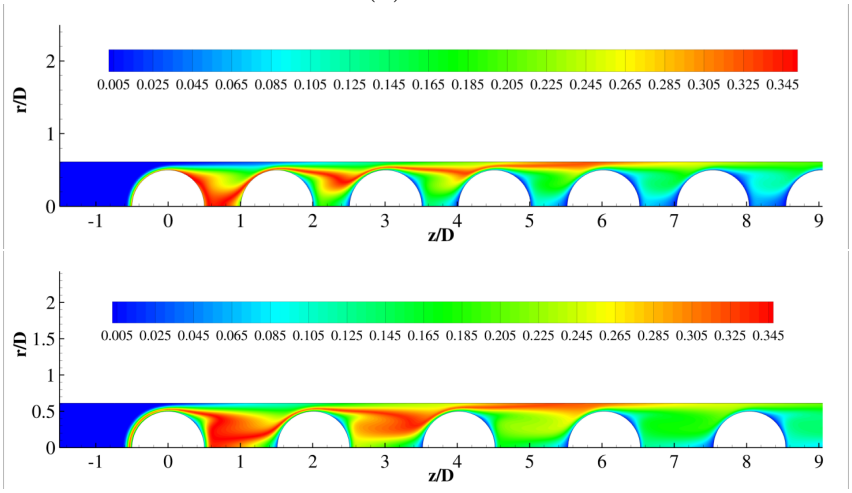


(c) Re 100

Figure 4.5: 2D contour plot representing $CO_2$ for arrangement of particles with '$0.5d_p$' and '$d_p$' separation where $Y_{O_2} = 0.233$ and $Y_{H_2O} = 0.001$ for the inlet gas; P-1 radiation model was included in these simulations

spaced models than that observed for the solid particles arrange without spaces. The value is approximated to be 0.323 for the former and 0.295 for the latter, as mentioned before. The right column of Fig.4.7 represents the comparison plots for the axial temperature. We see that the peak temperature along the axis increases with increase in spacing between particles, with a shift in the peak position downstream of the channel. The maximum increase was observed for $Re = 10$ of 25% in the peak axial temperature between non-spaced and spaced simulations($d_p$).

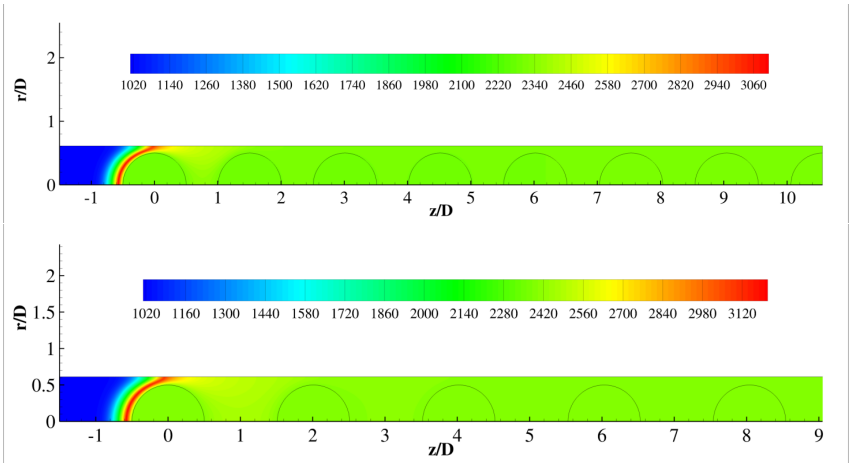


(a) Re 10

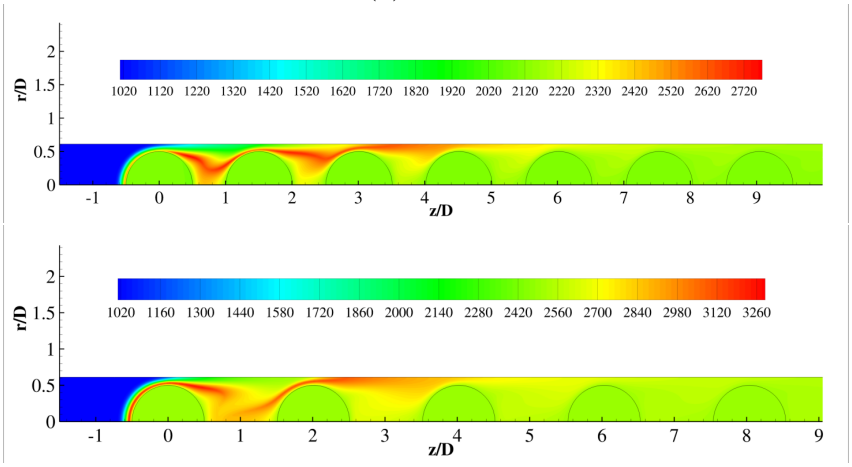


(b) Re 50

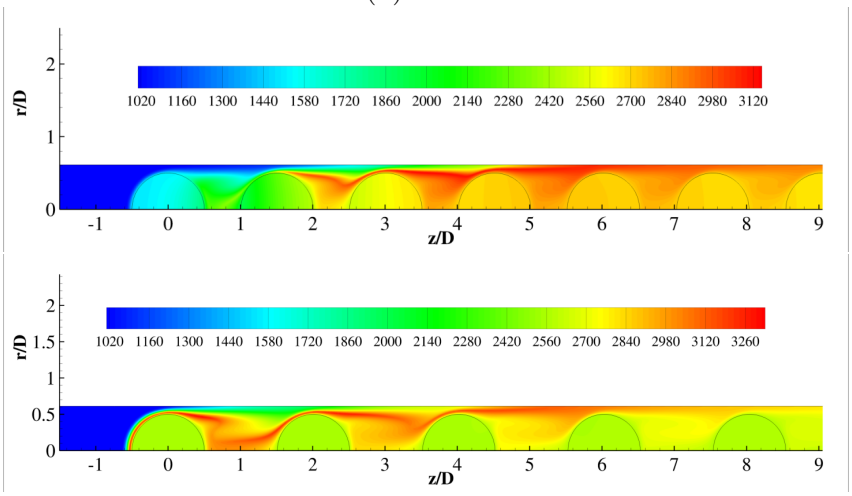


(c)Re 100

Figure 4.6: 2D contour plot representing temperature for arrangement of particles with '$0.5d_p$' and '$d_p$' separation where $Y_{O_2} = 0.233$ and $Y_{H_2O} = 0.001$ for the inlet gas; P-1 radiation model was included in these simulations

### 4.3.2 Gasification

This section presents the results for the spaced simulations in both the models for an inlet composition, $Y_{O_2} = 0.11$ and $Y_{H_2O} = 0.074$ at 1000K. This commonly represents a gasification ambience inside bed reactors. Fig.4.8 represents the $CO_2$ mass fraction contours for arrangement of particles with both the cases of separation($0.5$'$d_p$' and '$d_p$'). There is no continuous sheet visible for the $Re = 10$ for spacing of $0.5d_p$ and a thin layer of the peak $Y_{CO_2}$ is present very close to the particle surface. For the case of $Re = 50$, the flame sheet is very close to the surface of the particle and extends downstream of the channel. Towards the end, we see a diffused zone of maximum $CO_2$ without any definite flame sheet. There is a formation of long flame sheet for $Re = 100$ which extends upto the end of the channel.

For spacing of $d_p$, we can see a very short flame sheet over the first particle for $Re = 10$. The maximum $Y_{CO_2}$ was found to be 0.182, which is quite less than that found for dry-air gas inflow, $Y_{CO_2} = 0.345$, in both the cases. The flame sheet is thicker than that observed during combustion. Fig.4.9 shows the temperature contours obtained for the gasification reactions. We see that the temperature of the gas flow on the leading side of the particle is much lower than the trailing side. This is because of significant heat transfer to the cold inlet gas and there is not much air flow in the gap between the particles. In both the cases of $0.5d_p$ and $d_p$, this effect is limited to first three particles after which the temperature within the channel becomes uniform towards the interior of the channel.

Fig.4.10 shows the comparison of the axial temperature and $Y_{CO_2}$ for non-spaced and spaced($0.5d_p$ and $d_p$) models during the gasification reactions. The peak $Y_{CO_2}$ along the axis was 0.163 greater than that obtained for particle without spacings, $Y_{CO_2} = 0.142$. The temperature along the axis brought out some interesting conclusions for this case. For $Re = 10$, the peak temperature for $d_p$ spacing was 2000K was much higher than $0.5d_p$. For fixed beds, the peak was around 1700K which is 17.6% lower than the peak temperature observed for $d_p$ spaced results.

These results when applied to fixed and fluidized beds suggest that heat transfer inside a fluidized bed is much better than that for a fixed bed and the mass fraction of $CO_2$ is also observed to be higher for both cases of combustion and gasification within a fluidized bed.

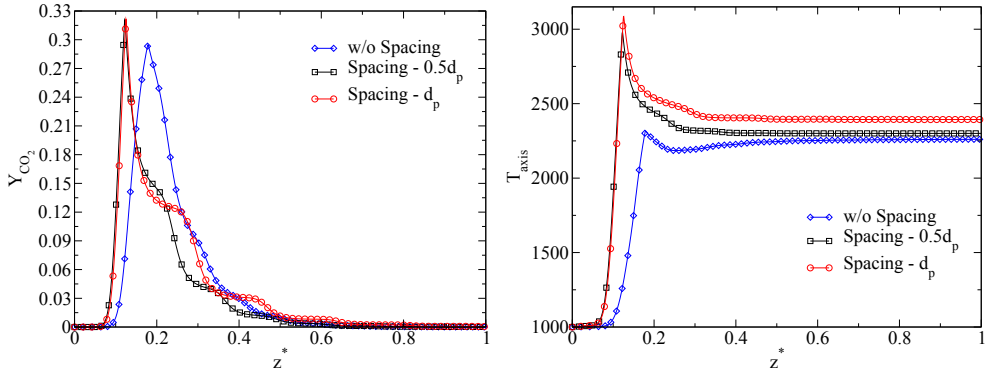


(a) Re 10

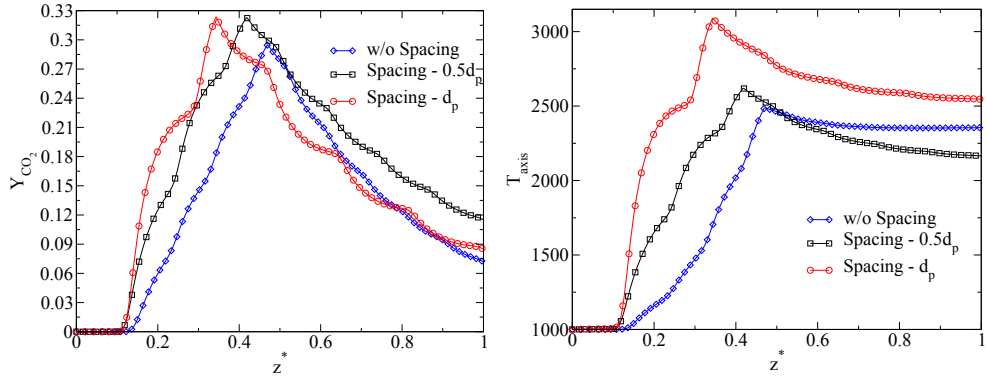


(b) Re 50

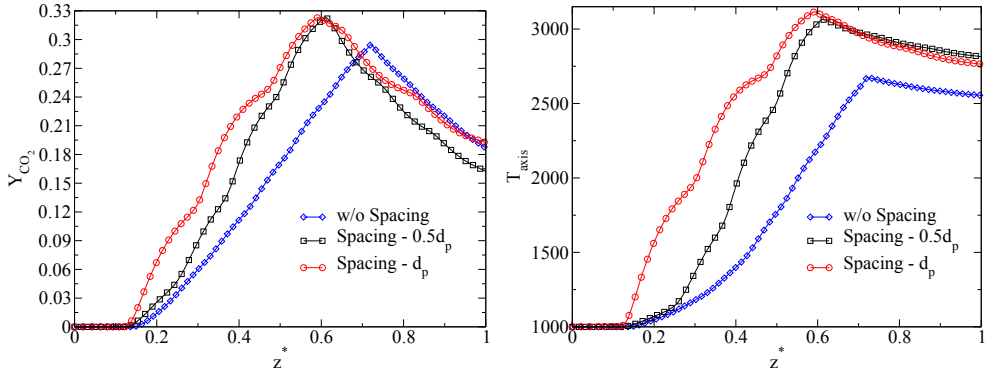


(c) Re 100

Figure 4.7: Comparison of the axial temperature and $Y_{CO_2}$ for non-spaced and spaced($0.5d_p$ and $d_p$) models. The composition of the inlet gas was taken as $Y_{O_2} = 0.233$ and $Y_{H_2O} = 0.001$ and $T_{in} = 1000$K; P-1 radiation model was included in these simulations

### 4.3.3 Combustion vs Gasification

Fig.4.11 illustrates the comparisons of carbon mass flux and surface averaged temperature at different Reynolds number for both $0.5d_p$ and $d_p$ spaced beds during combustion and gasification. The column on the left represents the model with $0.5d_p$ spacing while that on the right represents the case with $d_p$ spacing. Fig.4.11(a) shows the carbon mass flux for the participating solid particles with spacing of $0.5d_p$. As expected, the carbon mass flux is found to be minimum for $Re = 10$ and maximum for $Re = 100$. The carbon mass flux decreases as we move downstream of the channel for $Re = 10$ and $Re = 50$. However, for $Re = 100$ increases till the thrid particle and then gradually decreases till the outlet of the channel. The result of this effect can be seen in Fig.4.11(c), where the surface averaged temperature for the solid particle is the minimum near the inlet of the channel. We see that the effect of the P-1 radiation model is prominent in the case of $Re = 100$. The temperature drops significantly near the inlet and then increases downstream, which is a known phenomena.

However, for gasification, there is no observed effect of radiation and the carbon mass flux is quite low compared to the combustion, as seen in Fig.4.11(b). The carbon mass flux was observed to be higher for the $d_p$ spaced beds and radiation did not lead to a decrease in the carbon mass flux at the inlet of the channel. The carbon mass flux followed a steady trend, *i.e.*, it increases with Reynolds number and decreases along the channel. Similarly, the particle temperature increases with the Reynolds number and decreases as move downstream of the channel, as illustrated in Fig.4.11(d).

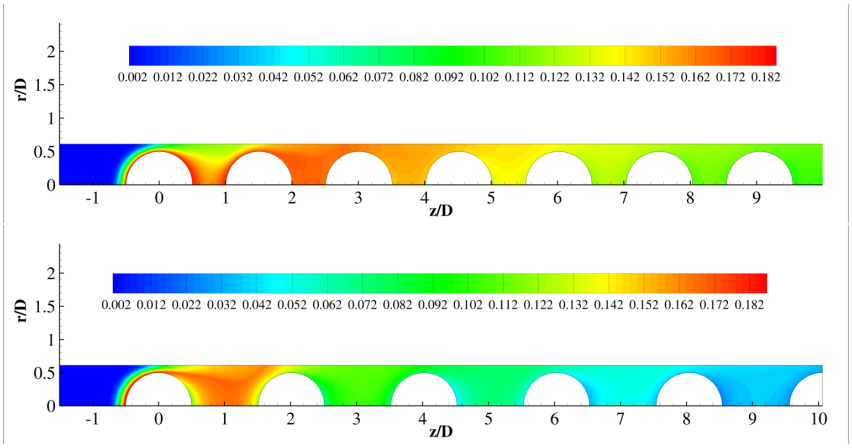


(a) Re 10

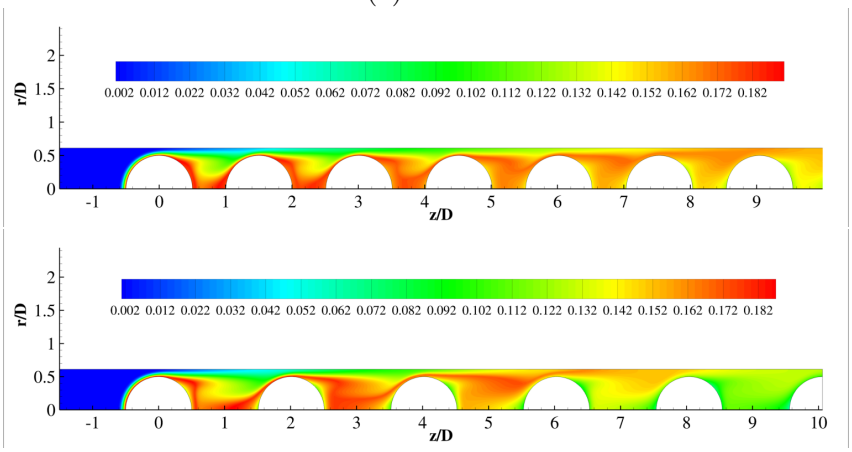


(b) Re 50

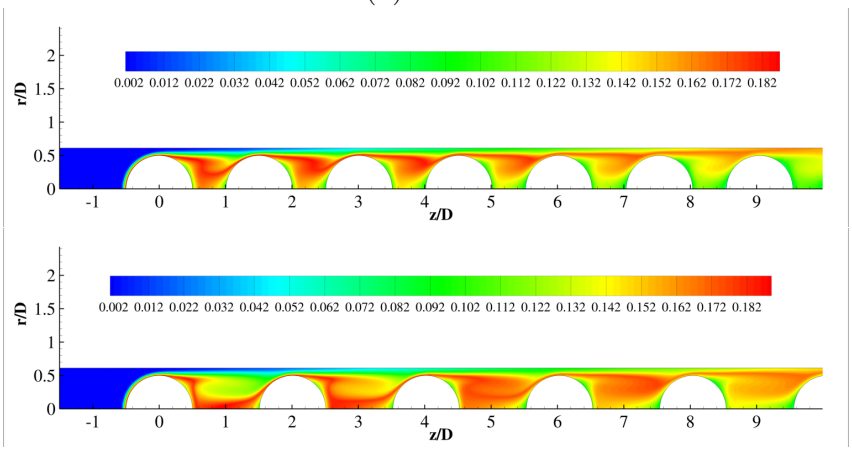


(c) Re 100

Figure 4.8: 2D contour plot representing $CO_2$ for arrangement of particles with '$0.5d_p$' and '$d_p$' separation where $Y_{O_2} = 0.11$ and $Y_{H_2O} = 0.074$ for the inlet gas; P-1 radiation model was included in these simulations

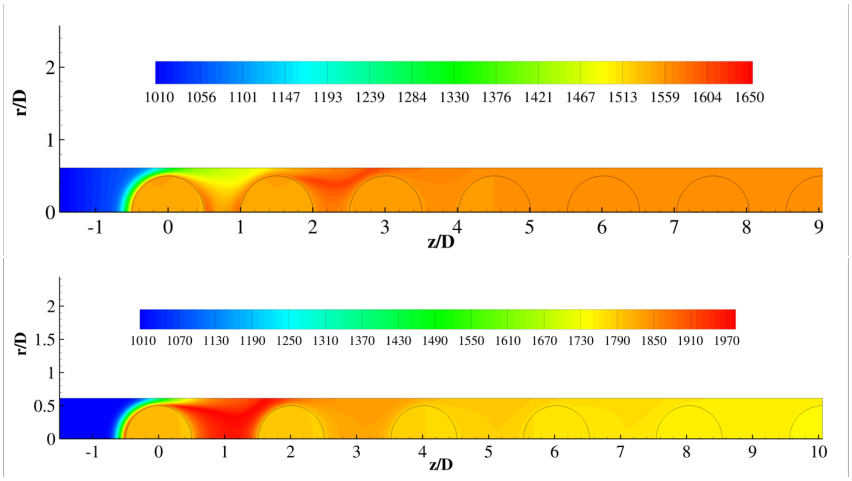


(a) Re 10

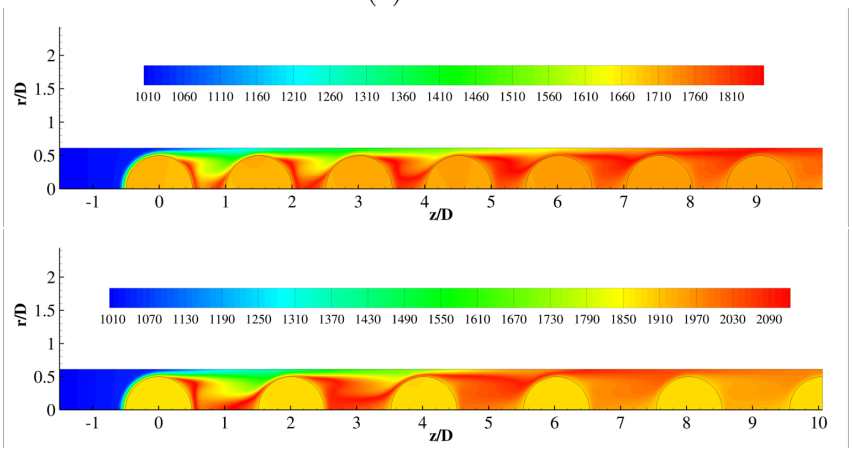


(b) Re 50

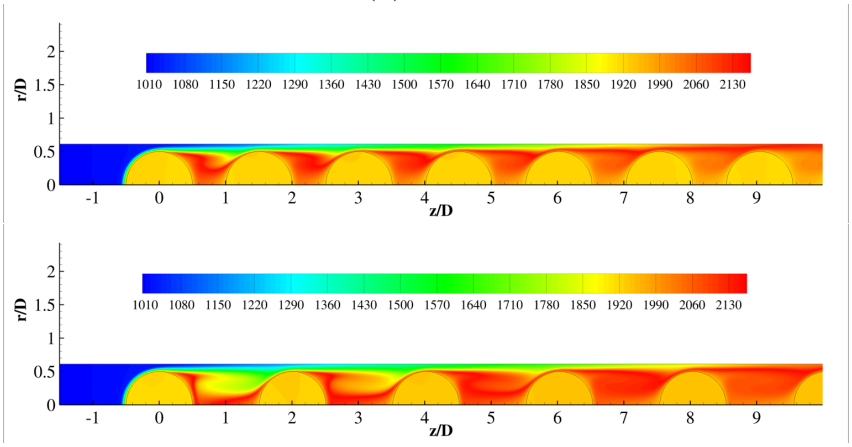


(c)Re 100

Figure 4.9: 2D contour plot representing temperature for arrangement of particles with '$0.5d_p$' and '$d_p$' separation where $Y_{O_2} = 0.11$ and $Y_{H_2O} = 0.074$ for the inlet gas; P-1 radiation model was included in these simulations

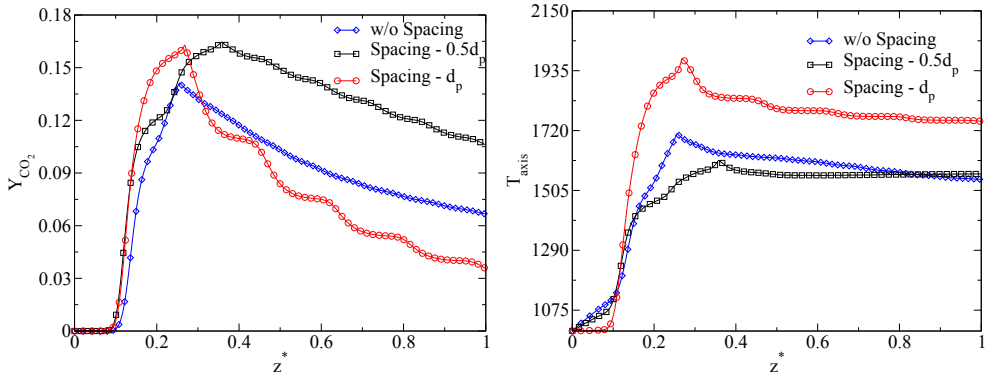


(a) Re 10

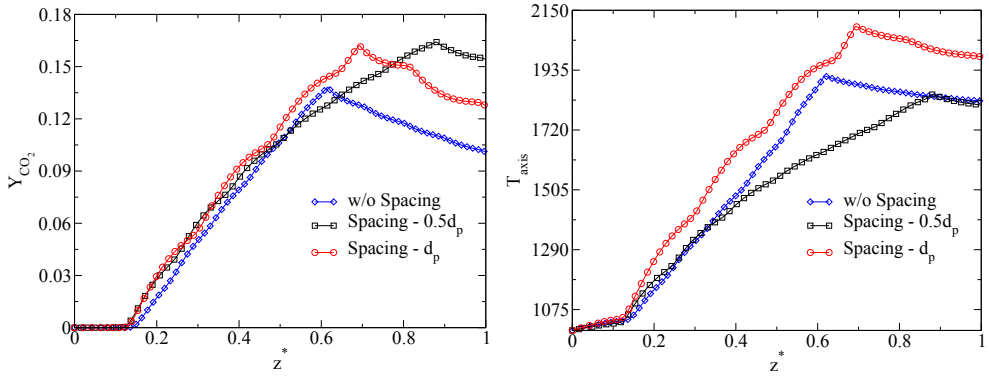


(b) Re 50

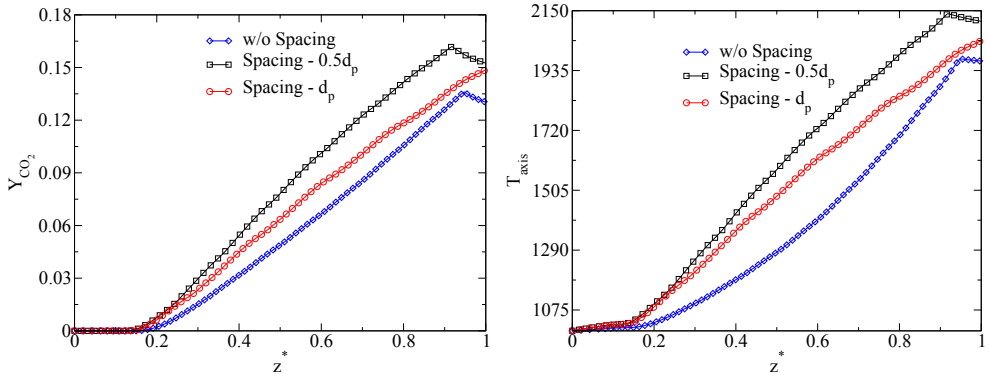


(c) Re 100

Figure 4.10: Comparison of the axial temperature and $Y_{CO_2}$ for non-spaced and spaced($0.5d_p$ and $d_p$) models. The composition of the inlet gas was taken as $Y_{O_2} = 0.11$ and $Y_{H_2O} = 0.074$ and $T_{in} = 1000$K; P-1 radiation model was included in these simulations

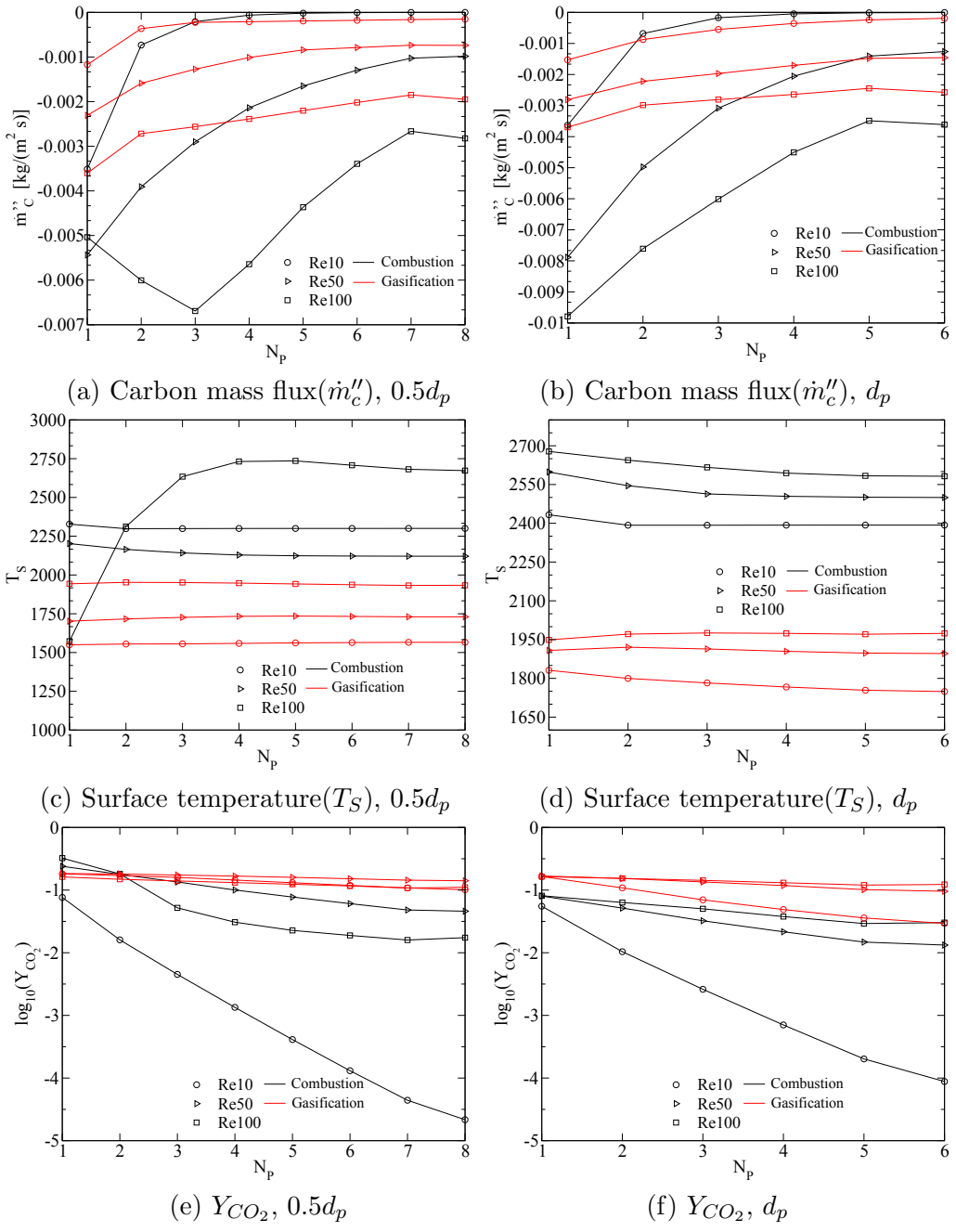


(a) Carbon mass flux($\dot{m}_c''$), $0.5d_p$

(b) Carbon mass flux($\dot{m}_c''$), $d_p$

(c) Surface temperature($T_S$), $0.5d_p$

(d) Surface temperature($T_S$), $d_p$

(e) $Y_{CO_2}$, $0.5d_p$

(f) $Y_{CO_2}$, $d_p$

Figure 4.11: Comparison plot for carbon mass flux, surface temperature and mass fraction of $CO_2$ on the surface of reacting char particles during combustion and gasification. *This case accounts for models with spacing of '$0.5d_p$' in the left column and '$d_p$' in the right column between the particles*

## 4.4 Summary

This chapter attempted to study the heat transfer, fluid flow and species characteristics within spaced beds of particles, applicable to fluidized bed reactors. Recent studies have concentrated their focus on the bulk properties of the reactor with a few studies based on the particle resolved simulations. Keeping this mind, we performed simulations using a 2D geometry, which was modified to take into account for the free moving particles within a fluidized bed. Combustion and gasification processes were studied and distances between the particles were kept at $0.5d_p$ and $d_p$. The results can be summarized as follows:-

- During combustion, the peak $Y_{CO_2}$ was observed to be 0.323 for spaced simulations which was definitely higher than that observed for fixed beds of 0.295. Also, we noted a huge increase of 15 - 25% in the peak axial temperature for fluidized beds at different Reynolds number.

- The peak $Y_{CO_2}$ along the axis was 0.163 and a 15% maximum increase in the peak temperature was observed at $Re = 10$.

- The flame penetration is much less for fluidized reactor beds as compared to fixed beds.

- As an engineering relevance, it should be noted that the mass flux of carbon from the surface decreases by $5 \times 10^{-3}\,\mathrm{kg/m^2{-}s}$ at the exit of the particle row during combustion, for all cases of Reynolds number for a higher spacing. However, the carbon mass flux decreases by only $1 \times 10^{-3}\,\mathrm{kg/m^2{-}s}$ during gasification.

- From an engineering point of view, it can be said that the surface temperature of the particle along the column observes a maximum change of 50 K in fluidized reactor beds within a length of 5 particles.

It was, hence, concluded that fluidized bed reactors have a higher heat transfer and species characteristics compared to fixed beds due to presence of spacing between the particles. Fixed bed creates dead zones between the particles which constrain the entry or flow of the inlet gas into these zones. Hence, there is a restricted increase in $Y_{CO_2}$ and temperature between the particles.

# Chapter 5

# Conclusions

This work attempts to develop a 2D model to approximate a 3D model of a fixed bed gasifier in order to save computational time and resources for future simulations. Comparisons were made during combustion at $T_{in} - 1000K$ and composition of the inlet gas was taken to be:-(i) $Y_{O_2} = 0.233$ and $Y_{H_2O} = 0.001$ during combustion and $Y_{O_2} = 0.11$ and $Y_{H_2O} = 0.0074$ during gasification. Our findings states:-

- Comparisons were made between the 2D and 3D models during combustion at $T_{in} - 1000K$ and composition of the inlet gas was taken as $Y_{O_2} = 0.233$ and $Y_{H_2O} = 0.001$.
  - The velocity profiles for the two models were in very good agreement with each other with a maximum difference of 8.33% for cold run.
  - Axial $Y_{CO_2}$ and temperature were also compared for the two models and plots showed excellent agreement with a maximum difference 7.46 % between the peak temperatures.
  - $Y_{CO_2}$ between the 2D and 3D model was found to be minimal with a maximum difference of 5.82% observed at $Re = 50$.
  - This model can be used reliably and robustly to study fixed bed gasifiers in replacement to the 3D model. This can save a huge amount of computational resources and time.
- Inclusion of heat transfer in solids in the above simulations was performed and discussed as follows:
  - Axial temperature generated similar profiles with a maximum 2.5% difference in the peak temperature at $Re = 100$.

- The peak mass fraction of $CO_2$ was 0.295 and found to be same for the particles and solids at all Reynolds number
- Surface averaged temperature and carbon mass flux were found to be essentially the same(small scale of decrease) between solids and particles at each Reynolds number.
- Lewis number was found to be 1 for the domain and Damkohler number was used to comment on the transport regimes for different Reynolds number.
- From an engineering point of view, the temperature of the particle is lower at the start of the channel by 50 - 70 K during combustion. However, the particle temperature inside the column is much higher as compared to the surface temperature and goes up to a maximum value of 180 K for $Re = 100$.

- Inspired by fluidized bed, we attempted to study fluidized bed gasifiers using a modified version of the 2-D geometry. Spacings were introduced into the row of particles to account for the freely moving char particles. We see that:-
  - During combustion, the peak $Y_{CO_2}$ was observed to be 0.323 for spaced simulations which was definitely higher than that observed for fixed beds of 0.295.
  - A huge increase of $\approx 15$ - 25% in the peak axial temperature was observed at different Reynolds number.
  - The peak $Y_{CO_2}$ along the axis was 0.163 and a 15% maximum increase in the peak temperature was observed at $Re = 10$ during gasification.
  - It was noted that fluidized bed reactors have a higher temperature and $CO_2$ mass fraction compared to fixed beds due to spacing between the particles.
  - As an engineering relevance, it should be noted that the mass flux of carbon from the surface decreases by $5 \times 10^{-3}\,\mathrm{kg/m^2{-}s}$ at the exit of the particle row during combustion, for all cases of Reynolds number for a higher spacing. However, the carbon mass flux decreases by only $1 \times 10^{-3}\,\mathrm{kg/m^2{-}s}$ during gasification.

# Bibliography


[1] ANSYS, Inc. ANSYS®-FLUENT™ V 14.0 – Commercially available CFD software package based on the Finite Volume method. Southpointe, 275 Technology Drive, Canonsburg, PA 15317, U.S.A., www.ansys.com, 2013.

[2] Petr A Nikrityuk and Bernd Meyer. *Gasification Processes: Modeling and Simulation*. John Wiley & Sons, 2014.

[3] Electric Power Research Institute, Inc. EPRI 3420 Hillview Avenue, Palo Alto, California 94304; www.epri.com, 2001-2014.

[4] M. Ertan Taskin, Anthony G. Dixon, and E. Hugh Stitt. CFD study of fluid flow and heat transfer in a fixed bed of cylinders. *Numerical Heat Transfer, Part A: Applications*, 52(3):203–218, 2007.

[5] Sabri Ergun. Fluid flow through packed columns. *Chemical Engineering Progress*, 48:89 – 94, 1952.

[6] Pierre Guimard, Daniel McNerny, Edmund Saw, and Allen Yang. Pressure drop for flow through packed beds. 2004, available at `http://www.os-cfd.ru/UserFiles/File/e-library/porousity/t4_s04.pdf`.

[7] Yuan Jia, Yan Li, and David Hlavka. Flow through packed beds. 2009, available at `http://www.me.rochester.edu/courses/ME241.gans/PackedBeds(11).pdf`.

[8] Rajendra P. Chhabra, Jacques Comiti, and Ivan Machač. Flow of non-newtonian fluids in fixed and fluidised beds. *Chemical Engineering Science*, 56(1):1 – 27, 2001. ISSN 0009-2509.

[9] Henry Darcy. *Les fontaines publiques de la ville de Dijon: exposition et application*. Victor Dalmont, 1856.

[10] Stephen Whitaker. Flow in porous media I: A theoretical derivation of Darcy's law. *Transport in porous media*, 1(1):3–25, 1986.

[11] Shijie Liu, Artin Afacan, and Jacob Masliyah. Steady incompressible laminar flow in porous media. *Chemical Engineering Science*, 49(21):3565 – 3586, 1994. ISSN 0009-2509.

[12] A. Z. Barak and Jacob Bear. Flow at high Reynolds numbers through anisotropic porous media. *Advances in Water Resources*, 4:54–66, 1981.

[13] R. F. Benenati and C. B. Brosilow. Void fraction distribution in beds of spheres. *AIChE Journal*, 8(3):359–361, 1962. ISSN 1547-5905.

[14] B Eisfeld and K Schnitzlein. The influence of confining walls on the pressure drop in packed beds. *Chemical Engineering Science*, 56(14):4321–4329, 2001.

[15] B Eisfeld and K Schnitzlein. A new pseudo-continuous model for the fluid flow in packed beds. *Chemical engineering science*, 60(15):4105–4117, 2005.

[16] Anthony G. Dixon, Michiel Nijemeisland, and E. Hugh Stitt. Systematic mesh development for 3d CFD simulation of fixed beds: Contact points study. *Computers & Chemical Engineering*, 48(0):135 – 153, 2013. ISSN 0098-1354.

[17] Michiel Nijemeisland and Anthony G. Dixon. Comparison of CFD simulations to experiment for convective heat transfer in a gas–solid fixed bed. *Chemical Engineering Journal*, 82(1–3):231 – 246, 2001. ISSN 1385-8947.

[18] Hua Bai, Jörg Theuerkauf, Paul A. Gillis, and Paul M. Witt. A coupled DEM and CFD simulation of flow field and pressure drop in fixed bed reactor with randomly packed catalyst particles. *Industrial $ Engineering Chemistry Research*, 48(8):4060–4074, 2009.

[19] A. Soleymani, I. Turunen, H. Yousefi, and D. Bastani. Numerical investigations of fluid flow and lateral fluid dispersion in bounded granular beds in a cylindrical coordinates system. *Chemical Engineering & Technology*, 30(10): 1369–1375, 2007. ISSN 1521-4125.

[20] Rodrigo J. G. Lopes and Rosa M. Quinta-Ferreira. Numerical simulation of trickle-bed reactor hydrodynamics with rans-based models using a volume of fluid technique. *Industrial & Engineering Chemistry Research*, 48(4):1740–1748, 2009.

[21] Alfredo Guardo, Miguel Coussirat, M. Angels Larrayoz, Francesc Recasens, and Eduard Egusquiza. CFD flow and heat transfer in nonregular packings for fixed bed equipment design. *Industrial & Engineering Chemistry Research*, 43(22):7049–7056, 2004.

[22] O. Laguerre, S. Ben Amara, G. Alvarez, and D. Flick. Transient heat transfer by free convection in a packed bed of spheres: Comparison between two modelling approaches and experimental results. *Applied Thermal Engineering*, 28 (1):14 – 24, 2008. ISSN 1359-4311.

[23] Rui-Na Xu and Pei-Xue Jiang. Numerical simulation of fluid flow in microporous media. *International Journal of Heat and Fluid Flow*, 29(5):1447 – 1455, 2008. ISSN 0142-727X.

[24] Jan Tobiś. Influence of bed geometry on its frictional resistance under turbulent flow conditions. *Chemical Engineering Science*, 55(22):5359 – 5366, 2000. ISSN 0009-2509.

[25] Shinichi Ookawara, Mayu Kuroki, David Street, and Kohei Ogawa. High-fidelity DEM-CFD modeling of packed bed reactors for process intensification. In *Proceedings of European Congress of Chemical Engineering (ECCE-6), Copenhagen*, pages 16–20, 2007.

[26] Mayu Kuroki, Shinichi Ookawara, David Street, and Kohei Ogawa. High-fidelity CFD modeling of particle-to-fluid heat transfer in packed bed reactors. *ECCE-6, Copenhagen*, pages 16–21, 2007.

[27] T Eppinger, K Seidler, and M Kraume. DEM-CFD simulations of fixed bed reactors with small tube to particle diameter ratios. *Chemical Engineering Journal*, 166(1):324–331, 2011.

[28] Marvin B Glaser and George Thodos. Heat and momentum transfer in the flow of gases through packed beds. *AIChE Journal*, 4(1):63–68, 1958.

[29] Chao Gai and Yuping Dong. Experimental study on non-woody biomass gasification in a downdraft gasifier. *International Journal of Hydrogen Energy*, 37 (6):4935–4944, 2012.

[30] Gerardo Gordillo and Kalyan Annamalai. Adiabatic fixed bed gasification of dairy biomass with air and steam. *Fuel*, 89(2):384–391, 2010.

[31] Enrico Maria Grieco and Giancarlo Baldi. Predictive model for countercurrent coal gasifiers. *Chemical Engineering Science*, 66(23):5749–5761, 2011.

[32] H. Yoon, J. Wei, and M.M. Denn. A model for moving-bed coal gasification reactor. *AIChE Journal*, 24:885–903, 1978.

[33] N.R. Amundson and L.E. Arri. Char gasification in a countercurrent reactor. *AIChE Journal*, 24:87–101, 1978.

[34] A. Bhattacharya, L. Salam, M.P. Dudukovic, , and B. Joseph. Experimental and modeling studies in fixed-bed char gasification. *Industrial & Engineering Chemistry Process Design and Development*, 25:988–996, 1986.

[35] M.L. Hobbs, P.T. Radulovic, , and L.D. Smoot. Modeling fixed-bed coal gasifiers. *AIChE Journal*, 38:681–702, 1992.

[36] Hugo A. Jakobsen, Havard Lindborg, and Vemund Handeland. A numerical study of the interactions between viscous flow, transport and kinetics in fixed bed reactors. *Computers & Chemical Engineering*, 26:333 – 357, 2002.

[37] Stein Harald Skaare. Reaction and heat transfer in a wall-cooled fixed bed reactor. 1993.

[38] Jiin-Yuh Jang and Yu-Wei Chiu. 3-d transient conjugated heat transfer and fluid flow analysis for the cooling process of sintered bed. *Applied Thermal Engineering*, 29(14–15):2895 – 2903, 2009. ISSN 1359-4311.

[39] J.R. Bunt and F.B. Waanders. Volatile trace element behaviour in the sasol® fixed-bed dry-bottom (FBDB)™ gasifier treating coals of different rank. *Fuel Processing Technology*, 92(8):1646 – 1655, 2011. ISSN 0378-3820.

[40] Luc Gerun, Maria Paraschiv, Razvan Vijeu, Jérôme Bellettre, Mohand Tazerout, Benny Gøbel, and Ulrik Henriksen. Numerical investigation of the partial oxidation in a two-stage downdraft gasifier. *Fuel*, 87(7):1383–1393, 2008.

[41] Myriam Lorena Melgarejo Navarro Cerutti, Antonio Augusto Ulson de Souza, and Selene Maria de Arruda Guelli Ulson de Souza. Solvent extraction of vegetable oils: Numerical and experimental study. *Food and Bioproducts Processing*, 90(2):199 – 204, 2012. ISSN 0960-3085.

[42] William Hallett, Brenda Green, Taras Machula, and Yue Yang. Packed bed combustion of non-uniformly sized char particles. *Chemical Engineering Science*, 2013.

[43] Y. S. Cho and B. Joseph. Heterogeneous model for moving-bed coal gasification reactors. *Industrial & Engineering Chemistry Process Design and Development*, 20(2):314–318, 1981. doi: 10.1021/i200013a021.

[44] A.G. Dixon, M. Nijemeisland, and E.H. Stitt. Packed tubular reactor modeling and catalyst design using computational fluid dynamics. *Advances in Chemical Engineering*, 31:307–389, 2006.

[45] Marcelo J.S. DeLemos. Numerical simulation of turbulent combustion in porous materials. *International Communications in Heat and Mass Transfer*, 36(10):996 – 1001, 2009. ISSN 0735-1933.

[46] José E.A. Coutinho and Marcelo J.S. de Lemos. Laminar flow with combustion in inert porous media. *International Communications in Heat and Mass Transfer*, 39(7):896 – 903, 2012. ISSN 0735-1933.

[47] Marcelo J.S. de Lemos. Analysis of turbulent combustion in inert porous media. *International Communications in Heat and Mass Transfer*, 37(4):331 – 336, 2010. ISSN 0735-1933.

[48] Marcelo J.S. de Lemos and Ana C. Pivem. Turbulent flow with combustion in a moving bed. *International Communications in Heat and Mass Transfer*, 39(1):1 – 7, 2012. ISSN 0735-1933.

[49] Ana C. Pivem and Marcelo J.S. de Lemos. Numerical simulation of a crossflow moving porous bed using a thermal non-equilibrium model. *International Journal of Heat and Mass Transfer*, 67(0):311 – 325, 2013. ISSN 0017-9310.

[50] Mohsen Behnam, Anthony G Dixon, Michiel Nijemeisland, and E Hugh Stitt. A new approach to fixed bed radial heat transfer modeling using velocity fields from computational fluid dynamics simulations. *Industrial & Engineering Chemistry Research*, 52(44):15244–15261, 2013.

[51] Xiaomin Chen, Jiu Dai, and Zhenghong Luo. CFD modeling using heterogeneous reaction kinetics for catalytic dehydrogenation syngas reactions in a fixed-bed reactor. *Particuology*, 11(6):703 – 714, 2013. ISSN 1674-2001.

[52] Ya-Ping Zhu Xi Gao and Zheng hong Luo. CFD modeling of gas flow in porous medium and catalytic coupling reaction from carbon monoxide to diethyl oxalate in fixed-bed reactors. *Chemical Engineering Science*, 66:6028 – 6038, 2011.

[53] MJ Keyser, M Conradie, M Coertzen, and JC Van Dyk. Effect of coal particle size distribution on packed bed pressure drop and gas flow distribution. *Fuel*, 85(10):1439–1445, 2006.

[54] Hannsjörg Freund, Thomas Zeiser, Florian Huber, Elias Klemm, Gunther Brenner, Franz Durst, and Gerhard Emig. Numerical simulations of single phase reacting flows in randomly packed fixed-bed reactors and experimental validation. *Chemical Engineering Science*, 58(3):903–910, 2003.

[55] Anthony G. Dixon, M. Ertan Taskin, E. Hugh Stitt, and Michiel Nijemeisland. 3d CFD simulations of steam reforming with resolved intraparticle reaction and gradients. *Chemical Engineering Science*, 62(18–20):4963 – 4966, 2007. ISSN 0009-2509. 19th International Symposium on Chemical Reaction Engineering - From Science to Innovative Engineering ISCRE-19.

[56] Michiel Nijemeisland and Anthony G. Dixon. CFD study of fluid flow and wall heat transfer in a fixed bed of spheres. *AIChE Journal*, 50:906 – 921, 2004.

[57] F. Augier, F. Idoux, and J.Y. Delenne. Numerical simulations of transfer and transport properties inside packed beds of spherical particles. *Chemical Engineering Science*, 2009.

[58] S.A. Logtenberg, M. Nijemeisland, and A.G. Dixon. Computational fluid dynamics simulations of fluid flow and heat transfer at the wall–particle contact points in a fixed-bed reactor. *Chemical Engineering Science*, 54(13–14):2433 – 2439, 1999. ISSN 0009-2509.

[59] J. Cooper and W.L.H. Hallett. A numerical model for packed-bed combustion of char particles. *Chemical Engineering Science*, 2000.

[60] S. Schulze and P.A. Nikrityuk. Three dimensional CFD-based numerical study of chemically reacting char particles in a fixed bed coal gasifier. The Clearwater Clean Coal Conference, June 3-7, 2012, Clearwater, Florida, USA, 2012.

[61] S. Schulze, P.A. Nikrityuk, and B. Meyer. Three dimensional CFD-based numerical study of chemically reacting carbon particles within a randomly packed bed. 2013 AIChE Annual Meeting, November 3-8, 2013, San-Francisco CA, USA, 2013. AIChE.

[62] ML Hobbs, PT Radulovic, and LD Smoot. Combustion and gasification of coals in fixed-beds. *Progress in Energy and Combustion Science*, 19(6):505–586, 1993.

[63] Predrag T Radulovic, M Usman Ghani, and L Douglas Smoot. An improved model for fixed bed coal combustion and gasification. *Fuel*, 74(4):582–594, 1995.

[64] Kenneth M Bryden and Kenneth W Ragland. Numerical modeling of a deep, fixed bed combustor. *Energy & Fuels*, 10(2):269–275, 1996.

[65] G Wehinger, T Eppinger, and M Kraume. Detailed numerical simulations of catalytic fixed-bed reactors: heterogeneous dry reforming of methane. *Chemical Engineering Science*, 122:197–209, 2015.

[66] Martin Gräbner, Sirko Ogriseck, and Bernd Meyer. Numerical simulation of coal gasification at circulating fluidised bed conditions. *Fuel Processing Technology*, 88(10):948–958, 2007.

[67] M Syamlal and LA Bissett. METC gasifier advanced simulation (MGAS) model. Technical report, USDOE Morgantown Energy Technology Center, WV (United States), 1992.

[68] Jian Yang, Qiuwang Wang, Min Zeng, and Akira Nakayama. Computational study of forced convective heat transfer in structured packed beds with spherical or ellipsoidal particles. *Chemical Engineering Science*, 65(2):726–738, 2010.

[69] Sebastian Schulze, Petr A Nikrityuk, and Bernd Meyer. Porosity distribution in monodisperse and polydisperse fixed beds and its impact on the fluid flow. *Particulate Science and Technology*, (just-accepted), 2014.

[70] S.R. Turns. *An Introduction to Combustion*. McGraw-Hill, 2006. 2nd. ed.

[71] Y. Wu, P.J. Smith, J. Zhang, J.N. Thornock, and G. Yue. Effects of turbulent mixing and controlling mechanisms in an entrained flow coal gasifier. *Energy & Fuels*, 24:1170–1175, 2010.

[72] H.S. Caram and N.R. Amundson. Diffusion and reaction in a stagnant boundary layer about a carbon particle. *Industrial & Engineering Chemistry Fundamentals*, 16:171–181, 1977.

[73] P. A. Libby and T. R. Blake. Burning carbon particles in the presence of water vapor. *Combustion and Flame*, 41:123 – 147, 1981.

[74] W.P. Jones and R.P. Lindstedt. Global reaction schemes for hydrocarbon combustion. *Combustion and Flame*, 73:233–249, 1988.

[75] S. Sundaresan and N.R. Amundson. Diffusion and reaction in a stagnant boundary layer about a carbon particle. 6. effect of water vapor on the pseudo-steady-state structure. *Industrial & Engineering Chemistry Fundamentals*, 19: 351–357, 1980.

[76] D. Safronov, M. Kestel, PA. Nikrityuk, and B. Meyer. CFD-based modelling of a carbon particle oxidation in a laminar flow. *Canadian J. Chem. Eng.*, in press, 2014.

[77] FJ Higuera. Combustion of a coal char particle in a stream of dry gas. *Combustion and Flame*, 152(1):230–244, 2008.

[78] M. Kestel, P.A. Nikrityuk, O. Henning, and Ch. Hasse. Numerical study of the partial oxidation of a coal particle in steam and dry air atmosphere. *Journal of Applied Mathematics*, 77:32–46, 2012.

[79] ANSYS Inc. *ANSYS-FLUENT Theory Guide*, Release 14.0, 2013.

[80] R.J. Kee, Coltrin M.E., and P. Glarborg. *Chemically Reacting Flow. Theory & Practice*. John Wiley & Sons, Inc., Hoboken, New Jersey, 2003.

[81] A. Richter, P.A. Nikrityuk, and M. Kestel. Numerical investigation of a chemically reacting carbon particle moving in a hot $o_2/co_2$ atmosphere. *Ind. Eng. & Chem. Res.*, 52:5815–5824, 2013.

[82] Paula A Bejarano and Yiannis A Levendis. Single-coal-particle combustion in $O_2/N_2$ and $O_2/CO_2$ environments. *Combustion and Flame*, 153(1):270–287, 2008.

[83] S. Schulze, M. Kestel, D. Safronov, and P. A. Nikrityuk. From detailed description of chemical reacting coal particles to subgrid models for CFD: model development and validation. *Oil. Gas. Sci. Technol.*, 68:1007–1026, 2013.

[84] A. Makino, K. Namikiri, , and K. Kimura. Combustion rates of graphite rods in the forward stagnation field with high-temperature airflow. *Combustion and Flame*, 132:743–753, 2003.

[85] F. Dierich and K. Wittig. Interface tracking during char particle gasification. In P. Nikrityuk and B. Meyer, editors, *Gasification Processes: Modeling*

*and Simulation*, pages 171–204. Willey-VCH Verlag GmbH & Co, Weinheim, Germany, 2014.

[86] T.F. Smith, Z.F. Shen, and Friedman J.N. Evaluation of coefficients for the weighted sum of gray gases model. *Journal of Heat Transfer*, 104:602–608, 1982.

[87] Hans Grabmüller and H-K Schädlich. Residence time distribution of plug flow in a finite packed-bed chemical reactor. *Chemical engineering science*, 38(9): 1543–1553, 1983.

[88] GF Froment. Analysis and design of fixed bed catalytic reactors. 1972.

[89] Klaas B van Gelder and K Roel Westerterp. Residence time distribution and hold-up in a cocurrent upflow packed bed reactor at elevated pressure. *Chemical engineering & technology*, 13(1):27–40, 1990.

[90] Roman G Szafran and Andrzej Kmiec. CFD modeling of heat and mass transfer in a spouted bed dryer. *Industrial & engineering chemistry research*, 43(4):1113–1124, 2004.

[91] A Guardo, M Coussirat, F Recasens, MA Larrayoz, and X Escaler. CFD study on particle-to-fluid heat transfer in fixed bed reactors: Convective heat transfer at low and high pressure. *Chemical Engineering Science*, 61(13):4341–4353, 2006.

[92] Th Zeiser, P Lammers, E Klemm, Y W Li, J Bernsdorf, and G Brenner. CFD-calculation of flow, dispersion and reaction in a catalyst filled tube by the lattice boltzmann method. *Chemical engineering science*, 56(4):1697–1704, 2001.

[93] Milind S Kulkarni and Milorad P Dudukovic. Dynamics of gas phase and solid phase reactions in fixed bed reactors. *Chemical engineering science*, 51(11): 3083–3088, 1996.

[94] R Byron Bird, Warren E Stewart, and Edwin N Lightfoot. *Transport phenomena*. John Wiley & Sons, 2007.

[95] Scott Cooper and Charles J Coronella. CFD simulations of particle mixing in a binary fluidized bed. *Powder Technology*, 151(1):27–36, 2005.

[96] Jack T Cornelissen, Fariborz Taghipour, Renaud Escudié, Naoko Ellis, and John R Grace. CFD modelling of a liquid–solid fluidized bed. *Chemical Engineering Science*, 62(22):6334–6348, 2007.

[97] Ernst-Ulrich Hartge, Lars Ratschow, Reiner Wischnewski, and Joachim Werther. CFD-simulation of a circulating fluidized bed riser. *Particuology*, 7 (4):283–296, 2009.

[98] Fariborz Taghipour, Naoko Ellis, and Clayton Wong. Experimental and computational study of gas–solid fluidized bed hydrodynamics. *Chemical Engineering Science*, 60(24):6857–6867, 2005.

[99] Sebastian Zimmermann and Fariborz Taghipour. CFD modeling of the hydrodynamics and reaction kinetics of FCC fluidized-bed reactors. *Industrial & engineering chemistry research*, 44(26):9818–9827, 2005.

[100] Yaghoub Behjat, Shahrokh Shahhosseini, and S Hassan Hashemabadi. Cfd modeling of hydrodynamic and heat transfer in fluidized bed reactors. *International Communications in Heat and Mass Transfer*, 35(3):357–368, 2008.